MEASUREMENT AND CORRELATION OF ACOUSTIC CAVITATION WITH CELLULAR AND TISSUE BIOEFFECTS

A Thesis
Presented to
The Academic Faculty

By

Daniel M. Hallow

In Partial Fulfillment
of the Requirements for the Degree
Doctor of Philosophy in Chemical Engineering

in the

School of Chemical & Biomolecular Engineering

Georgia Institute of Technology
December 2006

MEASUREMENT AND CORRELATION OF ACOUSTIC CAVITATION WITH CELLULAR AND TISSUE BIOEFFECTS

Approved by:

Dr. Mark Prausnitz, Advisor
School of Chemical & Biomolecular Engineering
Georgia Institute of Technology

Dr. Levent Degertekin
School of Mechanical Engineering
Georgia Institute of Technology

Dr. Athanassios Sambanis
School of Chemical & Biomolecular Engineering
Georgia Institute of Technology

Dr. W. Robert Taylor
Emory School of Medicine
Emory University

Dr. Carson Meredith
School of Chemical & Biomolecular Engineering
Georgia Institute of Technology

Date Approved:
August 18th, 2006

To my parents,
for their love, support, and guidance

ACKNOWLEDGEMENTS

I would like to thank my advisor, thesis committee members, funding sources, colleagues, friends, and family who have given me support and have helped make this thesis possible. I would like to thank my advisor Mark Prausnitz for his patience, intellect, and advice towards my thesis and in addition, for giving me the opportunity to work in his lab and helping me grow as a researcher and an individual. I would also like to thank Dr. Carson Meredith, Dr. Athanassios Sambanis, Dr. Levent Degertekin, and Dr. Robert Taylor for serving as members of my thesis committee and for their scientific advice. I would like to thank my funding sources: the National Institutes of Health, U.S. Department of Education Graduate Assistance in Areas of National Need (GAANN) fellowship, and the EKOS Corporation.

I would like to thank those past and present members of the Prausnitz Drug Delivery Laboratory who have helped me in my research and for being such great colleagues and friends: Jason (Ninghao) Jiang, my fellow classmate, for his help during our first year of classes, his constant humor, and "love taps"; Wijaya Martanto for his contributions, for being a great friend, and for helping me meet my wife; Robyn Schlicher for her biological expertise and friendship; Josh Hutcheson for his morning discussion of research, news, Braves, and finer episodes of "Good Eats"; Sean Sullivan for his constant ranting on everything from sports to sub sandwiches, introducing me to "Lost" (but not "24") and creating the candy drawer; Harvinder Gill for his advice and help in engineering so many small projects; Vladimir Zarnitsyn for his programming expertise and interesting perspectives; Mangesh Deshpande for showing his passion for

science, blaring Queen in the lab, and giving me a “hard-time”; Esi Ghartey-Tagoe for her patient help in the lab; Pavel Kamaev for his ultrasound and bubble expertise, and his contribution toward this work; and fellow labmates Samantha Andrews, Prerona Chakravarty, Ping Wang, Jeong-Woo Lee, Jung-Hwan Park, Samir Patel, Ying Liu, Jyoti Gupta, Yeu Chun Kim, and Kristy Rostad for their help and friendship.

I would especially like to thank the undergraduate researchers who have helped with this work: Todd McCutcheon for his help and willingness to work with such little sleep; Anuj Mahajan for his hard work and help with so much of this thesis; Richie Seeger for his work on microchannels, willingness to do the mundane sometimes, and humorus stories.

I would like to thank those in the IBB, Georgia Tech, and Emory who have helped with this thesis: Donna Bondy for help with nearly everything from orders to making sure I get paid, and especially for her delicious baking; Trudy Walker for her motherly advice; Johnafel Crowe for this confocal and flow cytometry expertise; Tracy Couse for her kind help with histology; Jeff Andrews and Brad Parker for their help in machining many projects and reminding me I should be finished; Mark Allen for allowing me to use his micromachining lab; Richard Schafer for his expertise with the laser equipment; Brian Wayman for teaching me to excise arteries and his enjoyable company during those early morning drives; and those in Dr. Taylor’s lab for their help and advice.

I would like to thank those at Holifield Farm for their donation of pig tissue and Tommy for his early morning humor and educating me on cuts of meat.

I would like thank Matt Kahle and Mark Gildersleeve, my first roommates in Atlanta, for their great friendship.

Most of all, I would like to acknowledge the family closest to me: my parents for their unconditional love and support. Their invaluable guidance provided the bearing in my life and I hope to continue in the example they have set. My father's wisdom and advice will always be remembered, and my mother's strength and motivation continues to inspire. I thank my sister for her love, support, and tolerance towards her little brother. I would like to acknowledge Melissa Hallow, my wife, for being my best friend, my love, and my companion. Her words of encouragement and contribution in my life and work cannot be overstated. Finally, but definitely not least, I would like to acknowledge Ana Grace Hallow, my daughter, for the love, laughter, and joy she brings into my life everyday.

TABLE OF CONTENTS

LIST OF TABLES

LIST OF FIGURES

LIST OF SYMBOLS AND ABBREVIATIONS

ANOVA	analysis of variance
AoSMC	aortic smooth muscle cells
BN	broadband noise measurement
BSA	bovine serum albumin
CSID	cell shearing injury device
CVD	cardiovascular disease
DMEM	Dulbecco's Modified Eagle's Medium
DNA	deoxyribonucleic acid
EDTA	ethylenediaminetetraacetic acid
EC	endothelial cell
eNOS	endothelial nitric oxide synthase
f	frequency
FDA	Food and Drug Administration
FG	function generator
FGF	fibroblast growth factor
FITC	Fluorescein isothiocyanate
FFT	fast-fourier transfrom
HBSS	Hank’s Balanced Salts Solution
MCDB	Modified Czapek Dox Broth
NADPH	nicotinamide adenine dinucleotide phosphate
PBS	phosphate buffered saline

PVDF	poly vinylidene flouride
RPMI	Roswell Park Memorial Institute medium
SEM	standard error of the mean
SMC	smooth muscle cell
SONAR	sound navigation and ranging
VEGF	vascular endothelial growth factor
VI	virtual instrument

SUMMARY

Targeted intracellular delivery is a goal of many novel drug delivery systems to treat site-specific diseases, such as cancerous tumors and atherosclerotic lesions, thereby increasing the effectiveness of drugs and reducing the side effects associated with current drug administration. The development of ultrasound-enhanced delivery is aimed at providing a targeted means to intracellularly deliver drugs and genes by utilizing ultrasound's unique ability to non-invasively focus energy into the body and generate cavitation, which has been found to cause transient poration of cells. Previous research of ultrasound-enhanced delivery has concentrated on delivery into *in vitro* cells in suspension and, most recently, in tissues of in vivo animal models in order to understand the cavitation-based mechanism, to control the bioeffects, to optimize intracellular uptake, and to advance this technique toward clinical applications. Despite the advancements made by these studies, many challenges remain before ultrasound-enhanced delivery can become a realistic therapy. To address some of these issues, the goals of this study were (i) to develop a measurement based on cavitation sound emissions to correlate with bioeffects for a means to predict and control intracellular uptake and loss of viability and (ii) to evaluate the ability of ultrasound to target intracellular delivery into endothelial and smooth muscle cells in viable *ex vivo* arteries for potential treatment of cardiovascular diseases and dysfunctions. In addition, this study sought to exploit the underlying shear mechanism of ultrasound-enhanced delivery by (iii) developing a simplified device to expose cells to shear stress and cause intracellular uptake of molecules.

The first objective of this work was to relate a measurement of cavitation to ultrasound-induced bioeffects. We sought to record and analyze the cavitation emissions while simultaneously measuring intracellular delivery and loss of cell viability mediated by cavitation in an *in vitro* cell suspension. Analysis of recorded cavitation emissions was performed by deriving the frequency spectra of the sound and monitoring the features indicating cavitation. The frequency spectra of cavitation emissions were found to exhibit characteristic features of cavitation, including subharmonics, ultraharmonics, and increased broadband noise levels. Concentrating on broadband noise, a common measure of inertial cavitation (i.e., cavitation associated with violent bubble implosions), we were able to monitor the kinetic activity of inertial cavitation. Broadband noise was found to increase sharply during the first 20 milliseconds to a peak value and then decayed with a half-life of tens to hundreds of milliseconds until reaching a point of constancy. From analysis of the kinetic behavior over a range of experimental and acoustic parameters, we proposed that cavitation activity was principally controlled by the initial number of bubbles capable of undergoing inertial cavitation (i.e., bubbles within the size range for inertial cavitation) and by the rate of destruction of bubbles by inertial cavitation. Furthermore, we analyzed cavitation while altering the acoustic and experimental parameters, including pressure, exposure time, frequency, microbubble concentration, and cell type, and measuring the cellular bioeffects, generating 350 data points. Calculating the time integral of broadband noise provided a measure of the inertial cavitation dose that correlated strongly to intracellular uptake and loss of viability. The inertial cavitation dose proved to be a unifying parameter that correlated to the bioeffects over the broad range of parameters tested. The significance of this study is

that we have demonstrated that broadband noise can provide an appropriate measure of inertial cavitation activity and, more importantly, we have shown broadband noise measurements can improve the correlation with cellular bioeffects compared to other measures of cavitation (e.g., acoustic energy or sonoluminescence measurements). Therefore, we believe broadband noise can be used to predict and control bioeffects in the lab or potentially in the clinic.

The second aim of this work was to evaluate intracellular drug delivery by ultrasound in viable arterial tissue for potential treatment of cardiovascular diseases and dysfunctions. For these studies, we focused on intracellular delivery into endothelial and smooth muscle cells by exposing viable *ex vivo* porcine carotid arteries to ultrasound. By analyzing the arteries using confocal microscopy, we found that ultrasound could cause targeted intracellular delivery to endothelial and smooth muscle cells and often caused loss of viability in the form of dead intact and denuded cells. Furthermore, quantification of bioeffects was used to determine the approximate acoustic energies required for a range of bioeffects. At low to intermediate ultrasound energy, ultrasound achieved targeted intracellular delivery into viable cells that represented 9 – 24% of exposed endothelial cells and also typically caused 7 - 25% endothelial cell death. At high energy, intracellular delivery was targeted to smooth muscle cells, which further caused denuding or death of proximal endothelial cells. Lastly, by experimentally testing intact arteries, we found that ultrasound can target delivery at near physiologic conditions. This study represents the first known in-depth study that has evaluated intracellular uptake of molecules into viable tissue by ultrasound.

The last aim of this work sought to develop a simple device to expose *in vitro* cells to shear forces, thereby causing intracellular uptake. By fabricating microchannels in Mylar® sheets with established micro-machining techniques, we designed a device that could force cells in suspension through microchannels, thereby exposing cells to high shear forces for short durations. By evaluating channels of various dimensions and geometries, we found that shear generated at channel diameters of approximately 40-50 μm and in a conical geometry yielded the best results, approximately 36% of cells with uptake and 80% viability. We further found that this technique could deliver small molecules to large macromolecues (e.g., proteins) into cells. Lastly, we designed a device that provided a quick, high-throughput method to deliver molecules into cells. The significance of this work is that we have developed a simple and inexpensive device that could be potentially used by the biological, medical, and biotechnology communities to cause intracellular delivery into cells.

In summary, this thesis has advanced advancement the field of ultrasound-enhanced delivery by (i) developing a measurement based on cavitation emissions, to correlate with ultrasound-mediated bioeffects, i.e., intracellular uptake and loss of viability and by (ii) evaluating the intracellular uptake into viable cells in tissue by ultrasound. The correlation of cavitation measurements with bioeffects suggests possible laboratory and clinical applications in ultrasound-enhanced delivery of drugs and genes into cells. By evaluating ultrasound-enhanced delivery in arterial tissue, we believe these findings indicate the approximate ultrasound energies for *in vivo* applications. Furthermore, this work suggests potential strategies for cardiovascular applications to deliver molecules into endothelial or smooth muscle cells. Lastly, by using shear forces

generated in microchannels, we have fabricated a simple and inexpensive device to cause intracellular uptake of small and large molecules into *in vitro* cells. We believe this device has the capability to be used in the lab, clinic, or plant to deliver bioactive molecules (e.g., genetic material or drugs) or diagnostic molecules (e.g., labeling probes) into cells.

CHAPTER 1

INTRODUCTION

With escalating advancements in new therapeutic drugs in recent decades, increasing attention has been focused on methods to deliver drugs in more efficient and effective manners (Langer 1998; Saltzman 2001). A large amount of research has been performed in drug delivery to improve administration, targeting, controlled release, effectiveness, and efficiency of drugs by chemical modifications to the drug (e.g., antibodies, proteins, polymers) (McCarron et al. 2005; Sapra et al. 2005; Veronese and Pasut 2005), the use of controlled release systems (e.g., polymeric degradation and diffusion, liposomal vesicles) (Chien 1992; Stubbe et al. 2004), and novel mechanical or electrical mechanisms (e.g., electroporation, iontophoresis, microneedles) (Batheja et al. 2006; Heller et al. 2005; Prausnitz 2004). Efficiently targeting specific cells and permeating the cell's natural regulating barriers (e.g., cellular membrane or nuclear membrane) to allow intra- and extra-cellular molecular transport remains a difficult challenge and limits the effectiveness and potential of many drugs and gene therapy treatments (Panyam and Labhasetwar 2004; Stein and Lieb 1986). A general method to deliver therapeutic agents in a more safe and effective manner would provide a great benefit in a broad range of drug delivery applications to increase the efficacy of current drugs, lower administrating costs, decrease side effects, and promote future gene therapy and drug design. A potential remedy to these difficulties in drug delivery is the method of ultrasound-enhanced drug delivery, a novel technique that offers the potential to efficiently deliver drugs to highly targeted regions of the body by a non-invasive method.

Ultrasound-enhanced drug delivery research is at the frontier of drug delivery and aims to develop a novel method to increase targeting to specific areas of the body, increase delivery efficiency, and release drugs in controlled doses (Mitragotri 2005). As a mechanical method that increases drug delivery targeting, ultrasound has the potential to be applied to a broad range of applications from chemotherapy treatment at specific tumor locations (Tachibana 2004) to treating atherosclerosis at the site of the disease (Bekeredjian et al. 2005). By exploiting the local mechanical and possibly chemical effects (e.g., high local temperatures and pressures, microstreaming, shear flow, and free radical formation) associated with the acoustic cavitation induced by pressure transients of ultrasound, this method is able to reversibly permeabilize the cells' regulating barrier to its extracellular environment and allow passive diffusion of extracellular compounds into the cell (Miller et al. 1996). The potential of ultrasound-enhanced drug delivery has been mainly shown in systems of *in vitro* cell suspensions, with encouraging results demonstrating improved delivery of DNA for gene therapy (Tsutsui et al. 2004) and loading of cells to equilibrium with the extracellular concentration of molecules of interest (e.g. calcein or fluorescent dextrans) (Guzman et al. 2002). Furthermore, ultrasound-enhanced drug delivery has also been studied in *ex vivo* tissue and *in vivo* animal models as a means to deliver therapeutic plasmids (Bekeredjian et al. 2005).

One of the greatest challenges with the application of ultrasound-enhanced drug delivery is the prediction of bioeffects based on the acoustic and experimental parameters. A means to control bioeffects based on a measurement of the input or output parameters would allow for feedback control by clinicians to optimize the amount of uptake and loss of viability for particular applications. The measurement of cavitation by

analyzing the acoustic emissions from cavitation and correlating this measurement with bioeffects is the scope of the first part of this thesis. Determining the capabilities of cavitation in systems beyond simple cells suspensions in *ex vivo* or *in vivo* tissue is also essential to the development of ultrasound-enhanced drug delivery. The second portion of this thesis investigates delivery into *ex vivo* arterial tissue to understand the effects and mechanism of cavitation. Based on the commonly held belief that shear forces from fluid flow is the cause of bioeffects by ultrasound-mediated cavitation, the last portion of this thesis investigates the use of microfluidic channels as a means to impart high shear forces on cells in suspension and cause bioeffects similar to cavitation.

CHAPTER 2

BACKGROUND

Drug Delivery

In recent years, novel and improved drug delivery systems have become a heightened focus for pharmaceutical and biomedical companies and academic research. Sales of advanced drug delivery systems in the U.S. have reached nearly $20 billion annually (Langer 2001). Research on improving drug delivery systems is aimed at enhancing the administration of drugs in safe and non-invasive manners, improving the targeting or effectiveness to specific tissues or cells, increasing the solubility, and controlling the release of drugs (Rosen and Abribat 2005). The range of current research in drug delivery systems spans chemical modifications of drugs, new particles for transport of drugs, improved polymeric release mechanisms, and new mechanical and electrical methods (Langer 1998).

Chemical modifications to drugs can enhance the targeting by antibody or microparticle linkages (McCarron et al. 2005), improve pharmacokinetics and solubility by attachment of degradable synthetic polymers (Aliabadi and Lavasanifar 2006; Duncan and Spreafico 1994), or alter immunogenicty of the drug by protein engineering and attachment of polymers such as polyethylene glycol to the drug (Veronese and Pasut 2005). Chemical alterations to drugs can also include creating microparticle or colloidal carriers for drugs. These carriers typically consist of proteins, lipids, or synthetic polymers (e.g., liposomes) (Gupta et al. 2005; Hofheinz et al. 2005) and aim to improve

systemic transport of the drug, create anti-immunogenic particles, improve targeting, or enhance transport through the lipid-based cellular membrane.

Controlled release delivery spans a wide variety of engineered systems, but in general, the goal is to administer drugs in controlled dosage levels and to avoid the peaks and valleys in systemic drug concentrations, which are common in many conventional methods (Conti et al. 2000). This is particularly important since many drugs must be above a certain concentration level threshold to be effective and below a certain level to avoid being toxic to the patient (Chien 1992).

Novel mechanical and electrical methods include techniques to improve administration. These include iontophoresis, electrically driving molecules across tissues (Batheja et al. 2006); electroporation, permeabilizing the impeding cell membrane (Gehl 2003); magnetic particles, carrying and releasing drugs under magnectic fields (Edelman et al. 1985); high velocity particles or jets, transdermal delivery by impacting the skin with high velocity injections (Burkoth et al. 1999); and microneedle injections, transdermal delivery by painless microscopic needles (Prausnitz 2004).

Ultrasound-enhanced drug delivery falls into the classification of novel mechanical methods. These novel techniques to deliver drugs have the potential to improve not only the market of current drugs, but also to promote future drug design and provide the necessary means to deliver the latest complex agents such as genetic material (Johnson-Saliba and Jans 2001), proteins (Kompella and Lee 2001), and other therapeutic agents.

Ultrasound

Sound is propagating pressure waves through a medium such as air or water at frequencies perceived by humans. Generally, mechanical vibrations create sound or pressure waves in an elastic medium, transferring energy into the medium and to any objects the sounds contact. Ultrasound is defined as sound in frequency ranges above the audible range of humans. The typical human range for audible sound is from 4 Hz to 20 kHz; therefore, ultrasound is classified as sound at frequencies above 20 kHz. Typically, ultrasound is generated from transducers composed of piezoelectric materials such as quartz or certain ceramics that resonate when electricity is passed through the material. These vibrations of the piezoelectric material convert electrical energy to mechanical energy in the form of high frequency sound (Pierce 1981). A common purpose of ultrasound is cavitation production for the application of imaging, cleaning, initiating chemical reactions, drug delivery, destruction of kidney stones, or surgically destroying cells (Apfel 1997).

Acoustic cavitation

Acoustic cavitation is defined as the bubble formation and/or oscillation of gas bubbles in liquid due to rapid variations in pressure caused by ultrasonic waves. Cavitation induced from acoustical activity is typically a result of either (1) liquid vapor that forms as a result of the local pressure falling below the vapor pressure of the liquid, (2) dissolved gases that come out of solution due to the low local pressures, or (3) pre-existing stabilized gas bubbles present in the liquid (Apfel 1997).

Cavitation can be further classified as either stable or inertial cavitation (also known as transient cavitation) based on the oscillations the bubbles undergo. At low

pressures, the bubbles oscillate in a stable manner for many cycles, hence termed stable cavitation. However, high-pressure oscillation can cause large fluctuations in the bubble size and can lead to a violent implosion of the bubble above a certain pressure threshold; this type of cavitation is termed inertial cavitation. The type of cavitation has drastically different local effects from the lesser impacting effects of stable cavitation to the more intriguing and intense activity of inertial cavitation (Leighton 1994).

The implosion of inertial cavitation occurs so quickly that it causes compression of the gas at near adiabatic conditions (Leighton 1994). As a result, the imploding bubble reaches extremely high temperatures and pressures (i.e, >5000^{o}C and > 500 atm) (Flint and Suslick 1991; Suslick 1990). These intense conditions can cause the formation of free radicals and a variety of chemical reactions that have been extensively researched for applications in the chemical industry (Suslick 1990). These sonochemical reactions have also been shown to cause light emissions, a phenomenon referred to as sonoluminescence (Crum 1994).

With bubbles in either stable or inertial cavitation, the surrounding liquid forms local streaming and mixing, creating local shear flow (Acoustical Society of America 2002). When a bubble collapses near an object, the collapse can occur non-uniformly and force a stream of liquid through the bubble towards the impinging object. These local small jets of water are called microstreaming and can cause intense mixing, high local shear flow, and damage to the objects (Lauterborn and Ohl 1997).

Just as the piezoelectric source vibrates to create ultrasound, the vibrations of the bubbles further cause their own sound emissions. The resonant frequency of a bubble is determined by its size and the viscosity of the surrounding liquid (Allen et al. 1997).

When sound is applied to a bubble at its resonant frequency (e.g., ~ 2 MHz for the mean size of Optison® bubbles), the bubble oscillates linearly and in phase with the pressure fluctuations of sound, emitting sound at the same frequency as the driving frequency. However, when the frequency of sound does not match the resonant frequency of the bubble, the bubble will oscillate non-linearly or out of phase with the pressure fluctuation. These non-linear vibrations can produce sound at frequencies other than the driving frequency, often emitting sound at subharmonics or ultraharmonics of the driving frequency (i.e, ½f, 3/2f, 2f, 5/2f,3f, etc) (Leighton 1994). These emissions of sound at the driving frequency and subsequent harmonics are further superimposed onto a level of broadband noise caused by erratic oscillations and the violent implosion of inertial cavitation (Neppiras 1968). Cavitation emissions are often studied to characterize the cavitation activity and used in an attempt to monitor the amount and quality of cavitation (Chen et al. 2003; Neppiras 1980).

The combination of these local effects of acoustic cavitation and ultrasound's ability to be applied in a focused and non-invasive manner make ultrasound a favorable tool for the medical industry. Using one or a combination of these local effects caused by ultrasound-induced cavitation, a variety of current medical applications can be achieved, including imaging, heating tissue, tissue destruction, or lithotripsy, and future applications such as ultrasound-enhanced drug delivery are being avidly pursued.

Ultrasound in Current Medical Applications

Ultrasound has a long history of use as a diagnostic and therapeutic instrument in the medical industry for applications in medical imaging, physical therapy, and lithotripsy. The uses of ultrasound range from conditions with minimal bodily impact for

medical imaging (e.g., myocardial diagnosis and fetus development) (Beach 1992) to conditions with high bodily impact for surgery such as lithotripsy (Madersbacher and Marberger 2003), which is the destruction of kidney stones and tissue by ultrasonic cavitation.

Ultrasound was first used as a medical tool in physical therapy. Ultrasound's ability to heat tissues and to be focused non-invasively in the body was first discovered in the 1930s and as a means to heat inner body tissues. Ultrasound has since developed into an accepted tool in the field of physical therapy for heating specific tissues (Ng and Liu 2002). The application of ultrasound to heat tissues has been further extended and researched to treat some cancers by heating tumors to help kill cancerous cells (Madersbacher et al. 1995).

The use of ultrasound as a diagnostic tool for imaging did not develop until the late 1940s and 1950s. When sound contacts another object or a medium with different physical properties, sound is not only transferred into the next medium but is also reflected back towards the source. Using this principle, imaging of the interior of the human body is possible by applying this pulse-echo technique, a method similar to the naval reconnaissance tool know as SONAR and the echolocation technique used by bats, dolphins and whales (Ng and Liu 2002). As ultrasound is non-invasively focused into the body, sound reflections are sent back to the source due to the different physical characteristics of tissue, bone, blood and other matter. These reflections are then recorded and analyzed to form distinctions between tissues and organs and further processed to generate an image. With vastly improving imaging resolution and the development of 3-D imaging over the last 50 years, ultrasound has become an

exceptionally popular diagnostic tool in the medical community, particularly for non-invasively monitoring fetus development in obstetrics and diagnosing myocardial abnormalities (Hollis and Thilaganathan 2001; Mittle et al. 2003).

In the past few decades, other improvements to imaging have been made through the use of contrast agents. Contrast agents are stabilized gas bubbles typically consisting of a protein- (i.e. albumin) or lipid- based shells filled with an inert gas (i.e., perflurocarbon gas), such as Optison® or Definity® (Goldberg et al. 1994; Miller and Nanda 2004). Contrast agents are intravenously introduced into the body's blood circulation. When imaging the circulation of blood in the heart or blood vessels, the bubbles serve as echogenic agents that produce more acoustic reflections to yield increased contrast between the blood and surrounding tissues (Forsberg et al. 2000). These contrast agents are widely used in myocardial imaging to delineate the endocardial borders in echocardiograms (Mittle et al. 2003) and give an improved image of muscle contractions and heart valves (Rosenzweig et al. 2001).

Ultrasound can also be used in high-energy conditions such as removing kidney stones by extracorpeal shock wave lithotripsy (Coleman and Saunders 1993). Approximately 75% of treated kidney stones are treated with lithotripsy (Holmes and Whitfield 1991). Using a spectrum of high-intensity acoustic waves, relative to diagnostic and physical therapy levels of ultrasound, acoustic energy is focused at the kidney stones to create intense inertial cavitation that destroys or breaks apart the kidney stones and allow them to be passed more easily by the patient (Coleman and Saunders 1993).

Ultrasound has developed into a tremendously useful tool for the medical community in a broad range of applications due to its non-invasive nature, ability to be targeted into the body, and wide range of intensity levels to impact the body. Exposure intensity levels of ultrasound in medical applications range from <0.5 W/cm^2 in diagnostic imaging, 0.5-3 W/cm^2 in therapeutic applications, and >10 W/cm^2 in lithotripsy treatments (Ng and Liu 2002). As ultrasound has become an established modality in a number of treatments, further novel applications of ultrasound are continually being explored and researched.

Ultrasound in Drug Delivery

The latest research has found ultrasound to be valuable in interesting applications for drug delivery. The remarkable benefits of ultrasound in drug delivery include its ability to be applied in non-invasive or minimally invasive manners and focused to affect only the specific tissues or cells of interest. As a mechanical method, in contrast to a chemical modification, ultrasound has the potential to be applied to a wide range of current and future drugs. By exploiting the local effects of acoustic cavitation induced by ultrasound, cavitation can cause reversible permeation across cell membranes, allowing the intracellular transport of molecules into the cell (Cooke 2000; Mitragotri 2005), and/or cause release from drug carriers such as micelles, liposomes, microbubbles, and polymers (Marin et al. 2002; Rapoport 2004; Unger et al. 2004).

The earliest application and research of ultrasound-enhanced drug delivery was a method to promote transdermal drug delivery of hydrocortisone ointment into inflamed tissues (Tyle and Agrawala 1989). Transdermal drug delivery is an avidly pursued method due to its potential ease of administration and its ability to bypass the

gastrointestinal system's harsh metabolism (Langer 1990). However, transdermal drug delivery remains a difficult challenge due to the daunting task of crossing the impermeable barrier presented by the stratum corneum, the outer most layer of dead skin (Edwards, 1994). Research of ultrasound for transdermal drug delivery, a phenomenon known as sonophoresis or phonophoresis, has been attempted for low molecular weight drugs and proteins such as insulin (Mitragotri et al. 1995). Ultrasound has been shown to increase the permeability of the skin by a mechanism believed to involve cavitation at the skin's surface, which can disorganize the stratum corneum layer, thereby promoting molecular transport across the layer of skin (Mitragotri et al. 1995). Even though early attempts at promoting transdermal drug delivery with megahertz-frequency ultrasound met with limited success, more recent work in the kilohertz range has effectively enhanced delivery of a range of different compounds (Barry 2001).

Understanding the local effects of cavitation induced by ultrasound has led studies to exploit these effects to cause cell permeabilization, allowing increased diffusion of extracellular compounds into the cell. Many researchers have investigated cavitation in terms of causing cell lysis and damage in erythrocytes (Daniels et al. 1995; Everbach et al. 1997) and other cell suspension systems (Brayman et al. 1999; Miller and Quddus 2001) to identify and prevent the negative effects ultrasound may cause in diagnostic treatments. However, other investigators have chosen to examine cavitation in a more positive sense and have explored the use of acoustically induced cavitation to cause reversible permeabilization of the cell membrane for therapeutic drug and gene delivery (Amabile et al. 2001; Guzman et al. 2001). The cell membrane is an arduous barrier for drug delivery (Stein and Lieb 1986), and various engineered techniques, including

ultrasound-enhanced drug delivery, are being explored to increase diffusion of drugs across the cellular membrane.

Acoustic cavitation's mechanism of cellular damage is hypothesized to be mainly a mechanical process in which the induced microstreaming and shear flow, namely from inertial cavitation, causes local damage to the cell (Miller et al. 1996; Schlicher et al. 2006; Wu et al. 2002). Others have also shown that the chemical effects of cavitation, such as free radical formation, can cause further bioeffects, hypothetically by cellular membrane destruction or inducing other cellular pathways such as apoptosis (Feril et al. 2003; Lagneaux et al. 2002). The ability of cavitation to cause local damage to the cell can potentially be a beneficial tool if the cellular damage allows increased molecular transport across the cell membrane and if the cell is able to repair damage, remain viable, and maintain normal metabolism and function.

Previous research has shown the potential of ultrasound-enhanced drug and gene delivery in cell suspension systems and cell monolayers, typically utilizing fluorescent molecules to monitor the molecular uptake (Chen et al. 2003; Greenleaf et al. 1998; Guzman et al. 2001; Guzman et al. 2002). Results of these experiments have been encouraging as they have shown its possible to cause reversible permeation, intracellular uptake is capable for molecular sizes up to 464 kDa, and intracellular uptake reaches equilibrium with extracellular concentrations (Guzman et al. 2002). Further research has shown positive results for increasing the uptake of genetic material and may be used to facilitate gene therapy treatments in combination with adenoviral or liposomal techniques (Beeri et al. 2002; Koch et al. 2000).

A large portion of research with ultrasound in *in vivo* animal models, have investigated this technique for gene therapy in the cardiovascular system. Many studies have shown positive results of delivery of therapeutic genes and tissue responses. This research has mostly focused on reducing or preventing neointimal formation in atherosclerotic plaques or promoting angiogenesis for the treatment of ischemic heart or peripheral injury (Bekeredjian et al. 2005). Others have also shown positive transfection results by ultrasound in *in vivo* tissues such as skeletal muscle (Lu et al. 2003), kidney (Koike et al. 2005), and liver (Kondo et al. 2004) for various applications. However, few studies have focused on the delivery of small molecules or proteins by ultrasound *in vivo* (Mitragotri 2005).

The current limitation of ultrasound-enhanced delivery is the low fraction of cells with uptake at low acoustic energies and the high loss of viability at high acoustic energies. However, in some treatments, the loss of viability may be a desirable effect, such as in treating cancerous cells or tumors (Kennedy 2005) or destroying fat cells (Pine et al. 2003). The loss of viability has been shown to inversely correlate with the amount of uptake. Many studies have attempted to correlate the bioeffects (i.e., uptake and loss of viability) with aspects of cavitation or the acoustic parameters (Cochran and Prausnitz 2001; Guzman et al. 2001; Sundaram et al. 2003).

Research has also focused on using ultrasound to control drug release by using acoustic cavitation as a triggering mechanism. By using micelles, liposomes, microbubbles, or polymers that encapsulate the drug, the mechanical or chemical effects induced by ultrasound have been shown to trigger drug release in a controlled manner (Marin et al. 2002; Rapoport 2004; Unger et al. 2004). This method would be especially

beneficial to cause targeted release by exploiting ultrasound's ability to be focused into the body. If further used in combination with cell permeation, these modalities may lead to a powerful technique for controlling drug release and targeting specific cells for drug delivery in a non-invasive manner.

Cardiovascular Drug Delivery

Cardiovascular disease (CVD) is currently one of the leading causes of death, resulting in nearly 17 million deaths per year worldwide (Smith et al. 2004). In the U.S. alone, CVD affects nearly 70 million people, accounts for 900,000 or 40% of the deaths per year, and remains the leading cause of death. Projected economic costs are estimated at $400 billion for 2006 in the U.S (Thom et al. 2006). CVD includes coronary and peripheral heart disease, hypercholesterolemia, and hypertension that can lead to heart attack or stroke. Other vascular dysfunctions include restenosis post percutaneous interventions, myocardial and peripheral ischemia, and vascular angiogenesis in tumorous cancers.

Blood vessels, i.e., arteries or veins, are composed of three distinct layers, known as the intima, media, and adventitia (Fig 2.1) (Davis et al. 2003). The intima consists of a monolayer of endothelial cells that rest upon an elastin protein matrix, the internal elastic lamina. The muscular portion of the vessel, known as the media, consists of smooth muscle cells that mainly serve to exert muscular contraction or relaxation. Lastly, the adventitia mainly consists of connective tissue of collagen but also contains fibroblasts, nerve bundles, and inflammatory cells (Belanger 1990).

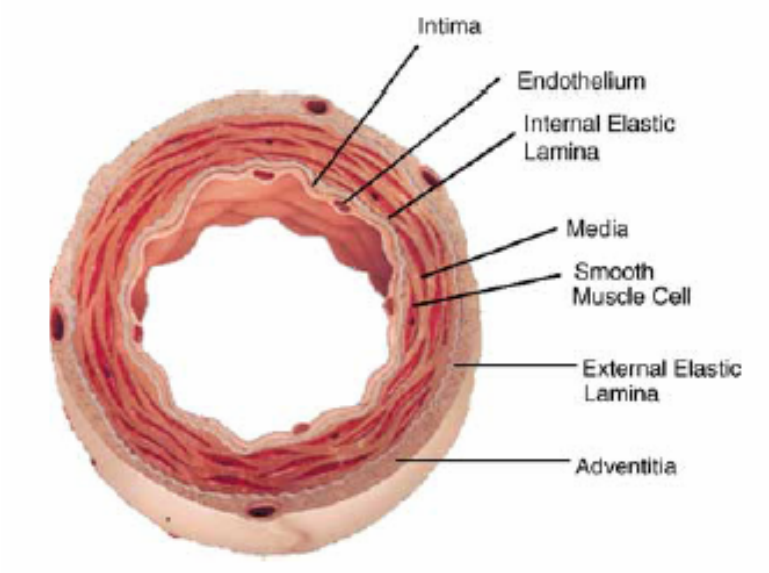

Figure 2.1: The vascular anatomy (Davis et al. 2003)

In the past, the endothelium was viewed only as a cell layer to provide a mechanical, non-thrombogenic barrier. The endothelium is now known to be a critical mediator in a number of chemical pathways that maintain homeostasis and vascular tone, regulate thrombosis and vascular permeability, mediate inflammatory responses, control smooth muscle cell proliferation, and initiate angiogenesis (Belanger 1990). Endothelial dysfunction occurs when endothelial homeostasis is disturbed due to pathological stresses, such as increased oxidative stress, hyperlipidemia, inflammation, and mechanical injury. Endothelial dysfunction can lead to a host of detrimental effects, such as an imbalance of vasodilator and vasoconstrictor agents (e.g., nitric oxide and prostacylcin, angiotesin II, and thromboxane), increased platelet adhesion, macrophage recruitment, and uncontrolled smooth muscle cell proliferation (Cines et al. 1998). The pathological results may be atherosclerotic lesions, hypertension, or re-narrowing of the artery in the case of restenosis (Cines et al. 1998). In cancerous tumors, an imbalance is caused by the over-production of angiogenic factors such as vascular endothelial growth

factor (VEGF). This imbalance leads to an uncontrolled and tortuous vascular system that allows tumors to grow to larger sizes and metastasize (Hanahan and Weinberg 2000; Sato 2003). In contrast, myocardial or peripheral ischemia is a condition caused by insufficient blood supply due to failing blood vessels from injury or disease (Madeddu 2005).

Due to the critical role of endothelial cells and smooth muscle cells in controlling vascular functions and dysfunction in a number of pathological conditions (Cines et al. 1998), targeted drug and gene therapy to the vascular endothelium and media has increasingly become a focus for treating cardiovascular diseases and dysfunctions (Cooke 2000; Feldman and Steg 1997; Melo et al. 2004; Quarck and Holvoet 2004). In many of these ailments, it is desired to have drug or gene delivery to the specific diseased site in order to locally treat the area or lesion while avoiding harsh or toxic systemic side effects. Currently, many drug delivery techniques, such as drug-elutings stents (Gershlick 2005), catheter-based delivery systems (Sharif et al. 2004), viral vectors, targeted liposomes (Quarck and Holvoet 2004), and targeted microbubbles (Kipshidze et al. 2005), are being studied to cause targeted drug or gene delivery to specific diseased sites in the cardiovascular system.

Current gene therapy research in the cardiovascular system is aimed at genetically manipulating the endothelium or smooth muscle cells by increasing protein expression or blocking protein expression of certain factors in order to reestablish a chemical balance and reaffirm homeostasis (e.g., eNOS or E2F decoy), promote angiogenesis (e.g.., VEGF or FGF) (Quarck and Holvoet 2004), or decrease or kill vasculature in tumors (e.g.., Caspase-9) (Song et al. 2005; Tozer et al. 2005). However, most current techniques lack

either the effectiveness or specificity to adequately treat these disorders while safely administering the therapeutic agent and avoiding toxic systemic effects. A safe and effective method to target delivery of genes to the specific disease site in the vasculature would greatly benefit treatment of cardiovascular diseases and dysfunctions.

A novel approach to targeting drug and gene administration is the method of ultrasound-enhanced delivery. The vascular endothelium is an attractive target for ultrasound-enhanced delivery because cavitation, often necessary in the mechanism of delivery by ultrasound, can be readily produced in the vasculature, as currently performed for diagnostic imaging (Correas et al. 2001). Moreover, cavitation is expected to have limited effects beyond cells layers directly experiencing cavitation activity, and the endothelium is the first point of contact to cavitation activity (Hwang et al. 2005). A number of researchers are currently studying ultrasound-enhanced gene therapy for cardiovascular disorders to control intimal hyperplasia, restore vascular function, or promote angiogenesis. These studies have shown expression of reporter plasmids as well as plasmids with a therapeutic purpose and delivery of drugs and proteins (Bekeredjian et al. 2005). Clinical potential of this method has been shown by causing protein expression by plasmid DNA (Amabile et al. 2001; Huber et al. 2003; Taniyama et al. 2002; Teupe et al. 2002) or blocking specific proteins by gene blocking siRNA (Miura et al. 2002) and decoy oligonucleotides (Hashiya et al. 2004). A recognized limitation of this method is the low number of cells with drug uptake or gene expression (Bekeredjian et al. 2005). However, few studies have been directed at analyzing the uptake efficiency and imaging the bioeffects, i.e., intracellular uptake and loss of viability, caused by ultrasound-enhanced delivery in viable tissue (Mitragotri 2005). It is important to know

the uptake efficiency at different ultrasound energies in order to design and apply this technique for drug or gene delivery applications.

Shear-Induced Bioeffects

Biological research in industry and academia rely on techniques including electroporation (Gehl 2003), liposomes (Goyal et al. 2005; Simoes et al. 2005), viral vectors (Young et al. 2006), microinjection (Jensen et al. 2003), cell penetrating proteins (Kerkis et al. 2006), and other emerging technologies to deliver small molecules to macromolecules intracellularly for *in vitro* studies. These studies aim to deliver molecules such as genetic material to alter protein expression, macromolecules to alter cellular processes, or labeling probes to stain cell organelles or structures. Establishing a means to uniformly cause poration in cells by a simple and effective means, would have many applications in *in vitro* procedures.

Cellular membrane poration by mechanical forces has been studied using a variety of techniques to bypass the barrier imposed by the membrane for intracellular delivery and to understand the cellular response to mechanical injury. Membrane tension is believed to be the central event by which these mechanical means cause poration or wounds in the lipid bilayer cell membrane (Lokhandwalla and Sturtevant 2001).

The first studies on pore formation by membrane tension were performed using osmotic swelling or micropipetting techniques on red blood cells. These studies found that membrane poration and subsequently cell lysis in red blood cells, which lack the ability to repair actively, occur at the critical areal strain of 2-3% and the critical tension of 10 mN/m^3 (Evans et al. 1976). Beyond directly inducing membrane tension, many techniques have used shear stress to generate membrane tension and cause poration. It is

theorized by Lokhandwalla et al. (Lokhandwalla and Sturtevant 2001) that shear stress from shock waves or cavitation cause cell deformation due to extensional flow, causing tension and poration of the cell membrane. The techniques to induce shear forces upon the cell include fluid flow in viscometers or syringes (Clarke and McNeil 1992), cell scraping (McNeil et al. 1984), shock waves by lasers (Doukas and Kollias 2004; Kodama et al. 2002; Mulholland et al. 1999) or ultrasound (Lokhandwalla and Sturtevant 2001), and cavitation activity induced by lasers or ultrasound (Miller et al. 1996; Ohl and Wolfrum 2003; Rau et al. 2004). Furthermore, it is suspected that cell shear is a critical event in injury (i.e., tramatic brain injury) leading to cell death or dysfunction (Prado et al. 2005). From these studies, it is clear that shear stress is a powerful mediator of cell poration and may be developed to cause intracellular uptake for medical or laboratory applications.

CHAPTER 3

MATERIAL AND METHODS

Measurement and Correlation of Acoustic Cavitation with Cellular Bioeffects

Cell sample preparation

Cell culture and preparation was performed as described by Guzman et al. (2001). In brief, human prostate cancer cells (DU145, American Type Culture Collection, Manassas, VA, USA, item no. HTB-81) were cultured as monolayers in a humidified atmosphere of 95% air and 5% CO_2 at 37^{o}C in RMPI-1640 medium, supplemented with 100 μg/ml penicillin-streptomycin (Cellgro, Mediatech, Herndon, VA, USA) and 10% (v/v) heat inactivated fetal bovine serum (Atlanta Biologicals, Atlanta, GA, USA). Human aortic smooth muscle cells (AoSMC, Cambrex, East Rutherford, NJ, USA, catalog no. CC-2572, lot no. 2FO653) were initiated from a cryopreserved stock and harvested at passage seven prior to each experiment. They were cultured as monolayers in a humidified atmosphere of 95% air and 5% CO_2 at 37^{o}C in MCDB-131 medium, supplemented with 100 μg/ml penicillin-streptomycin and 10% (v/v) heat inactivated fetal bovine serum. Both cell types were harvested by trypsin/EDTA (Cellgro) digestion, washed and resuspended in pure RPMI for DU145 cells and pure MCDB-131 for AoSMC.

Prior to ultrasound exposure, samples were prepared at a cell concentration of 10^6 cells/ml, a calcein concentration of 10 μM and Optison® concentrations of 0.25% v/v (~ 1.6 x 10^6 bubble/ml), 1.7% v/v (~ 1.1 x 10^7 bubble/ml) and 14.3% v/v (~ 9.3 x 10^7 bubble/ml). Calcein (623 Da, radius = 0.6 nm; Molecular Probes, Eugene, OR, USA,

catalog no. C481), a green fluorescent molecule that cannot cross intact cell membranes, was used to quantify molecular uptake into viable cells. Optison® (Mallinckrodt, St. Louis, MO, USA. catalog no. 2707-03) is a suspension of perfluorcarbon gas bubbles stabilized with denatured human albumin that was used to serve as nuclei to promote cavitation activity.

Ultrasound apparatus

Ultrasound was produced using an immersible, focused, piezoceramic transducer (Sonic Concepts, Woodinville, WA, USA, model no. H-101), supplied with two different matching resistance networks allowing production of sound at 1.1 MHz (vicinity of fundamental node) and 3.1 MHz (vicinity of third harmonic). The transducer had a diameter of 70 mm, a 52 mm focal length and a 1.5 mm focal width at half-amplitude (-6 dB).

A sinusoidal waveform was produced by two programmable waveform generators (Standford Research Instruments, Sunnyvale, CA, USA, model no. DS345 and Agilent, Austin, TX, USA, model no. 33120A) used in conjunction to control pulse length, frequency and peak-to-peak voltage. The sinusoidal waveform was then amplified by a RF broadband power amplifier (Electronic Navigation Industries, Rochester, NY, USA, model no. 3100LA) before passing through a matching network and then, finally, controlling the response of the transducer.

The transducer was housed in a polycarbonate tank (30.5 x 29 x 37 cm) containing approximately 26 l of deionized, distilled and partially degassed water at room temperature, 22-23 ^{o}C. A 5-cm thick acoustic absorber (SC-501 Acoustic Rubber, Sonic Concepts) was mounted opposite the transducer to minimize standing-wave formation. A

three-axis positioning system (10 μm resolution, Velmex, Bloomfield, NY, USA) was mounted on top of the tank to position samples and a hydrophone at desired locations in the tank. A PVDF membrane hydrophone (NTR Systems, Seattle, WA, USA, model no. MHA200A) was used to measure spatial-peak-temporal-peak negative pressure in order to map and calibrate the acoustic field produced by the transducer versus the peak-to-peak voltage signal provided by the function generator.

Experimental protocol

Prior to every experiment, the desired sample placement in the acoustic field was found using the PVDF membrane hydrophone. This location was approximately 1 cm and 0.5 cm out of the ultrasound's focus towards the transducer for 1.1 and 3.1 MHz, respectively. The acoustic pressure was calibrated versus the peak-to-peak voltage of the signal created by the function generator, using the PVDF membrane hydrophone at the desired location. These out-of-focus locations had a broader acoustic beam than at the focus, approximately 10.4 mm and 2.4 mm wide at half-amplitude (-6 dB) for 1.1 and 3.1 MHz, respectively. This broader acoustic beam was favorable to have a more uniform acoustic exposure across the sample to reduce "dead zones" where cells or microbubbles were not exposed uniformly. In addition to the broad exposure zone, vigorous mixing caused by cavitation during ultrasound exposure further enabled a more uniform exposure of all cells.

Samples were placed within chambers constructed from the bulb of polyethylene transfer pipets (Samaco, San Fernando, CA, USA, cat. no. 293). The bulb was cut from the transfer pipet approximately 3 mm from the top of the bulb. At the other end, the bulb had a small hollow stub that was cut and filled with silicone rubber sealant (Dow

Corning, Midland, MI, USA) to prevent entrapment of the sample solution. The final dimensions of the approximately cylindrical sample chamber were 1.4 cm in height and 0.6 cm in diameter.

A sample solution was slowly aliquoted via a 3-ml syringe (Becton Dickinson, Franklin Lakes, NJ, USA) with a 22-gauge needle (Perkin Elmer, Foster City, CA, USA) into a sample chamber, while making sure completely to fill the chamber, without air bubbles. A metal rod was immediately inserted into the open end of the sample chamber and then attached to the three-axis positioning system, placing the sample in the desired location as determined by the hydrophone. After sample placement, the computer program was initiated to record hydrophone output and the exposure was begun by triggering the function generator with the desired settings. Exposures were performed at a burst length of 1 ms, 1% duty cycle (i.e., 10 pulses per second); pressures of 0.5, 0.8, 1.2, 1.7 and 2 MPa; total exposure times of 3, 10, 30, 100, 300, 1000 and 3000 ms; and frequencies of 1.1 and 3.1 MHz. Total exposure time is the amount of time a sample was exposed to ultrasound, calculated by multiplying the number of bursts times the burst length. After ultrasound exposure, samples were immediately transferred into 1.5 ml microcentrifuge tubes (Eppendorf, Brinkman, Westbury, NY, USA) and allowed to "recover" for 5 min at room temperature. Samples in microcentrifuge tubes were then placed on ice and allowed to incubate until all samples had been exposed (1 – 2 h).

After all samples had been exposed, samples were washed with PBS (Cellgro) and centrifuged (800 x G, 3 min, Eppendorf 5415C, Brinkman, Westbury, NY, USA) three times to remove extracellular calcein in the supernatant. The subsequent cell pellets were resuspended in a final volume of 205 μl of PBS containing 2 μg/ml of propidium

iodide (Molecular Probes, catalog no. P-1304), a viability marker that stains nonviable cells with red fluorescence.

Quantification of bioeffects

Flow cytometry was used to determine molecular uptake, i.e., fraction of cells containing intracellular calcein, and loss of cell viability by detecting the fluorescence intensity from calcein and propidium iodide, respectively, on a cell-by-cell basis. A BD LSR benchtop flow cytometer (BD Biosciences, San Jose, CA, USA) was used to measure the fluorescence of cells with calcein uptake (FITC fluorescence, 530/28 nm bandpass filter) and to distinguish viable from nonviable cells by the red fluorescence of propidium iodide (Per CP fluorescence, 670 nm longpass filter). Typical analyses sampled approximately 10000 cells. The viability of a sonicated sample compared with a "sham" sonicated cell population, was determined by accounting for lysed cells, intact dead cells and viable cells. Viable cells were counted in each sample, normalized based on the fluid volume analyzed by the flow cytometer and then normalized to the viability of a control sample. The analysis time of a sample in the flow cytometer was used as a measure of the sample volume analyzed, since the flow cytometer operated at a constant flow rate. A similar technique was used with fluorescent beads, as described by Guzman et al. (2001).

Broadband noise detection and calculations

A passive cavitation detection system was used to monitor cavitation and consisted of a custom broadband piezopolymer hydrophone (bandwidth of 1 kHz to 13 MHz, Sonic Concepts) with an active diameter of 13 mm. The hydrophone was placed at

an angle of 90º to the direction of sound propagation and approximately 7.5 cm from the sample position to collect only sound scattered from the sample or emitted from cavitation occurring within the sample. The signal from the hydrophone was amplified (Sonic Concepts) and then recorded by a flexible, high-speed, high-resolution digitizer (NI 5911, National Instruments, Austin, TX, USA) and LabVIEW software (National Instruments) operating on a personal computer. The digitizer was synced to the function generator that controlled the duty cycle of the ultrasound so recordings were only collected during the on-time of ultrasound exposure. The data acquisition card was used at a collection frequency of 12.5×10^6 samples per second and 11 bit accuracy. To analyze the acoustic emissions, the recorded data were processed using fast-fourier transform (FFT) analysis in MATLAB (MathWorks, Natlick, MA, USA) to create frequency spectra of the recorded sound. Each burst of 1 ms yielded 12500 discrete points that were analyzed by FFT analysis, creating one frequency spectrum graph for every millisecond of exposure.

To measure cavitation, a value based on the broadband noise was calculated and termed the cavitation dose. A representative value of the broadband noise for each burst of ultrasound was determined by averaging the signal magnitude from 2.3-2.5 MHz on the frequency spectrum graphs. Average broadband noise measurements were graphed over the total number of bursts (exposure time) of each sample and characteristic features of the cavitation activity, including peak broadband noise, exposure time at peak broadband noise and half-life of broadband noise, were measured. The cavitation dose was calculated by summing the broadband noise on each frequency spectrum graph until the broadband noise decayed to a constant value. At this point, the cavitation activity

was considered to be insignificant and the broadband noise magnitude at this level was subtracted from all spectra as background. In samples where the broadband noise did not decrease to a constant level, i.e., samples with short exposure times, the broadband noise level of samples without Optison® exposed at the same pressure was subtracted as the background.

Statistical Analysis

For conditions at 1.7% v/v Optison® at 1.1 and 3.1 MHz, a minimum of three replicates were performed for all acoustic conditions (i.e., pressure and exposure time). Replicates enabled calculation of means, standard deviations and standard errors of the mean for all conditions. Analysis of variance (ANOVA, α=0.05) was utilized to compare all parameters to determine their statistical significance in affecting molecular uptake and loss of viability. To test the robustness of the correlation of bioeffects with broadband noise, a broader range of experimental conditions were tested without any replicates, including samples at 0.25% v/v and 14.3% v/ v Optison®. The experimental and acoustic conditions are summarized in Table 3.1. The strength of the correlation of bioeffects with broadband noise was determined by fitting the data to exponential equations and comparing R^2, as described in the Results, Chapter 4.

Table 3.1: Replicates performed for the experimental and acoustic condition tested, resulting in 350 data points of bioeffects.

			Experimental Conditions			
			Cell Type	DU145	DU145	DU145	AoSMC
			Optison Concentration	0.25 vol%	1.7 vol%	14.3 vol%	1.7 vol%
Acoustic conditions			**Calcein Concentraion**	10 μM	10 μM	10 μM	10 μM
Frequency	**Pressure**	**Exposure Time**					
1.1 MHz	0.5, 0.8, 1.2, 1.7, 2.0 MPa	3, 10, 30, 100, 300, 1000, 3000 ms		**n=1**	**n=3**	**n=1**	**n=1**
3.1 MHz	0.5, 0.8, 1.2, 1.7, 2.0 MPa	3, 10, 30, 100, 300, 1000, 3000 ms			**n=3**		**n=1**

Ultrasonically Targeted Delivery into Vascular Cells in *Ex Vivo* Arteries

Porcine carotid artery isolation and preparation

Porcine carotid arteries were chosen for this study because they can be delicately excised without tissue damage, preserving an intact and viable endothelium. Furthermore, carotid arteries are relatively straight vessels without much branching, simplifying handling and imaging of the artery. Porcine carotid arteries were harvested from freshly killed female swine at a local abattoir (Holifield Farms, Convington, GA). Excised arteries were immediately rinsed with sterile phosphate-buffered saline (PBS, MediaTech, Herndon, VA) and placed in 15-ml conical tubes filled with Dulbecco's Modified Eagle Medium (DMEM, MediaTech) supplemented with 100 μg/ml penicillin-streptomycin (MediaTech) and 10% (v/v) heat-inactivated fetal bovine serum (Atlanta Biologicals, Atlanta, GA). Arteries were then placed on ice for approximately 1 h during transport to the laboratory. Upon return to the laboratory, arteries were placed in fresh DMEM with 15 μM sodium nitroprusside (Sigma, St. Louis, MO) and incubated at 37^{o}C for approximately 30 min while the ultrasound apparatus was prepared. Sodium nitroprusside, a nitric oxide donor, was added to the media to relax the arteries, improving the *en face* images of the artery (as described below). By testing additional samples without sodium nitroprusside incubation, we showed that sodium nitroprusside did not significantly affect the bioeffects observed after ultrasound exposure (data not shown). Arteries were then cleaned of adventitial adipose and connective tissue while submerged in DMEM.

Flat artery experiments

To prepare flat arteries for simplified exposure and analysis, the ends of the intact arteries were first discarded where the artery was handled with forceps, which likely caused tissue damage. Arteries were then cut cross-sectionally into 1-cm length segments and cut lengthwise to expose the endothelial surface. To approximate physiologic tension, artery segments were stretched to ~150% of their resting length (Chesler et al. 1998), sutured to acoutically transparent TPX® plastic disks (25 mm dia., Ajedium Film, Newark, DE) with the endothelium exposed (Figure 3.1), submerged in DMEM, and incubated at 37°C. In select experiments, the artery endothelium was removed by rubbing the endothelial surface with a plastic cell scraper denuding the artery completely, as verified by microscopy.

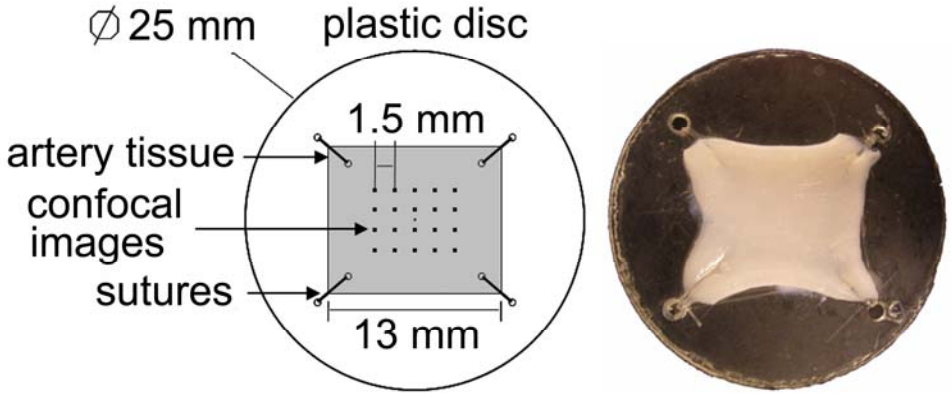

Figure 3.1: Artery segments were sutured to TPX® plastic disks exposing the endothelium for flat artery experiments. Confocal images for quantification of bioeffects were captured in a 5 x 4 array, where each image was spaced by 1.5 mm.

Intact artery experiments

To better mimic the *in vivo* geometry and environment, intact arteries were cut into 2.5-cm length segments and cannulated on each end in custom-built chambers for ultrasound exposure. Chambers were rectangular-shaped boxes constructed of acrylic plastic with metal cannulas on each end to suspend the artery lengthwise and acoustically transparent windows constructed of Mylar® (DuPont, Wilmington, DE) plastic to allow ultrasound exposure with minimal attenuation. Physiologic stretch and pressure were obtained by stretching the artery by ~150% and pressurizing the artery with DMEM or blood to 100 mmHg. The volume outside the artery was filled with DMEM, and then the chamber was incubated at 37°C.

Ultrasound apparatus

Ultrasound was produced using an immersible, focused, piezoceramic transducer (Sonic Concepts, Woodinville, WA, model no. H-101) at 1.1 MHz. The transducer had a 70-mm diameter, 52-mm focal length, and 1.5-mm focal width at half amplitude (-6 dB). Megahertz ultrasound was used in this study because frequencies in the vicinity of 1.1 MHz have been well established in our lab and many others to nucleate microbubbles and cause intracellular uptake of drugs and genes (Mitragotri 2005). Megahertz ultrasound is widely studied because it can be highly focused and is considered safer than lower frequencies, since it is less likely to spontaneously produce cavitation. Megahertz ultrasound therefore requires microbubbles to nucleate cavitation and thereby adds another element of control by allowing one to also regulate cavitation by the microbubbles added to the system.

A sinusoidal waveform was produced by two function generators (Standford Research Instruments, Sunnyvale, CA, model no. DS345 and Agilent, Austin, TX, model no. 33120A) used in conjunction to control pulse length, frequency and peak-to-peak voltage. The sinusoidal waveform was amplified by a RF broadband power amplifier (Electronic Navigation Industries, Rochester, NY, model no. 3100LA) before passing through a matching resistance network and controlling the response of the transducer.

The transducer was housed in a polycarbonate tank (30.5 x 29 x 37 cm) containing approximately 26 L of deionized and distilled water at 37^{o}C. A 5-cm thick acoustic absorber (SC-501 Acoustic Rubber, Sonic Concepts) was mounted opposite the transducer to minimize standing wave formation. A three-axis positioning system (10 μm resolution, Velmex, Bloomfield, NY) was mounted on top of the tank to position samples and a hydrophone at desired locations in the tank. A PVDF membrane hydrophone (NTR Systems, Seattle, WA, model no. MHA200A) was used to measure spatial-peak-temporal-peak negative pressure in order to map and calibrate the acoustic field produced by the transducer.

Experimental protocol

Prior to every experiment, the desired sample placement in the acoustic field was found using a needle hydrophone (NTR Systems, model no. TNU001A). This location was approximately 1 cm out of the ultrasound's focus towards the transducer.

Prior to ultrasound exposure, a solution for each sample was prepared with DMEM, 4 μM TO-PRO®-1 (Invitrogen, Molecular Probes, Eugene, OR), and 1.7% v/v (~ 1.1 x 10^7 bubble/ml) Optison® (Mallinckrodt, St. Louis, MO). TO-PRO®-1, a green fluorescent nucleic acid stain that is impermeable to intact cell membranes, was used as a

model drug and to quantify intracellular uptake into viable cells. TO-PRO®-1 emits little fluorescence until it binds to nucleic acids inside cells, which facilitates analysis by confocal microscopy by almost eliminating background noise from extracellular TO-PRO®-1. In select intact artery experiments, whole porcine blood, collected from the abattoir, with 5 USP units/ml of heparin (Baxter, Deerfield, IL) was used in place of DMEM to further imitate physiologic conditions.

Optison® is a suspension of perfluorcarbon gas bubbles stabilized with denatured human albumin that is a FDA-approved ultrasound imaging contrast agent but was used in this study to nucleate cavitation activity (Kamaev et al. 2004). Optison® bubbles of mean diameter 3-5 μm are expected to have a resonant frequency of ~2 MHz and a peak negative pressure threshold for inertial cavitation of ~0.4 MPa at 1.1 MHz (Leighton 1994). Optison is considered unstable when exposed to air and can be difficult to keep in a homogenous suspension due to buoyancy of the bubbles. Therefore, Optison was only added immediately before ultrasound exposure. During long ultrasound exposure, intense mixing caused by cavitation activity was expected to keep the solution homogenous. It is envisioned that microbubbles of the relatively high concentrations used in this study could be obtained in the body by local catheter release of microbubbles (Amabile et al. 2001) or by targeted microbubbles (Klibanov 2006).

Flat arteries were placed in cylindrical sample chambers that had the ends sealed with acoustically transparent TPX® plastic. Immediately before ultrasound exposure, sample chambers containing flat arteries were filled with a sample solution of media, model drug, and Optison®. Intact arteries were filled with the sample solution to physiologic pressure (~100 mmHg). Sample chambers were then placed in the desired

location in the ultrasound apparatus using the three-axis positioning system to orient the flat artery surface and the intact artery segment perpendicular to the acoustic beam.

Ultrasound was applied to each sample at 1.1 MHz and acoustic energies of 5.0 (0.7 MPa – 300 ms), 66 (1.4 MPa – 1000 ms), or 630 J/cm^2 (2.5 MPa – 3000 ms), referred to as low, intermediate, and high ultrasound energy, respectively. To avoid heating, ultrasound was applied in 1-ms bursts followed by 99 ms of off time, a 1% duty cycle. Inertial cavitation production during ultrasound exposure was verified using a passive cavitation detection system (i.e., monitoring broadband noise). Cavitation detection further showed that cavitation activity was sustained for many bursts equivalent to several hundreds of milliseconds of ultrasound exposure. After ultrasound exposure, samples were immediately incubated at 37^{o}C for 15 min to allow arteries to "recover". Arteries were then rinsed with DMEM and incubated at 37^{o}C for < 20 min until all samples had been exposed.

After ultrasound exposure, intact arteries were removed from their chambers, cut open lengthwise and sutured to rectangular TPX® plactic slides exposing the endothelium. Artery segments were then placed in DMEM with 0.07 mg/ml Hoechst 33342 (Invitrogen) and 7 μg/ml propidium iodide (Invitrogen) for 30 min in the incubator. Hoechst 33342 stains the nuclei of all cells with blue fluorescence, while propidium iodide only stains the nuclei of non-viable cells with red fluorescence.

Microscopy

Artery segments were observed using a Zeiss LSM 510 confocal laser-scanning microscope or Zeiss LSM META/NLO 510 multiphoton microscope (Zeiss, Thornwood, NY). Images of the endothelium and media were captured by directing a 40X

magnification oil objective or a 10X magnification objective at the endothelial surface of the artery. To grasp the extent and pattern of the bioeffects, a larger area of the endothelium was captured by taking four overlapping confocal images at 10X magnification and arranging them as a montage.

Quantification and statistical analysis

Quantification of endothelial bioeffects was objectively determined by capturing 20 images at specific locations relative to suturing holes that affixed the artery to the plastic disk. Twenty images of the artery endothelium were captured in a 5 by 4 array at 40X magnification for each sample of the flat artery experiments (Figure 3.1). Images were then processed in Image-Pro® Plus (Media Cybernetics, Silver Spring, MD) to count all ECs (blue florescence), non-viable cells (red fluorescence), and viable cells with model drug uptake (green fluorescence). Typical control samples would contain at least 4,000 ECs. The number of cells for each population was averaged for each energy and normalized to the control sample.

Statistical analysis was performed by use of Paired Student's t-Tests and analysis of variance (ANOVA) on quantified bioeffects from flat artery experiments. Values of $P < 0.05$ were considered statistically significant.

Shear-Induced Loading of Cells with Macromolecules by Controlled Microfluidics

Cell culture

Cell culture was performed as described by Guzman et al. (2001). In brief, human prostate cancer cells (DU145, American Type Culture Collection, Manassas, VA, item no. HTB-81) were cultured as monolayers in a humidified atmosphere of 95% air and 5% CO_2 at 37^{o}C in RMPI-1640 media (Cellgro, Mediatech, Herndon, VA), supplemented with 100 μg/ml penicillin-streptomycin (Cellgro) and 10% (v/v) heat-inactivated fetal bovine serum (Atlanta Biologicals, Atlanta, GA). DU145 cells were harvested by trypsin/EDTA (Cellgro) digestion, washed, and resuspended in culture media.

Cone-and-plate shearing device

DU145 cells were subjected to a high-magnitude, short-duration pulse of fluid shear stress using a custom-built, cell-shearing injury device (CSID) capable of delivering high magnitudes of shear stress, at rapid rates, to cell cultures (Prado et al. 2005). The CSID consisted of a servo motor-driven cone (0.5^{o}) that rotates above the cell culture surface at controlled speeds and rates of acceleration. Hank's Balanced Salt Solution (HBSS) (Sigma, St. Louis, MO) was placed between the cone and cell plate to serve as shearing buffer, transferring momentum from the rotating cone to the plate of seeded cells and producing a uniform shear stress across the culture plate.

Prior to shear exposure, cells were counted and seeded (density = 1.00 – 1.25 x 10^5 cells / cm^2) onto customized culture plates. Culture plates consisted of glass plates that were briefly flamed and subsequently coated with a poly-L-lysine solution (0.0023%

w/v; Sigma) for at least 12 h at 37 ^{o}C, 95% relative humidity before cell seeding. Cells were cultured as monolayers with culture media and in an incubator, as described above.

Shear stress experiments were conducted by removing culture plates from the incubator and rinsing them with HBSS. Cells were then incubated at 37 ^{o}C in the buffer containing calcein (0.34 mM, Molecular Probes, Eugene, OR) for 10 min and mounted in the CSID. The cone of the CSID was lowered until its apex contacted the center of cell plate, and then shearing buffer (HBSS) was added through a perfusion port in order to fill the gap between the cone and the plate. The applied shear stress magnitude and duration were 140 dynes/cm^2 and 300 ms, respectively. The rise time, which is defined to be the length of time for the cone to reach maximum velocity, was 20 ms. Cells were immediately removed from the CSID and analyzed by flow cytometry to determine viability and intracellular uptake of calcein, as described below. Cells exposed to shear were compared to cells in sham samples (i.e., cells treated exactly the same but not exposed to shear).

Microchannel fabrication

Sheets of polyethylene terephthalate (Mylar®, Dupont, Wilmington, DE) were used to make microchannels because this material is inexpensive, available in many different thicknesses, and easily cut using established laser-cutting techniques. Mylar® sheets measuring 100 μm and 250 μm in thickness were first cut into 15-mm diameter disks using a CO_2 laser (LS500XL, Gravograph-New Hermes, Duluth, GA). The CO_2 laser was operated with 30% power and 10% speed in the circular pattern until the laser cut completely through the sheet. Microchannels were created in each disk as a single

cylindrical channel, a single conical channel, or an array of conical channels by drilling near the center with an ultraviolet excimer laser (Resonetics Micromaster, Nashau, NH).

As shown in Figure 3.2 A, the relatively flat energy profile of the excimer laser allowed nearly cylindrical microchannels to be created in the Mylar®sheets with only a slight taper: typically a 10 μm difference between the inlet and outlet diameter over 100 μm of channel length (Davis et al. 2005). The laser was operated at 60 Hz with a 248 nm wavelength and energy of 200 mJ per pulse. To create a more uniform cylindrical profile, Mylar® disks were drilled with the excimer laser from both sides, which eliminated most of the taper such that inlet and outlet diameters differed by less than 5 μm over a 100-μm channel length. A wide range of microchannel diameters and lengths could be created using different sized masks for the excimer laser and the many available thicknesses of the Mylar® sheets, respectively.

To create conical channels in the Mylar® disk, the excimer laser was operated in a trepanning mode (Davis et al. 2005), as shown in Figure 3.2 B. During trepanning, the disk was moved in an overlapping circular motion allowing the excimer laser to ablate the Mylar® with greater intensity at the center of the circular path than at the edges, thereby creating a conical profile. Various conical profiles could be created by using different sized masks and controlling the laser energy, speed, and radius.

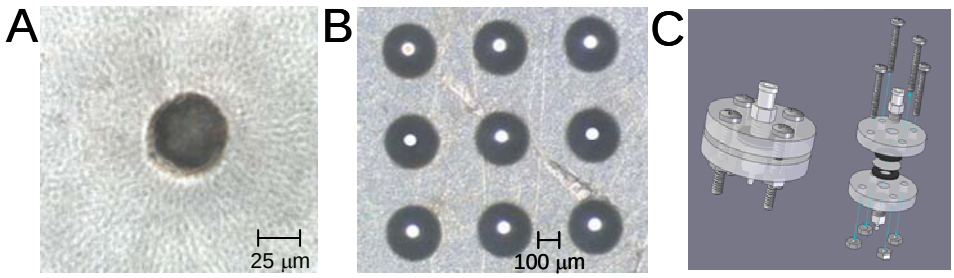

Figure 3.1: Microchannels were drilled in Mylar® sheets to produce (A) cylindrical or (B) conical microchannels as (A) a single channel or (B) as an array of channels. (A) displays a single cylindrical microchannel with a diameter of 50 μm, while (B) displays a 3 x 3 array of conical microchannel with an inlet diameter of 300 μm and an outlet diameter of 50 μm. (C) A device was created to secure microchannel disks in place with a water-tight seal to ensure flow through microchannels and to couple a syringe and tubing for dispensing and collecting of cell solution, respectively.

Microchannel device

To flow cell suspensions through the microchannels, a device was created to securely hold the Mylar® disk in place and allow coupling to tubing and a syringe (Figure 1C). To secure the Mylar® disks, two flanges constructed of 1/4-in. thick polymethylmethacrylate (acrylic, McMaster-Carr, Atlanta, GA) were used. Each acrylic flanges had a hole drilled in the center to allow fluid flow and four holes near the edge of the flange for securing screws. To prevent leakage within the flange, gaskets were cut from rubber gasket sheets (SBR rubber, 1/16-in thick, McMaster-Carr, Atlanta, GA) with an outer diameter of 15 mm and a hole was removed from the center with a diameter of 3 mm. Two gaskets were centered on each side of the Mylar® disk and held securely in place using the acrylic flanges and screws. To couple tubing and a syringe to the flange, a nozzle tip connection for 1/8-in. tubing was screwed into the outlet of the flange and a male luer fitting screwed into the inlet of the flange.

Experimental protocol of microchannel exposure

Prior to fluid flow through microchannels, samples were prepared at a cell concentration of 5 x 10^5 cells/ml. To test the ability of this device to cause intracellular uptake, one of several different cell-impermeant, green-fluorescent molecules of different sizes was added to the cell sample: calcein (10 μM, 623 Da, Molecular Probes), FITC-labeled dextrans (150, 500, and 2000 kDa, Sigma, St. Louis, MO), and FITC- labeled BSA (66 kDa, Sigma).

A 2-ml sample solution was aliquoted into a 3-ml syringe (Becton Dickinson, Franklin Lakes, NJ) and any entrapped air was removed from the syringe. The male luer connection on the microchannel device was then filled with additional cell solution, which displaced any air in the fitting upstream from the microchannel, and was connected to the syringe. To accurately flow the sample through the microchannel and thereby expose cells to a controlled shear, a syringe pump (Genie, Kent Scientific Corp, Torrington, CT) was used to set the flow rate at 30, 70, or 100 ml/h. Approximately 0.5 ml of sample was allowed to flow through the microchannel before any sample was collected, and then at least 1.0 ml of sample solution was collected in a 1.5 ml microcentrifuge tube (Eppendorf, Brinkman, Westbury, NY). Cells were allowed to "recover" for 5 min at room temperature, and then microcentrifuge tubes were incubated on ice until all samples had been exposed (< 2 h).

After all samples had been exposed, 1.0 ml of sample solution was pipetted from each collected sample and dispensed into a new microcentrifuge tube for analysis. Cells were then centrifuged (800 x g, 3 min, Eppendorf 5415C, Brinkman, Westbury, NY) and washed with PBS (Cellgro) three times to remove extracellular fluorescent molecules in

the supernatant. The subsequent cell pellets were resuspended in a final volume of 205 μl of PBS containing 2 μg/ml of propidium iodide (Molecular Probes), which is a viability marker that stains non-viable cells with red fluorescence.

Quantification of bioeffects

Flow cytometry was used to determine molecular uptake, i.e., fraction of cells containing intracellular fluorescent molecules, and loss of cell viability by detecting the fluorescence intensity from uptake molecules and propidium iodide, respectively, on a cell-by-cell basis. A BD LSR benchtop flow cytometer (BD Biosciences, San Jose, CA) was used to measure the green fluorescence of cells with intracellular uptake (FITC fluorescence, 530/28 nm bandpass filter) and to distinguish viable from non-viable cells by the red fluorescence of propidium iodide (Per CP fluorescence, 670 nm longpass filter). Typical analyses each included approximately 30,000 cells per sample. Since the flow cytometer could not count fragmented cells, the rate of viable cells counted in each sample was normalized to the rate of all cells counted in a non-exposed sample. Since the flow cytometer operated a constant flow rate, this method accounted for both intact and fragmented non-viable cells.

Statistical analysis

A minimum of three replicates was performed for all conditions. Replicates enabled calculations of means and standard errors of the mean (SEM). Analysis of variance (ANOVA, α=0.05) was utilized to compare all parameters to determine their statistical significance in affecting molecular uptake and loss of viability.

CHAPTER 4

MEASUREMENT AND CORRELATION OF ACOUSTIC CAVITATION WITH CELLULAR BIOEFFECTS[1]

Using broadband noise as a measure of cavitation activity, this study determined the kinetics of cavitation during sonication of Optison® contrast agent and tested whether cellular bioeffects can be predicted by cavitation dose. Cell suspensions were exposed to ultrasound at varying acoustic frequency, pressure, exposure time, Optison® concentration and cell type to obtain a broad range of bioeffects, i.e., intracellular uptake and loss of viability, as quantified by flow cytometry. We found that cavitation activity measured by broadband noise increased and peaked within 20 ms and then decayed with a half-life of tens to hundreds of milliseconds. Intracellular uptake and loss of viability correlated well with the cavitation dose determined by the time integral of broadband noise magnitude. These results demonstrate that broadband noise correlates with bioeffects over a broad range of experimental conditions, which suggests a noninvasive feedback method to control ultrasound's bioeffects in real time.

Introduction

Intracellular delivery of drugs, proteins and genes is often critical to the success of biopharmaceutical therapy, but is limited by the transport barrier imposed by the cell membrane (Stein and Lieb 1986). A wide variety of techniques is therefore being studied to drive molecules across the cell membrane and into cells. These include

[1]This work was published in Ultrasound in Medicine Biology: Hallow DM, Mahajan AD, McCutchen TE, Prausnitz MR. Measurement and correlation of acoustic cavitation with cellular bioeffects. Ultrasound in Medicine and Biology 2006; 32 (7): 1111-1122.

physical approaches, such as acoustic cavitation (Mitragotri 2005), shock waves (Doukas and Flotte 1996) and electroporation (Gehl 2003); chemical methods, such as lipid- and polymer-based complexes and particles (Langer 1998); and biological means, such as viral vectors (Gardlik et al. 2005) and receptor targeting (Vyas et al. 2001). Ultrasound-enhanced delivery, a physical method temporarily to permeabilize cells using cavitation, has received growing attention over the past decade, because of its potential to noninvasively deliver drugs, DNA and other molecules into targeted cells (Ng and Liu 2002; Unger et al. 2001).

Ultrasound has been studied in various experimental systems ranging from cell suspensions to monolayers to tissues, both *in vitro* and *in vivo*, and with intracellular delivery into a variety of cell types, including mammalian and plant cells (Bekeredjian et al. 2005; Liu et al. 2005; Mitragotri 2005). Cells have been studied using a range of different compounds ranging from small fluorescent molecules to macromolecules, such as proteins and DNA (Miller et al. 2002), to nanoparticles (Mehier-Humbert et al. 2005). Furthermore, a wide range of ultrasound parameters has been tested by varying acoustic frequency, pressure, energy, exposure time and duty cycle.

In general, experimental systems and acoustic conditions have been designed to produce cavitation, which is believed to be responsible for bioeffects (Miller et al. 1996). The mechanism is thought to involve localized shear forces from microstreaming and bubble collapse that disrupt cell membrane microstructure enough to allow transport of molecules into the cell (Lokhandwalla and Sturtevant 2001) but not so much to injure the cell beyond repair (McNeil and Steinhardt 2003; Schlicher et al. 2006).

To advance ultrasound-enhanced delivery for medical and biological applications, additional research is needed to control ultrasound's bioeffects reliably in various *in vitro* and *in vivo* environments. Bioeffects can be difficult to control and reproduce, even in simplified *in vitro* systems, because cavitation activity is typically a complex milieu of stochastic bubble oscillations and collapses (Apfel 1997). Different acoustic parameters, such as pressure, frequency and exposure time, and experimental conditions, such as nucleation bubble concentration and viscosity, can result in vastly different amounts and intensities of cavitation.

To develop methods to predict and to control ultrasound's bioeffects reproducibly, some research has focused on correlating acoustic and experimental input parameters with the bioeffects (Guzman et al. 2001). For example, acoustic energy exposure has been shown to correlate with bioeffects over a range of pressures and exposure times, but fails when acoustic frequency or nucleation bubble concentration are changed (Guzman et al. 2003; Sundaram et al. 2003). This failure may be explained by considering the mechanism of ultrasound's effects. Cavitation activity is believed to be directly responsible for bioeffects, whereas ultrasound, which is used to produce cavitation, is only indirectly associated with bioeffects. We therefore expect that measurements of output parameters produced by cavitation should correlate with bioeffects better than the input parameters of ultrasound used to generate cavitation.

Guided by this rationale, this study is designed to test the hypothesis that measurement of broadband noise produced by inertial cavitation correlates broadly with bioeffects. This hypothesis is supported by previous studies that correlated bioeffects with measurements of inertial cavitation, such as sonoluminescence (Cochran and

Prausnitz 2001), free radical formation (Kondo et al. 1993) and frequency spectrum analysis (Chen et al. 2003; Daniels et al. 1995; Liu et al. 1998; Sundaram et al. 2003). In this study, we measured intracellular uptake of molecules and loss of cell viability over a wide range of acoustic pressure, exposure time, frequency, cell type and contrast agent concentration. We then sought to correlate these bioeffects with measurements of broadband noise, with the goal of identifying a unifying parameter that correlates with bioeffects over the large set of parameters tested. Broadband noise could be measured during sonication to provide real-time feedback about the cavitation and bioeffects produced by ultrasound, which may provide a means actively to control acoustic bioeffects under diverse experimental conditions.

Results

Measurement of cavitation activity nucleated by contrast agent

Because inertial cavitation bubble collapse is believed to be responsible for ultrasound's bioeffects, our first goal was to measure this cavitation activity during sonication. Cavitation was characterized by analyzing acoustic emissions from cell samples exposed to ultrasound. Sound was recorded with a hydrophone and later analyzed by FFT analysis to extract frequency spectra.

Figure 4.1 A and B shows representative frequency spectra collected during sonication of cell suspensions with Optison®. Features of the acoustic spectra consist of a strong signal at the driving frequency (f, 1.1 or 3.1 MHz) as well as characteristic markers of cavitation, such as subharmonics (i.e., f/2), ultraharmonics (i.e., 3/2f, 2f) and high levels of broadband noise. Samples exposed to ultrasound without cells but with

Optison® exhibited similar features and magnitudes in the frequency spectra (data not shown). It is generally accepted that harmonic, subharmonic and ultraharomic signals are produced at the onset of cavitation and typically arise from stable cavitation bubbles oscillating linearly and nonlinearly with the pressure transients of ultrasound (Leighton 1994). These features are superimposed onto a level of broadband noise that results from erratic oscillations and bubble collapse, primarily from inertial cavitation (Neppiras 1980).

We focused on broadband noise measurements as a measure of inertial cavitation (ASA, 2002) based on the expectation that observed bioeffects result from inertial bubble collapse (Miller et al. 1996). By monitoring the broadband noise, we were attempting to measure the energy output in the form of sound from bubble collapses of inertial cavitation (ASA, 2002). Representative broadband noise measurements were obtained from the frequency spectra by averaging the signal magnitude from 2.3 to 2.5 MHz, a sampling region absent of any harmonics at 1.1 or 3.1 MHz (Figure 4.1A and B).

Average broadband noise levels are shown in Figure 4.2 as a function of the exposure time to display the dependence of cavitation activity kinetics on acoustic frequency (Figure 4.2A), acoustic pressure (Figure 4.2B) and Optison® concentration (Figure 4.2C). The measured cavitation was found to be a transient response, increasing to a maximum within 20 ms of ultrasound exposure time and then decreasing to background values over tens to hundreds of milliseconds. In general, the total cavitation activity, as measured by the time integral of broadband noise, generally increased with increasing pressure, decreasing frequency and increasing Optison® concentration.

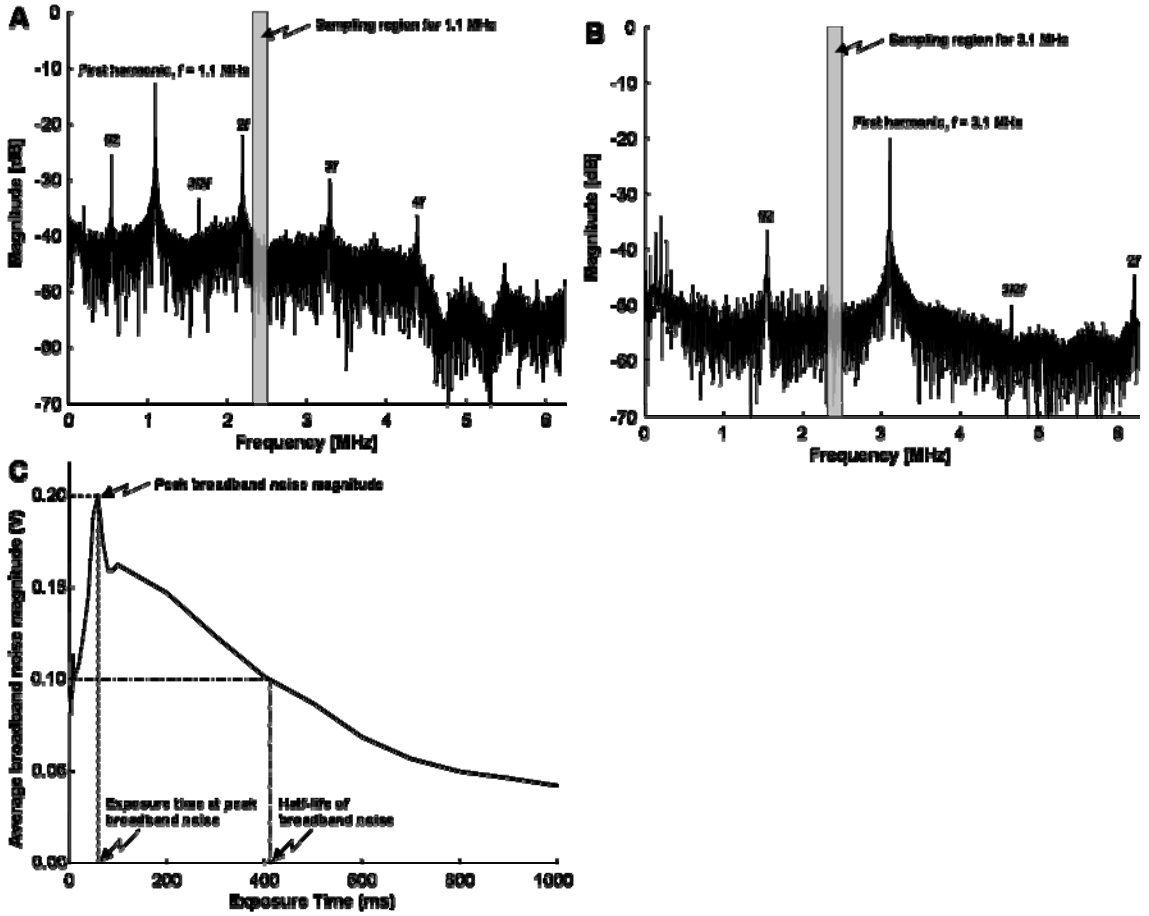

Figure 4.1: Representative frequency spectra derived from acoustic emissions of cell samples exposed to (A) 1.1 MHz and (B) 3.1 MHz ultrasound. Frequency spectra exhibit characteristic markers of cavitation, including subharmonics, ultraharmonics and high levels of broadband noise. The sampling region to measure the average broadband noise was chosen between 2.3 and 2.5 MHz, absent of any harmonic signals. (C) Representative graph displaying characteristic measurements of cavitation activity, including peak broadband noise magnitude, exposure time at peak broadband noise and half-life of broadband noise.

We can further interpret these data by recognizing that broadband noise is generated by both the initial rupture of stabilized gas bubbles added as nucleation sites and the destruction or dissolution of secondary bubbles generated and recycled over time. Strong broadband noise during the first milliseconds is believed to represent the emission

and scattering of sound by the initially large concentration of Optison® bubbles. In most cases, broadband noise increased during the first several bursts, which is believed to be caused by the initial collapse of Optison® bubbles and the resulting increase in secondary bubbles collapsing. This characteristic increase has been previously observed by monitoring cavitation emissions (Chen et al. 2002). The subsequent decrease in broadband noise is believed to indicate the loss of bubbles that are destroyed by inertial collapse or loss of stability, which reduce both sound scatter and emissions. Eventually, broadband noise decreases until it remains relatively constant near background levels, the point where inertial cavitation activity should no longer exist or be significant to induce bioeffects.

The kinetic activity in Figure 4.2 further depends on experimental parameters. Specifically, the peak broadband noise depends strongly on frequency and pressure, and the delay time until peak broadband noise and rate of destruction also strongly depend on Optison® concentration. To investigate these characteristic features further, a quantitative analysis of the data was performed to show characteristic features of cavitation activity as a function of frequency (Figure 4.3A), pressure (Figure 4.3B) and Optison® concentration (Figure 4.3C). These features, shown in the representative graph Figure 4.1C, include peak broadband noise magnitude (interpreted as the point when the largest number of bubbles was collapsing inertially), the corresponding exposure time at peak broadband noise and the half-life of broadband noise, which is a measure of the rate of bubble destruction.

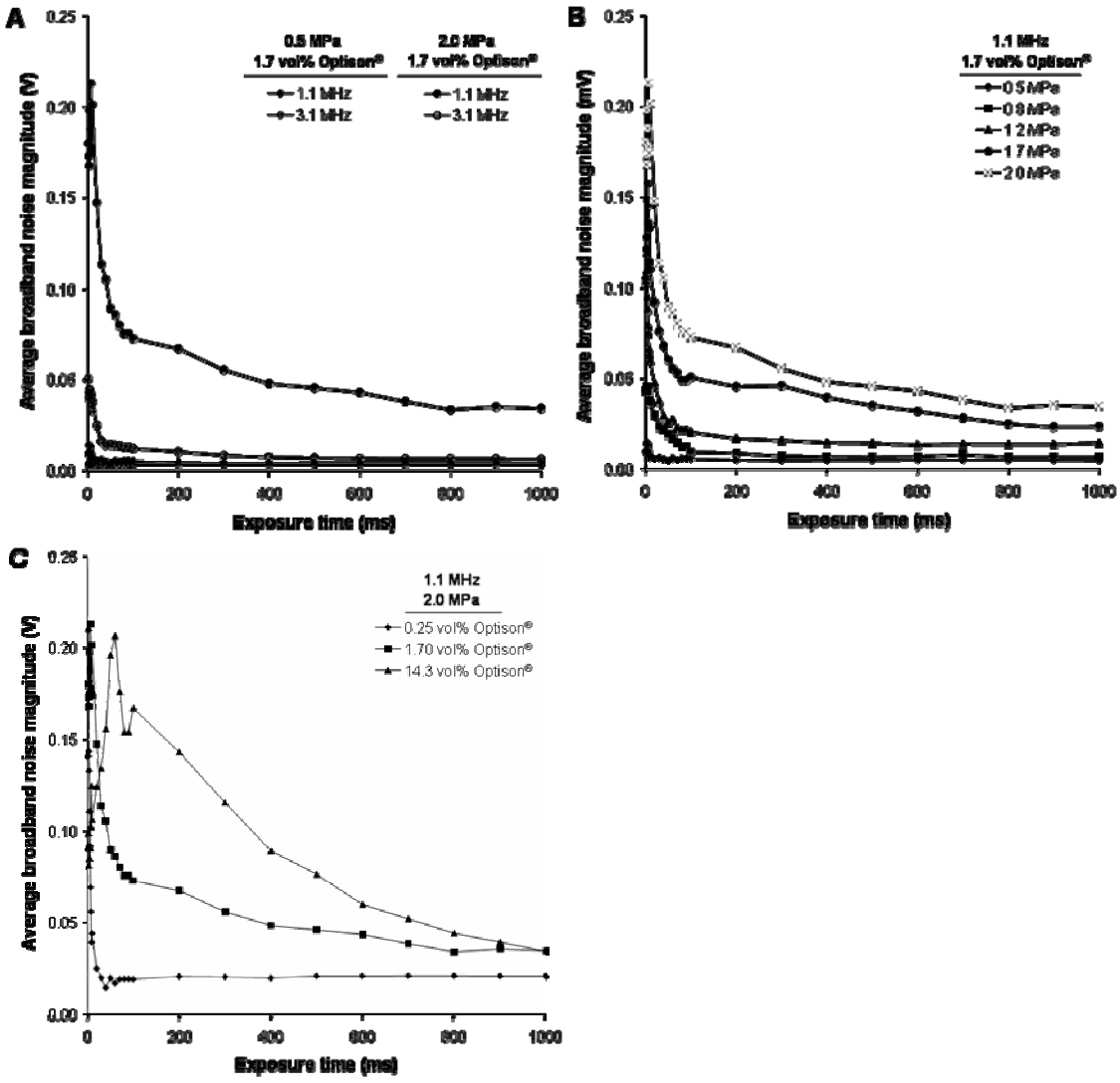

Figure 4.2: Kinetic activity of cavitation measured by broadband noise and dependence on acoustic and experimental parameters. Cavitation activity rapidly achieved a peak value and then decayed over time. (A) Exposure as a function of frequency (1.1 and 3.1 MHz) at two different pressures (0.5 and 2.0 MPa). Higher frequency yielded lower levels of cavitation activity. (B) Exposure as a function of pressure (0.5 – 2.0 MPa). Cavitation activity decreased with decreasing pressure. (C) Exposure as a function of Optison® concentration (0.25 – 14.3 vol%). Increasing Optison® concentration increased amount and duration of cavitation activity. Samples contained suspensions of DU145 prostate cancer cells. Most data represent the averages of n = 3 replicates.

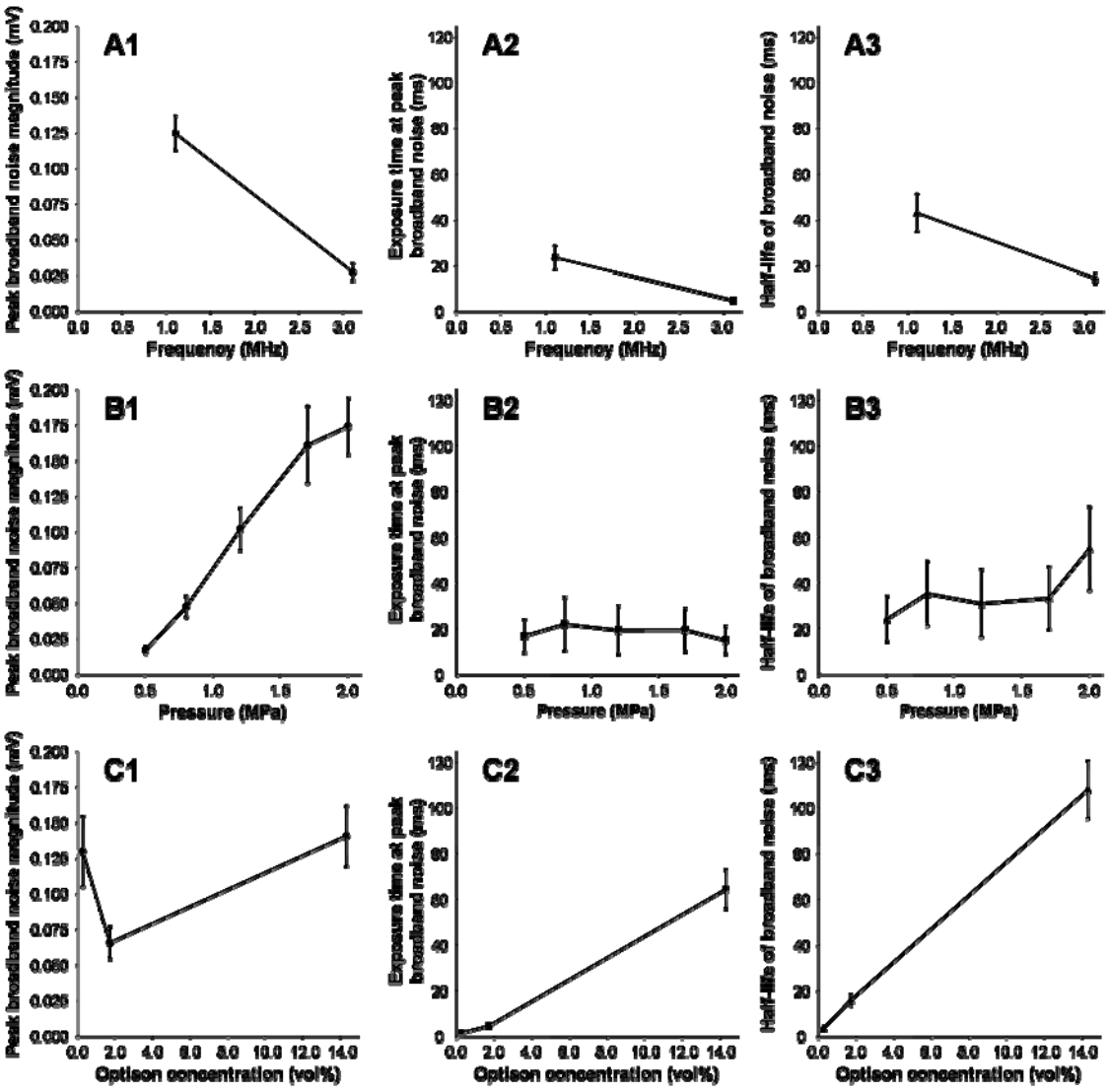

Figure 4.3: Characteristic features of cavitation activity derived from Figure 4.1 showing the effect of (A) Acoustic frequency, (B) Pressure and (C) Optison® concentration on (1) peak broadband noise magnitude, (2) exposure time at peak broadband noise magnitude and (3) half-life of broadband noise. Data represent the averages of n ≥ 12 with SEM error bars.

Considering the effects of ultrasound frequency, Figure 4.3 A shows that increasing frequency decreased peak cavitation activity (Figure 4.3 A1; ANOVA, $P<0.0001$), but did not have a statistically significant effect on the time constants associated with onset and decay of cavitation (Figures 4.3 A2-A3; ANOVA, $P=0.958$ and

P=0.756, respectively). In contrast, elevated pressures, as shown in Figure 4.3B, produced higher peak levels of inertial cavitation (Figure 4.3 B1; ANOVA, P<0.0001) that reached peak levels and decayed with similar time constants (Figures 4.3 B2-B3; ANOVA, P=0.895 and P=0.0566, respectively). In Figure 4.3 C, increasing Optison® concentration did not affect peak cavitation levels with a coherent trend (Figure 4.3C1; ANOVA, P=0.0247), but did increase the delay to onset and decay of cavitation (Figures 4.3C2-C3; ANOVA, P<0.0001 and P<0.0001, respectively).

Dependence of bioeffects on acoustic and experimental parameters

Having established a means to quantify inertial cavitation activity using broadband noise, our next objective was to quantify cellular bioeffects resulting from that cavitation activity. Over the same range of ultrasound exposure conditions assessed in Figures 4.2 and 4.3, we measured intracellular uptake of a fluorescent marker compound (calcein) and measured cell viability.

Figures 4.4 and 4.5 display the wide range of acoustic and experimental conditions tested and the broad range of resulting bioeffects. These bioeffects varied from mild conditions that caused low levels of uptake or almost no cell death, to moderate conditions that caused uptake into as many as one-third of cells and some cell death, to strong conditions that killed almost all cells. In each figure, the total height of each bar represents the percent of cells remaining viable after sonication, which is subdivided into a black bar, representing the percent of viable cells with uptake (the typically desirable population), and a grey bar, representing the percent viable cells without uptake (the apparently unaffected population). All samples were normalized to

the control sample (i.e., "sham" sonication) taken to represent 100% viability and 0% uptake.

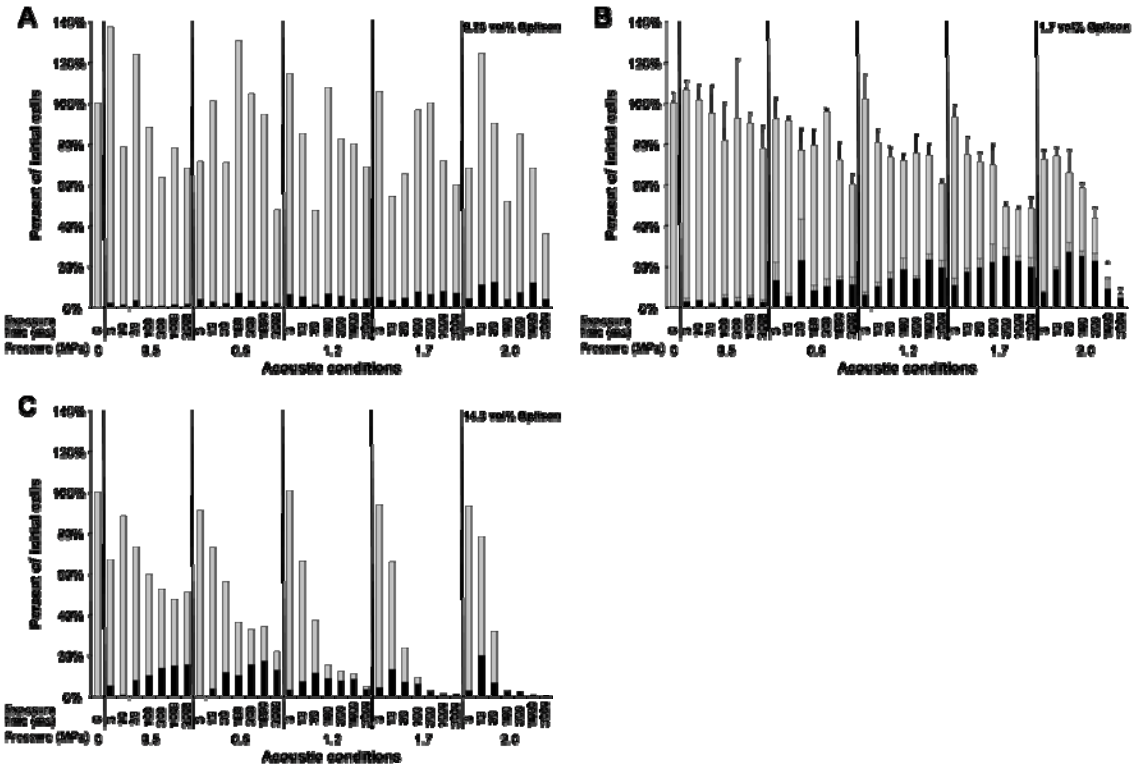

Figure 4.4: Cell viability and intracellular uptake populations following sonication over a range of pressures, exposure times and Optison® concentrations. The total height of each bar represents the fraction of cells remaining viable, the size of the black stripe represents the fraction of cells with significant levels of intracellular uptake and the size of the grey stripe represents the fraction of cells that were apparently unaffected. Ultrasound was applied at 1.1 MHz to samples containing a suspension of DU145 prostate cancer cells and Optison® at concentrations of (A) 0.25 vol%, (B) 1.7 vol% and (C) 14.3 vol%. Data in (B) represent the averages of n = 3 replicates with SEM shown, while data in (A) and (C) represent n = 1.

Figure 4.4 displays the effect of changing the concentration of Optison®, i.e., nucleation sites for cavitation, over a range of pressures and exposure times. The effects of frequency and cell type are shown in Figure 4.5, where two different cell types, aortic smooth muscle cells and prostate cancer cells, were sonicated at two different frequencies, 1.1 and 3.1 MHz, over the same range of pressures and exposure times.

In Figures 4.4 and 4.5, independently increasing pressure or exposure time increased the fraction of cells affected by cavitation activity by increasing both the fraction of cells with uptake and the fraction of cells killed (ANOVA, $P<0.0001$). The interaction of pressure and exposure time also had a statistically synergistic effect (ANOVA, $P<0.0001$). Increasing Optison® concentration (Figure 4.4) and decreasing frequency (Figure 4.5) also increased bioeffects, by increasing uptake and cell death (ANOVA, $P < 0.001$). In general, greater uptake and lesser cell death were seen in DU145 cells than in AoSMC cells (Figure 4.5). These finding are generally consistent with previous work (Guzman et al. 2001). They are also consistent with a cavitation-based mechanism for bioeffects; cavitation activity is known to show the same qualitative dependence on experimental conditions, where increased pressure, exposure time and Optison® concentration, as well as decreased frequency, all increase cavitation activity (Leighton 1994). A quantitative analysis of this relationship follows immediately below.

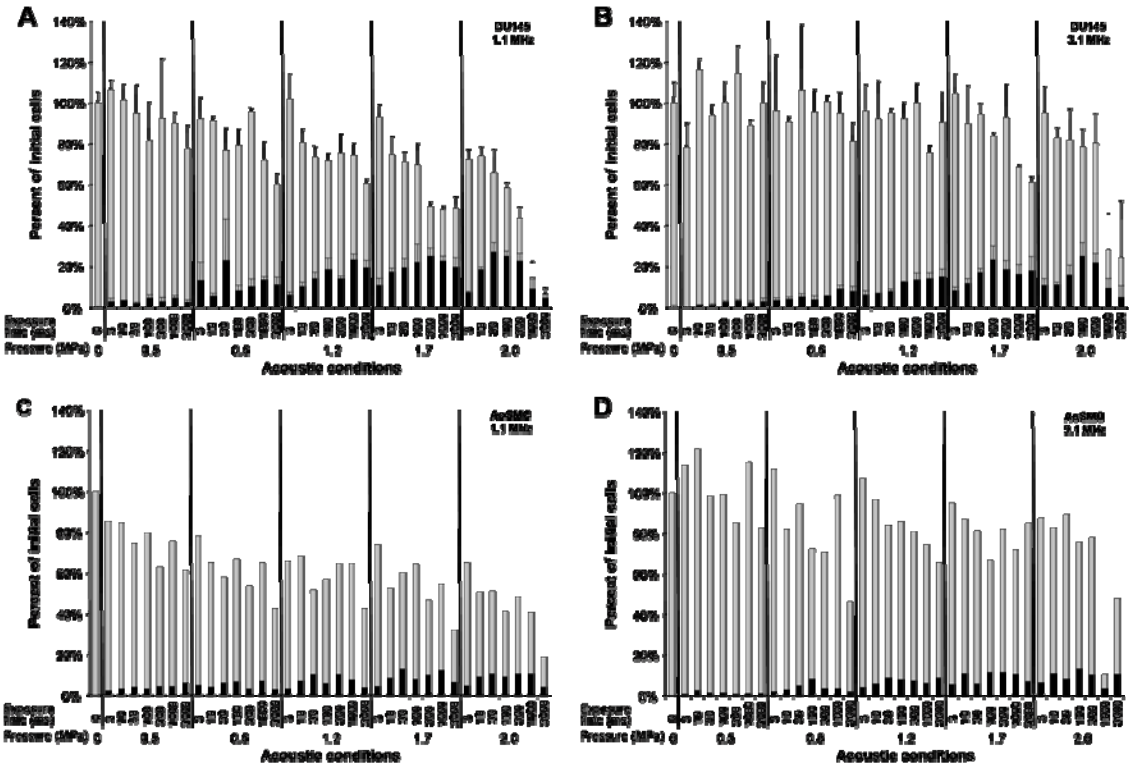

Figure 4.5: Cell viability and intracellular uptake populations following sonication over a range of pressures, exposure times, frequencies and cell types. The total height of each bar represents the fraction of cells remaining viable, the size of the black stripe represents the fraction of cells with significant levels of intracellular uptake and the size of the grey stripe represents the fraction of cells that were apparently unaffected. Ultrasound was applied at (A,C) 1.1 MHz and (B,D) 3.1 MHz to a suspension of (A,B) DU145 prostate cancer cells and (C,D) AoSMC at an Optison® concentration of 1.7 vol%. Data in (A) and (B) represent the averages of n = 3 replicates with SEM shown, while data in (C) and (D) represent n = 1.

Correlation of bioeffects with measurement of cavitation activity

Having collected paired data sets of cavitation activity and bioeffects caused by the same ultrasound exposures, we could now test the hypothesis that broadband noise provides a single measurement that broadly correlates with acoustic bioeffects. This hypothesis is guided by the expectation that measuring an experimental output parameter generated by the cavitation mechanistically responsible for bioeffects should provide

better correlation than experimental input parameters, such as acoustic conditions and Optison® concentration, which are only indirectly related to the mechanistic driving force.

To test this hypothesis, Figures 4.6A–C contain all of the 350 bioeffects data points shown in Figures 4.4 and 4.5 involving different pressures, exposure times, frequencies, Optison® concentrations and cell types plotted versus acoustic energy exposure, i.e., an experimental input parameter. Previous studies have shown that intracellular uptake and cell viability correlate with energy exposure over a broad range of acoustic conditions, since the energy of cavitation is related to the total acoustic energy input (Leighton 1994). However, energy exposure correlated poorly with our data set ($R^2 < 0.1$), probably because the single parameter of energy exposure is not sufficient to account for the effects of ultrasound frequency or Optison® concentration.

Instead of relying on an acoustic input parameter, Figures 4.6D–F show acoustic bioeffects as a function of a cavitation output parameter based on broadband noise measurement. The x-axis represents the integral of broadband noise pressure over time determined from graphs such as those shown in Figure 4.2. Measurements of the "cavitation dose" in this manner has previously been shown to correlate with hemolysis (Chen et al. 2003; Everbach et al. 1997; Liu et al. 1998) and with molecular uptake and viability (Sundaram et al. 2003).

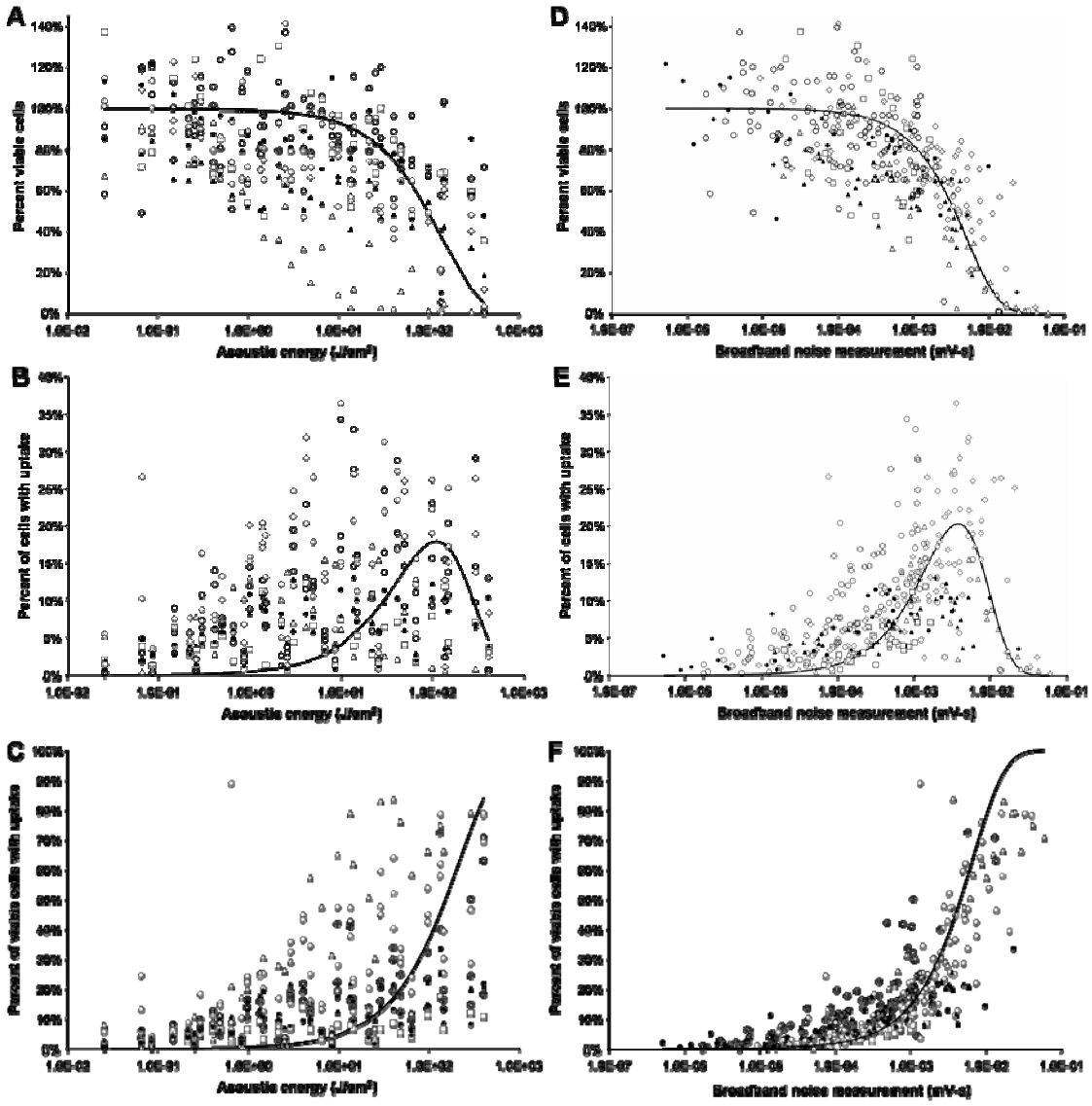

Figure 4.6: Correlation between (A,B,C) Acoustic energy and (D,E,F) Broadband noise measurement with (A,D) Percent viable cells, (B,E) Percent of cells with uptake and (C,F) Percent of viable cells with uptake from data shown in Figures 4.4 and 4.5. These bioeffects correlated poorly with acoustic energy input, but correlated better with cavitation dose based on broadband noise. Generally, increasing cavitation dose decreased viability and increased uptake into viable cells. Data represents experimental conditions of DU145 – 1.1 MHz – 0.25 vol% Optison (open square), DU145 – 1.1 MHz – 1.7 vol% Optison (open diamond), DU145 – 1.1 MHz – 14.3 vol% Optison (open triangle), DU145 – 3.1 MHz – 1.7 vol% Optison (open circle), AosMC – 1.1 MHz – 1.7 vol% Optison (closed triangle), AoSMC – 3.1 MHz – 1.7 vol% Optison (closed circle).

In Figure 4.6D, cell viability correlated with the cavitation dose (R^2 = 0.49), despite some scatter, and generally decreased with increasing cavitation dose above a threshold value. In Figure 4.6E, the percent cells with uptake also generally correlated with the cavitation dose (R^2 = 0.2) and generally increased with increasing cavitation dose, except at very large cavitation doses, where gains in uptake were outweighed by losses in cell viability. Unlike Figure 4.6E, that examines cellular uptake as a function of all cells initially present in the sample, Figure 4.6F considers cellular uptake among only those cells remaining viable after sonication. This uptake population also generally correlated with the cavitation dose (R^2 = 0.23) and increased with increasing cavitation dose. These results demonstrate that, unlike measuring acoustic input parameters that are indirectly associated with the cavitation mechanism, directly monitoring broadband noise signals generated by inertial cavitation activity can be used to correlate with cavitation-dependent bioeffects over a broad range of acoustic and experimental parameters.

To serve as concise mathematical representations of these correlations with cavitation dose, the data in Figures 4.6D–F can be summarized according to the following empirical expressions generated by least-squares regression:

$$V = e^{-203 \cdot BN}, \tag{4.1}$$

$$U = V - e^{-437 \cdot BN}, \tag{4.2}$$

and

$$U/V = (1 - e^{-234 \cdot BN}). \tag{4.3}$$

In these expressions, V is the viability as a percentage of the initial cells present, U is the uptake as a percentage of initial cells present and BN is the broadband noise measurement based on the integral of the average broadband noise over the exposure time. Equations 4.1 and 4.2 were independently fitted to the data shown in Figure 4.6D and Figure 4.6E, respectively. Equation 4.3 is the quotient of Equations 4.1 and 4.2. The form of these equations was suggested by the results of Sundaram et al. (2003), who proposed a "single bubble interaction model" that predicts the uptake and viability based on the distribution of cells within a certain distance from a cavitating bubble. We therefore expected broadband noise, a measure of the number of cavitation events, also to fit the uptake and viability data by these exponential forms.

Discussion

In this study, the kinetic activity of inertial cavitation nucleated by Optison® was quantified by measuring broadband noise emissions produced from bubble oscillation and collapse. Furthermore, the dependence of cavitation activity on a number of different acoustic and experimental parameters was determined by varying the acoustic pressure, exposure time, frequency, Optison® concentration and cell type. However, the most significant result of this work was the correlation between inertial cavitation activity and cellular bioeffects. The inertial cavitation dose, as measured by integrating the average broadband noise over the exposure time, correlated over a broad range of parameters with molecular uptake and loss of viability.

Potential applications

This correlation suggests possible laboratory and clinical applications in ultrasound-enhanced delivery of drugs and genes into cells. As proposed and demonstrated previously, ultrasound can be used to drive drugs, proteins, DNA and other compounds into cells both *in vitro* and *in vivo* (Bekeredjian et al. 2005). However, it is not always clear which ultrasound conditions are optimal, due to the unpredictable nature of stochastic cavitation. Rather than trying to estimate the acoustic conditions that lead to optimal cavitation, directly measuring the cavitation dose using broadband noise could provide a facile means to determine the resulting bioeffects and thereby to operate at optimal ultrasound conditions using a noninvasive, real-time feedback measurement of cavitation activity. For example, cavitation produced by targeted ultrasound in the body could be monitored by noninvasively recording emissions due to inertial bubble collapses and processed to yield a measure of the cavitation dose in real time. This measurement would allow the device or its clinical operator to end ultrasound exposure when the cavitation dose reached a predetermined optimal level to achieve the desired bioeffect.

The bioeffects observed as a function of cavitation dose can be classified into two overall regions: (i) low cavitation doses produce some uptake and retain high viabilities and (ii) high cavitation doses kill many cells, but produce high levels of uptake among those cells remaining viable. Different applications may prefer one of these regions over the other. For example, most drug or gene delivery applications would favor the first region to deliver compounds into cells while retaining high viability. In contrast, applications like chemotherapy, where the goal is to destroy cancerous cells at a tumor

site, might prefer the second region to elicit extensive cell death with large amounts of drug delivery to destroy the remaining viable cells with the chemotherapeutic agent.

This technique passively to detect cavitation by recording acoustic emissions is attractive because it can be used noninvasively, and it also provides a direct measure of inertial cavitation activity. Previous research has shown that correlations of bioeffects exist with sonoluminesnce (Cochran and Prausnitz 2001) and free radical activity (Kondo et al. 1993), which are other measures of inertial cavitation; however, they are less attractive because they would require more invasive and complicated systems to measure inertial cavitation inside the body. Others have shown that input parameters such as acoustic energy can correlate with bioeffects (Guzman et al. 2001; Miller and Dou 2004; Sundaram et al. 2003). However, input parameters of ultrasound are indirect and incomplete measures of cavitation activity and, therefore, correlations with bioeffects break down outside of limited ranges of applicability (e.g., Figure 4.6). We therefore believe that measuring cavitation activity with sound emissions, specifically broadband noise, is the most promising scenario to measure cavitation dose for correlation with bioeffects over a broad range of acoustic and experimental parameters.

Kinetic activity of cavitation

This study also presented data describing the kinetic activity of cavitation and its dependence on acoustic pressure, frequency and Optison® concentration. Guided by these observations, we hypothesize that two factors principally control the kinetic activity of inertial cavitation in our system and hence the measured broadband noise: these are (1) the initial number of bubbles capable of undergoing inertial cavitation (i.e., bubbles within the size range for inertial cavitation, which depends primarily on acoustic pressure

and frequency) and (2) the rate of destruction of bubbles by inertial cavitation, which depends on the volume of the sample exposed to a pressure above the pressure threshold for inertial cavitation.

In our experimental system, the cell sample is exposed to a non-uniform acoustic field. Perpendicular to the ultrasound beam, we have measured at the site of the sample chamber the pressure profile to have a half-amplitude (-6 dB) width of approximately 10.4 mm and 2.4 mm for 1.1 and 3.1 MHz, respectively. In the direction of the ultrasound beam, acoustic scattering by high concentrations of Optison® can cause significant attenuation, which can approach 100% during the initial bursts of ultrasound (data not shown). Given these non-uniformities, only a fraction of the sample volume is exposed to a pressure above the threshold for inertial cavitation. This size of this "cavitation zone" is expected to depend primarily on ultrasound pressure, frequency and Optison® concentration.

The preceding analysis is consistent with the observed timescales of cavitation activity shown in Figures 4.2 and 4.3, where broadband noise decays with time constants of 10's of milliseconds of "on" time, which corresponds to 1000's of milliseconds of total experimental time (given a 1% duty cycle). In contrast, previous studies show that uniform ultrasound exposure at high pressure (e.g, 2 MPa) should lead to inertial bubble collapse within microseconds (Chen et al. 2002; Leighton 1994). The fact that bubble destruction occurred in our system orders of magnitude slower than predicted for a uniform ultrasound exposure suggests that bubbles circulate in our sample and collapse in only regions with high ultrasonic pressures.

Guided by this analysis, we believe we can explain the trends observed in Figure 4.3. Increasing acoustic frequency should decrease the ultrasound beam width and decrease the initial number of bubbles available for inertial cavitation by increasing the pressure threshold for inertial cavitation. Therefore, we expect increasing frequency to decrease the size of the cavitation zone and thereby lower levels of peak broadband noise, as seen in Figure 4.3A1. In contrast, elevated pressure should increase the initial number of bubbles for inertial cavitation by exceeding the pressure threshold for a greater number of bubbles and thereby enlarge the cavitation zone. Thus, elevated pressure should increase peak broadband noise levels, as seen in Figure 4.3B1. Finally, increasing Optison® concentration increases the initial number of Optison® bubbles available for inertial cavitation but decreases the size of the cavitation zone due to increased attenuation. Therefore, we expect a lower rate of bubble destruction, which leads to longer times to reach the peak and half-life of cavitation, as seen in Figures 4.3C2-3.

Dependence of bioeffects on acoustic parameters

Another notable observation from this study was the dependence of bioeffects on acoustic pressure, exposure time, frequency and Optison® concentration. It was observed that bioffects generally increased in uptake and decreased in viablity with increasing pressure, increasing exposure time, increasing Optison® concentration and decreasing frequency. Furthermore, a significant synergistic effect was observed between pressure and exposure time. These trends are in agreement with previous research observations (Guzman et al. 2001). Taking in account the significant correlation of broadband noise with bioeffects and the dependence of bioeffects on these experimental parameters, these

results support an inertial cavitation-based mechanism, as previously proposed (Miller et al. 1996).

In conclusion, the results of this work demonstrate the potential of passively detecting acoustic emissions to measure cavitation activity, specifically using broadband noise measurements from acoustic frequency spectra. Furthermore, the cavitation dose based on broadband noise measurements was shown to correlate with intracellular uptake and loss of viability, which suggests a unifying parameter to correlate with bioeffects. Using acoustic spectral analysis of cavitation activity for real-time feedback about bioeffects may be useful for future experimental and clinical work in ultrasound-enhanced drug delivery applications.

CHAPTER 5

ULTRASONICALLY TARGETED DELIVERY INTO VASCULAR CELLS IN *EX VIVO* ARTERIES

This study tested the hypothesis that ultrasound can target intracellular uptake of drugs into vascular endothelial cells (ECs) at low to intermediate energy and into smooth muscle cells (SMCs) at high energy. Ultrasound-enhanced delivery has been shown to enhance and target intracellular drug and gene delivery in the vasculature to treat cardiovascular disease, but quantitative studies of the delivery process are lacking. Viable *ex vivo* porcine carotid arteries were placed in a solution containing a model drug, TO-PRO®-1, and Optison® microbubbles. Arteries were exposed to ultrasound at 1.1 MHz and acoustic energies of 5.0, 66, or 630 J/cm^2. Using confocal microscopy and fluorescent labeling of cells, the artery endothelium and media were imaged to determine the localization and to quantify intracellular uptake and cell death. At low to intermediate ultrasound energy, ultrasound was shown to target intracellular delivery into viable cells that represented 9 – 24% of exposed ECs. These conditions also typically caused 7 - 25% EC death. At high energy, intracellular delivery was targeted to SMCs, which was associated with denuding or death of proximal ECs. Significant intracellular uptake of molecules can be targeted into ECs and SMCs by ultrasound-enhanced delivery suggesting possible applications for treatment of cardivascular diseases and dysfunctions.

Introduction

Cardiovascular disease is one of the leading causes of death worldwide, resulting in nearly 17 million deaths annually (Smith et al. 2004). Targeted drug and gene delivery

to vascular endothelial cells (ECs) and smooth muscle cells (SMCs) has increasingly become a focus for treating cardiovascular diseases and dysfunctions, such as coronary artery disease, hypercholesterolemia, hypertension, and restenosis, because of the pivotal role of these cells in controlling and maintaining vascular functions (Cines et al. 1998; Cooke 2000; Melo et al. 2004). In addition, targeted drug and gene delivery to the endothelium is being used to treat cancerous tumors by anti-vascular therapy (Tozer et al. 2005) and myocardial and peripheral ischemia by promoting angiogenesis (Malecki et al. 2005). Many drug and gene delivery systems are being developed to increase targeting to vascular cells, such as drug-eluting stents (Saia et al. 2005), catheter-based systems (Sharif et al. 2004), viral vectors (Baker et al. 2005; Quarck and Holvoet 2004), and targeted liposomes (Niidome and Huang 2002) and microbubbles (Kipshidze et al. 2005). However, most current techniques lack either the effectiveness or specificity to adequately treat these disorders while safely administering the therapeutic and avoiding toxic systemic effects or require significantly invasive intervention. A safe, effective, and non-invasive method to target delivery of drugs or genes to the specific disease site in the vasculature would greatly benefit cardiovascular treatments.

A novel approach to targeting drug and gene administration is the method of ultrasound-enhanced delivery (Unger et al. 2001). Ultrasound-enhanced delivery often exploits cavitation bubble activity, a secondary effect of ultrasound, which can be produced by pressure oscillations of ultrasound (Mitragotri 2005). Furthermore, ultrasound pressures above a certain threshold can cause oscillating bubbles to undergo violent collapse known as inertial cavitation (Leighton 1994). Inertial cavitation is believed to cause transient disruptions in cell membranes, enabling transport of

extracellular molecules (e.g., drugs or genes) into viable cells (Schlicher et al. 2006; Sundaram et al. 2003). Cavitation-mediated cellular disruptions can allow uptake of small molecules, macromolecules (e.g., proteins), and genetic material (e.g., plasmid DNA or siRNA). Furthermore, ultrasound-enhanced delivery has been studied in a variety of *in vitro* and *in vivo* scenarios and has demonstrated promising therapeutic results after intracellular uptake of drugs and gene expression (Bekeredjian et al. 2005; Mitragotri 2005). Most importantly, ultrasound can be focused in the body by non-invasive extracorporeal targeted ultrasound (Huber et al. 2003) or by minimally invasive catheter-based transducers (Amabile et al. 2001). Greater efficacy and reduced side effects could be realized by this targeted therapy.

The vascular endothelium is an attractive target for ultrasound-enhanced delivery because cavitation can be readily produced in the vasculature, which currently occurs to a mild extent during diagnostic imaging (Correas et al. 2001). Moreover, cavitation is expected to have limited effects beyond cell layers directly experiencing cavitation activity, and the endothelium is the first point of contact to cavitation activity (Hwang et al. 2005). A number of researchers are currently studying ultrasound-enhanced gene therapy for cardiovascular disorders in order to control intimal hyperplasia, restore vascular function, or promote angiogenesis (Bekeredjian et al. 2005). These studies have shown expression of reporter plasmids as well as plasmids with a therapeutic purpose. Clinical potential of this method has been shown by causing protein expression by plasmid DNA (Taniyama et al. 2002) or blocking specific proteins by oligonucleotides (Hashiya et al. 2004).

A recognized limitation of ultrasound-enhanced delivery is the need for more cells with drug uptake or gene expression (Bekeredjian et al. 2005). Many studies have demonstrated gene transfection and tissue response in *ex vivo* and *in vivo* systems, however, few studies have been directed at quantifying the intracellular uptake of molecules and imaging bioeffects (i.e., intracellular uptake and loss of viability) caused by ultrasound-enhanced delivery in viable tissue (Mitragotri 2005; Mukherjee et al. 2000). It is important to know the uptake efficiency at different ultrasound energies in order to design and apply this technique for drug or gene delivery applications. In this study, we sought to determine whether ultrasound-enhanced delivery of a model drug can be targeted into ECs and SMCs in *ex vivo* arteries. This work represents the first known in-depth study to quantify and image the intracellular uptake of molecules and loss of viability to vascular cells by ultrasound-enhanced delivery. We hypothesize that ultrasound can target intracellular uptake of drugs into the vascular endothelium at low to intermediate energy and into SMCs at high energy. To assess this hypothesis, our goals in this study were to image the localization of (i) intracellular uptake of a model drug and (ii) loss of viability to vascular cells and (iii) to specifically quantify endothelial bioeffects in the targeted region.

Results

Endothelial bioeffects

To test the hypothesis that ultrasound-mediated cavitation can cause intracellular uptake into ECs, we exposed *ex vivo* arterial segments to ultrasound at three different acoustic energies - termed low, intermediate, and high - and compared these tissues to

control artery segments without ultrasound exposure (i.e., sham exposure). Figure 5.1 displays representative *en face* images of the endothelium of a control tissue and a tissue exposed to ultrasound at the intermediate energy. ECs are recognized by their rounded nuclei morphology and orientation parallel to the direction of blood flow.

Figure 5.1A1-A2 displays the endothelium of a representative control sample. The control artery appears to have a complete endothelium with high viability, as indicated by the continuum of ECs stained with blue fluorescent Hoechst 33342 (Figure 5.1A1) and few ECs stained with red fluorescent propidium iodide (Figure 5.1A2). None of the viable ECs appears to have green fluorescent TOPRO-1 staining, verifying that TOPRO-1 was membrane impermeable. These images indicate that arteries were isolated and handled in a manner that retained an intact endothelium and sustained the viability of the artery over the course of the experiment.

We next investigated if ultrasound caused intracellular uptake in the endothelium. Figure 5.1B1-B2 displays the endothelium of a representative artery exposed to ultrasound at intermediate energy. Fluorescently green stained ECs observed in the exposed sample (Figure 5.1B2) clearly indicate intracellular uptake of the model drug, TO-PRO®-1. Thus, we conclude that ultrasound exposure significantly increased intracellular uptake into ECs.

We also observed that intracellular uptake appeared in a pattern of discreet regions or "patches" of fluorescently green nuclei on the surface of the artery (Figure 5.1B2). This localized pattern of intracellular uptake was regularly seen in tissues exposed to ultrasound. We expect these regions of uptake can be explained by considering the cavitation-mediated mechanism causing bioeffects. It is commonly

believed that bioeffects observed by this technique are due to discreet cavitation events and are heterogeneous within a sample due to the stochastic nature of cavitation. Similar patterns of discreet regions of bioeffects have been observed in *in vitro* monolayers of cells exposed to ultrasound-mediated cavitation and attributed to individual cavitation events occurring near the surface of the monolayer (Brayman et al. 1999; Ohl and Wolfrum 2003). We therefore hypothesize that intracellular uptake is caused by many individual cavitation events occurring near the surface of the artery and creates the observed scattered patches of intracellular uptake in the targeted region of the artery.

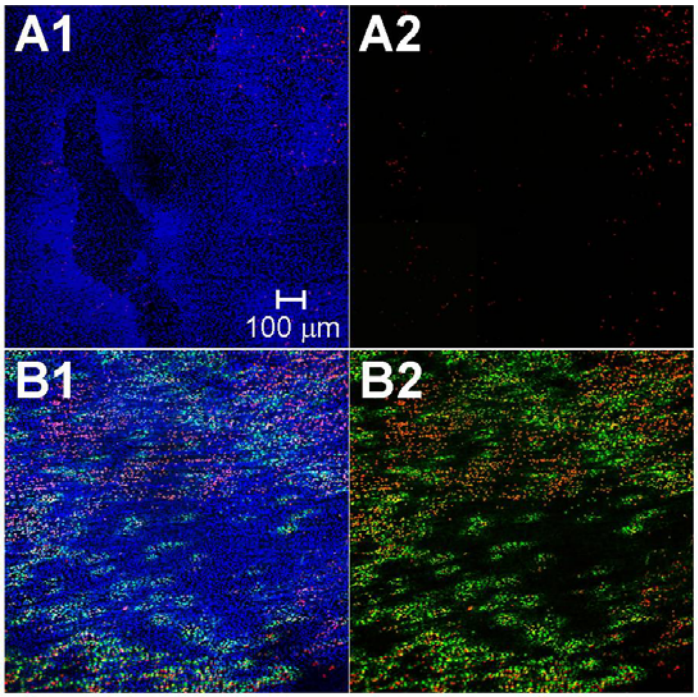

Figure 5.1: Confocal microscopy 2x2 image montages (10X magnification) displaying the localization of intracellular uptake enhanced by ultrasound. Images depict the endothelium of (A) a control sample and (B) a sample exposed to intermediate ultrasound energy. EC nuclei were labeled with Hoechst 33342 (blue) to stain all cells, propidium iodide (red) to stain dead cells, and TO-PRO®-1 (green) to indicate intracellular uptake. (A2) and (B2) are shown without blue fluorescence to more clearly view intracellular uptake and cell death.

In addition to intracellular uptake, we also sought to assess the extent to which ultrasound exposure caused loss of cell viability. In Figure 5.1B2, a decrease in viability of the exposed sample was observed, as shown by an increase in the number of fluorescently red nuclei compared to the control sample (Figure 5.1A2). This indicates ultrasound exposure can cause EC death.

Guided by the general findings in Figure 5.1, we wanted to assess endothelial bioeffects of intracellular uptake and loss of viability in greater detail at different ultrasound energies. In Figure 5.2, representative confocal images of control samples and samples exposed at low, intermediate, and high ultrasound energies are shown at two different magnifications. The extent of bioeffects appears to sharply increase with increasing ultrasound energy. The bioeffects ranged from (i) little intracellular uptake or cell death at the lowest energy (Figure 5.2C-D) to (ii) widespread intracellular uptake and reduced viabilities at the intermediate energy (Figure 5.2E-F) to (iii) widespread denuding of the endothelium and cell death at the highest ultrasound energy (Figure 5.2G-H). In Figure 5.2G1-H1, denuding of the endothelium is recognized by the lack of ECs and, instead, the characteristic image of the internal elastic lamina, which is highly autofluorescent in the blue and green channels.

Quantification of endothelial bioeffects

We next wanted to quantify the extent of intracellular uptake, loss of viability and denuding present after different ultrasound exposures. We used multiple *en face* images at 40X magnification (e.g., Figures 5.2B, D, F, and H) of each sample for analysis using image processing software to quantify the number of ECs that were (i) viable, (ii) viable

with intracellular uptake, (iii) non-viable, and (iv) removed from the artery (presumed non-viable).

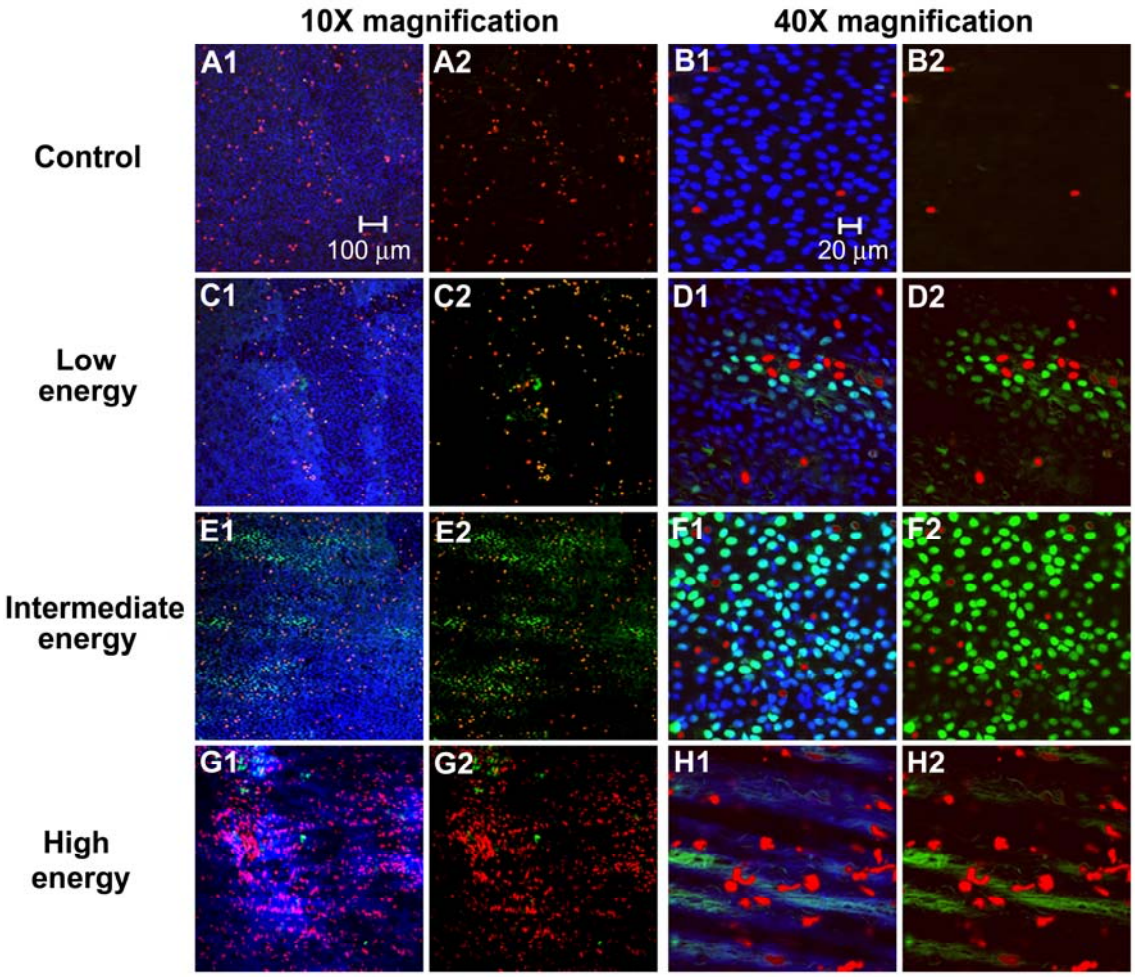

Figure 5.2: Confocal microscopy images of the artery surface at 10X (A, C, E, G) and 40X magnification (B, D, G, H) showing the range of bioeffects at different ultrasound energies. Images depict (A-B) a control sample and samples exposed to ultrasound at (C-D) low, (E-F) intermediate, and (G-H) high energies. Figures A2-H2 are shown without blue fluorescence to more clearly view intracellular uptake and cell death.

Figure 5.3 displays the percentage of cells in each of these four populations at low, intermediate, and high acoustic energy. The number of viable cells with

intracellular uptake increased with increasing energy from the control (0% of cells) to low energy (9% of cells) to intermediate energy (24% of cells) (ANOVA, $P < 0.002$). The number of cells with intracellular uptake at the highest acoustic energy (8% of cells) decreased due to substantial loss in viability.

Figure 5.3 further indicates that the total number of cells present on the artery surface and the number of viable ECs decreased with increasing acoustic energy (ANOVA, $P < 0.001$ and $P < 0.001$, respectively). The difference in the total number of ECs compared to the control indicated the amount of denuding was only statistically significant at the highest acoustic energy (~67% of cells were removed, $P<0.001$). The number of viable ECs was only significantly different when comparing the high acoustic energy (~25% of cells remained viable) to the control ($P<0.004$) and comparing the intermediate energy (~82%) to the control ($P < 0.03$). The viability at the low energy (~93%) was not significantly different from the control ($P = 0.07$).

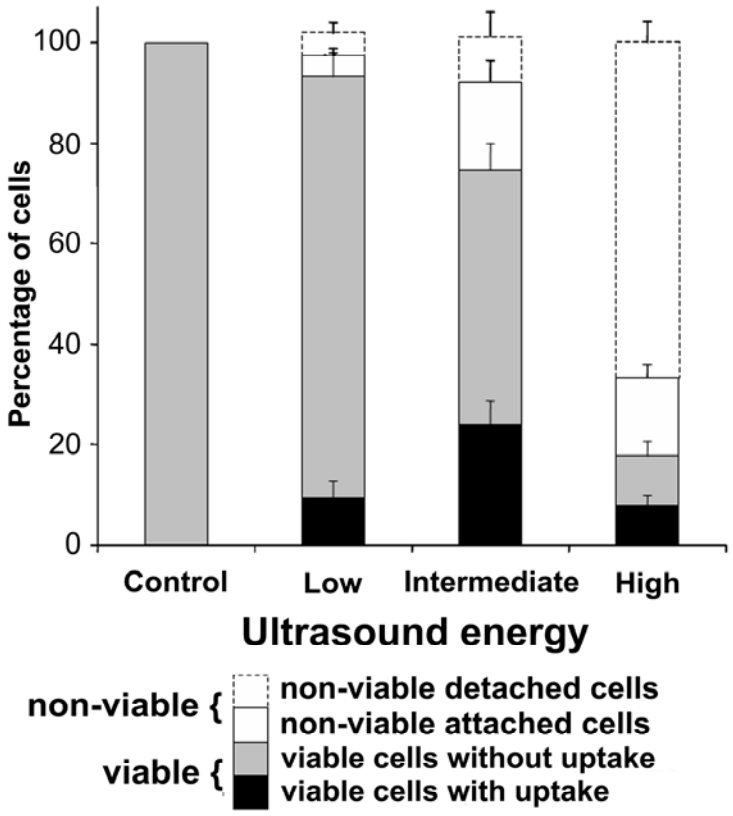

Figure 5.3: Quantification of endothelial bioeffects following ultrasound exposure. Data represent the averages of n ≥ 5 replicates with SEM shown.

Considering drug delivery applications, these results suggest that low proportions of intracellular uptake with insignificant loss in viability can be obtained at low energies, whereas a higher proportion of intracellular uptake with some loss of viability can be achieved at intermediate energy. Finally, if a large loss of viability and significant denuding is tolerable (or desired), intracellular uptake can be achieved among remaining viable cells by applying high ultrasound energies.

Medial bioeffects

Having observed and quantified endothelial bioeffects caused by ultrasound-mediated cavitation, we next determined if cavitation had any effects deeper into arterial

tissue to the SMCs present in the medial layer. In some drug delivery applications, it may be preferable to induce intracellular uptake to the underlying SMCs, such as to inhibit SMC proliferation.

By changing the focus depth of the confocal microscope, it was possible to optically slice the artery and capture images deeper in the tissue to approximately 40 μm below the endothelial surface. In Figure 5.4A, the surface of an artery exposed to the highest acoustic energy was captured. Extensive denuding of the artery was evident, based on the lack of ECs and the exposure of the internal elastic lamina. Images captured deeper in the tissue, as shown in Figures 5.4B-C, display SMCs that are recognized by their long and slender nuclei and orientation perpendicular to the direction of original blood flow. As indicated by propidium iodide and TO-PRO®-1 staining, SMCs in Figures 5.4B-C exhibited intracellular uptake, as well as loss of viability. In tissues exposed at lower acoustic energies, the medial layer did not show intracellular uptake or loss of viability (data not shown).

To determine if the presence of endothelial cells was a barrier to cavitation effects to smooth muscle cells, we pre-denuded arteries by rubbing the endothelial surface with a cell scraper. Confocal images from these studies (data not shown), indicated that SMC bioeffects (i.e., intracellular uptake and loss of viability) were small at low to intermediate energy and widespread at high energy, similar to Figure 5.4. This result suggests that the internal elastic lamina serves as the main barrier to cavitation, and high acoustic energies are necessary to mediate intracellular uptake to SMC.

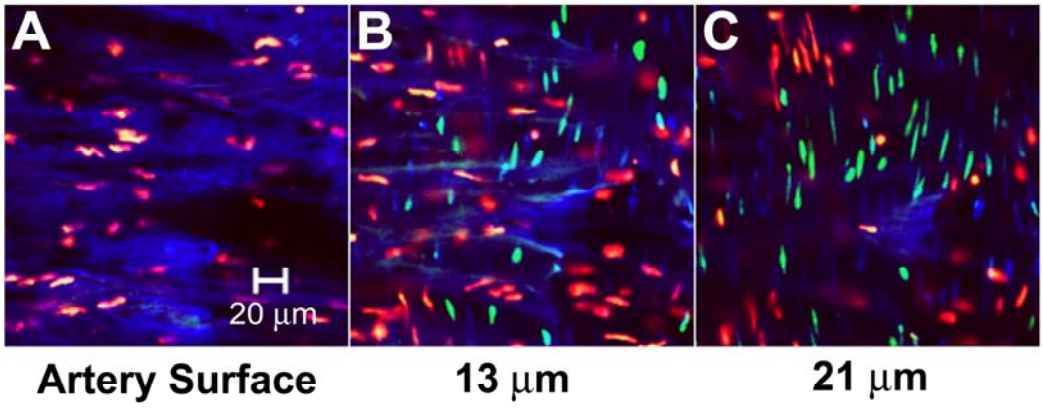

Figure 5.4: Confocal microscopy images at multiple depths in the artery displaying bioeffects to medial SMCs. Images were captured at (A) the artery surface and (B) 13 μm and (C) 21 μm below the artery surface.

Overall these results demonstrate that bioeffects be can directed to SMCs in the medial layer of the artery; however, we expect that effects are limited to the superficial layers of the media considering the cavitation-mediated mechanism, which is expected to have limited depth penetration (Hwang et al. 2005). This treatment of SMCs may be applicable in cases where denuding of the artery is tolerable or has already occurred due to some pretreatment, such as percutaneous coronary interventions.

Intact arteries

Lastly, we wanted to determine the role of physiological conditions such as geometry, pressure, tension, or presence of blood (a higher viscosity fluid) on bioeffects induced by ultrasound exposure. To better mimic physiologic geometry and conditions, intact arteries were stretched and pressurized to approximately physiologic tension and pressure during exposure to ultrasound at the intermediate and high acoustic energies. The arteries were also filled with DMEM or whole porcine blood containing Optison® and TOPRO-1.

Figure 5.5A-B display representative confocal microcopy images of an intact artery filled with DMEM and exposed at the intermediate and high acoustic energies. Similarly, Fig 5.5C-D display representative confocal microcopy images of the endothelium of an intact artery that was filled with whole blood and exposed to ultrasound at intermediate and high acoustic energies. Intact arteries filled with either DMEM or whole blood and exposed at either energy displayed similar bioeffects to the results found in the flat artery experiments (Figure 5.1) and, therefore, show that the geometry and presence of blood in a pressurized and stretched vessel did not significantly influence ultrasound exposure to cause bioeffects. These results also suggest that the bioeffects observed may be relevant for realistic drug delivery scenarios.

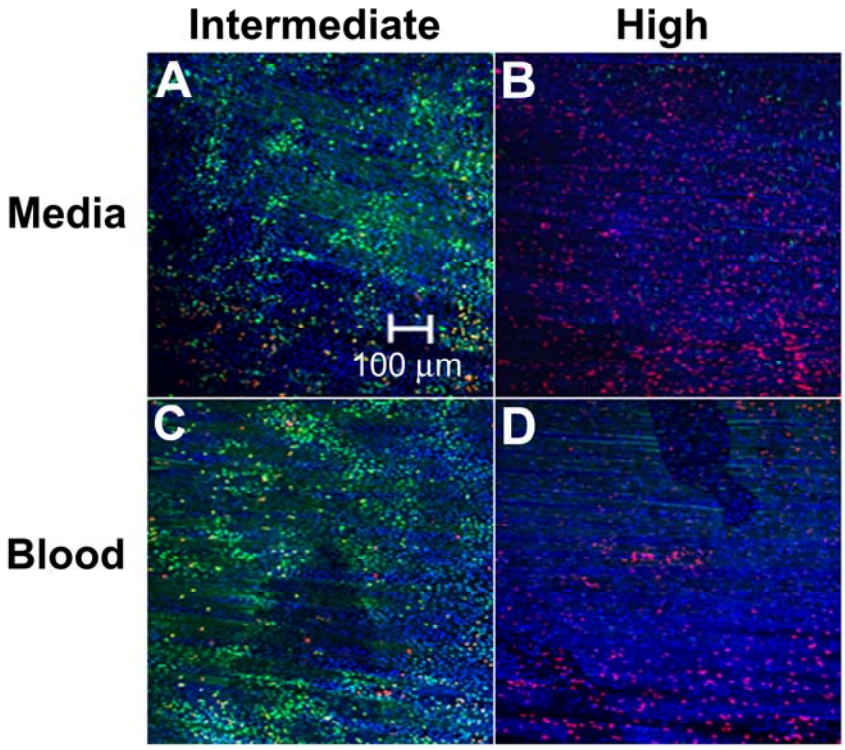

Figure 5.5: Confocal microscopy images of endothelium displaying bioeffects mediated by ultrasound exposure to intact arteries at near physiologic conditions. Ultrasound was applied at (A, C) intermediate and (B, D) high energy while the artery was filled with (A, B) DMEM or (C, D) blood.

Discussion

Previous studies utilizing ultrasound-enhanced gene therapy have shown promising results of positive gene transfection in *ex vivo* (Teupe et al. 2002) and *in vivo* (Taniyama et al. 2002) cardiovascular tissues. However, few studies have shown intracellular uptake of small molecules or macromolecules (e.g., proteins) for drug delivery applications in *ex vivo* or *in vivo* cardiovascular tissues (Bekeredjian et al. 2005; Mitragotri 2005). Moreover, there is a lack of knowledge on the efficiency of this technique in terms of the number of cells affected and the relevant populations. In this study, viable *ex vivo* porcine carotid arteries were exposed to ultrasound and demonstrated the ability of this method to cause intracellular uptake of small molecules into ECs and SMCs. Furthermore, quantitative data showed the approximate energies that are relevant for drug delivery applications.

Many cardiovascular diseases and dysfunctions would benefit from a targeted means to deliver drugs or genes to the endothelium (Melo et al. 2004). Quantitative results (Figure 5.3) suggest that low to intermediate ultrasound energies would be appropriate for drug or gene delivery applications to cause intracellular uptake or possibly transfect a large number of cells without a large loss of viability. Extensive cell death could be a drawback for drug delivery applications, since endothelial injury in the form of death or denudation could initiate an inflammation response or even thrombosis (Davis et al. 2003). Intracellular uptake results suggest that potential applications might be limited to drug or gene delivery to a minority of the cell population, yet some gene delivery applications may not require a high transfection efficiency if the expressed protein is excreted and has a local effect. To cause intracellular uptake to the majority of

the endothelium, repeated applications of ultrasound or other optimization approaches may facilitate higher uptake percentages without a harmful loss of viability. Cardiovascular diseases that could benefit from this method of targeted delivery include diseased sites such as vulnerable atherosclerotic plaques and ischemic heart or peripheral tissue. Intracellular therapeutic targets such as NADPH oxidases or gene expression of eNOS in the endothelium could help control neointimal formation and restore vascular function (Melo et al. 2004; Ray and Shah 2005). Promoting angiogenesis by intracellular delivery or gene expression agents such as VEGF or FGF in the endothelium could also benefit ischemic injuries in the myocardium or peripheral vasculature (Quarck and Holvoet 2004).

In other cardiovascular diseases, drug or gene delivery to SMCs may be desired, especially to control SMC proliferation (Quarck and Holvoet 2004). We found that ultrasound exposure could also cause medial bioeffects, which were only observed at high ultrasound energies. Results suggest that cavitation is obstructed by the internal elastic lamina and limited to superficial cell layers. Intracellular uptake to SMCs might be used in applications where denuding and loss of viability is acceptable or has already occurred, such as treatment for restenosis post-angioplasty. In this potential application, extensive denuding and injury to the endothelium typically occurs from balloon inflation during percutaneous coronary interventions (Davis et al. 2003). At this point, it may be advantageous to use ultrasound-enhanced cavitation to deliver drugs or genes to SMCs to inhibit smooth muscle proliferation and promote re-endothelialization for vascular recovery (Quarck and Holvoet 2004).

At higher ultrasound energies, extensive denuding of the endothelium was produced at the targeted site, as imaged in Figure 5.2 G-H and quantified in Figure 5.3. A targeted loss of viability or denuding may be not be desirable for drug or gene delivery applications but may be beneficial for other therapeutic applications. A number of vascular targeting agents, such as combretastatins, are currently being studied to cause EC death for anti-vascular targeting (Thorpe 2004). This therapy aims to selectively destroy endothelium of tumor blood vessels and subsequently cause vascular shutdown, which limits sustaining nutrients and waste removal required by the tumor (Tozer et al. 2005). High ultrasound energies focused at a tumor may be able to create this desired effect by denuding the artery.

In conclusion, this work supported the hypothesis that ultrasound-mediated cavitation can target intracellular uptake into ECs. Furthermore, we have for the first time imaged the localized patterns of intracellular uptake and shown them to be heterogeneously scattered patches that may correspond to ultrasonic cavitation events. These regions of uptake and cell death often appeared to be several cells in diameter, a dimension consistent with estimates of "blast radii" from single cavitation events (Guzman et al. 2003; Sundaram et al. 2003) and related observations of denuding cells off cultured monolayers (Ohl and Wolfrum 2003). We have also quantified the endothelial bioeffects due to ultrasound-enhanced delivery and found that intracellular uptake can occur in up to 24% of ECs at intermediate ultrasound energy and that widespread denuding of ECs from the arterial surface can occur at high energy. Using intact arteries as an ex vivo drug delivery model, this study showed that the same bioeffects occur at near physiologic conditions. These results exhibit advantages and

limitations of ultrasound-enhanced delivery that can further guide research on this technique for drug or gene delivery applications to treat cardiovascular diseases and dysfunctions.

CHAPTER 6

SHEAR-INDUCED LOADING OF CELLS WITH MACROMOLECULES BY CONTROLLED MICROFLUIDICS[2]

Introduction

Advances in biotechnology rely on techniques such as electroporation (Gehl 2003), liposomes (Goyal et al. 2005; Simoes et al. 2005), viral vectors (Young et al. 2006), microinjection (Jensen et al. 2003), and other emerging technologies to intracellularly deliver molecules into the cytoplasm and/or nucleus to modulate cellular behavior. These studies often aim to deliver bioactive molecules, such as genetic material or proteins, (Azzam and Domb 2004) or diagnostic molecules in order to label organelles or cellular structures (Barber et al. 1996). Current techniques to permeabilize cells for intracellular uptake encompass many different mechanisms to bypass the cell membrane, an impediment to molecular transport. These include electric means as with electroporation (Li 2004); chemicals to package molecules for delivery as with liposomes (Barber et al. 1996) or cell penetrating proteins (Kerkis et al. 2006); chemical fixation followed by permeablizing detergents (Melan 1994); direct injection of material by microinjection (Dice 1988); and mechanical means to apply shear stress to open cells as with scrape loading (McNeil et al. 1984), shockwaves (Kodama et al. 2002), and cavitation (Schlicher et al. 2006). Even though all of these techniques have developed into effective methods, they each have disadvantages such as requiring expensive

[2]This work was carried out in collaboration with Dr. Pavel Kamaev, whose contribution included the study of DU145 cells exposed to the cell shearing injury device (CSID).

equipment or chemicals, being complex to perform and time-intensive, being effective for only a small number of cells, or only being capable with non-viable cells as with chemical fixation and detergent protocols. Developing a means that is inexpensive, simple to perform, and effective at intracellular delivery of molecules into viable cells would greatly benefit biological research, biotechnology processes, and possibly the clinic.

A novel solution, which is being developed in our lab, is cell permeabilization by shear forces from fluid flow. We have found that flow of *in vitro* cells in suspension through microchannels, thereby exposing cells to high shear, can cause intracellular uptake of molecules. The potential advantages of this device are its low cost, ease of use, ability to be used for high throughput, and effective intracellular delivery.

Shear permeablization of cells is commonly believed to cause increased membrane tension and subsequent poration of the cell membrane (Lokhandwalla and Sturtevant 2001; Netz and Schick 1996). The first studies of membrane tension involved pore formation by using micropipetting techniques on red blood cells. These studies found that the critical areal strain is 2-3% and the critical tension is approximately 10 mN/m^3 before membrane poration and subsequently cell lysis in red blood cells, which lack the ability to repair actively (Evans et al. 1976). Later developed techniques to induce shear forces and tension upon cells include fluid flow in viscometers (Clarke and McNeil 1992) or hypodermic needles (Clarke and McNeil 1992), shock waves induced by lasers (Doukas and Kollias 2004; Kodama et al. 2002; Mulholland et al. 1999) or ultrasound (Lokhandwalla and Sturtevant 2001), and cavitation activity mediated by lasers or ultrasound (Miller et al. 1996; Ohl and Wolfrum 2003; Rau et al. 2004).

Furthermore, it is believed that cellular shearing is a critical event in injury (i.e., traumatic brain injury) leading to cell death or dysfunction due to cell permeablization (Prado et al. 2005).

Guided by these findings, we sought to (i) systematically study the effects of different shearing environments on cellular uptake and viability, (ii) assess the breadth of applications of uptake of different sized molecules, and (iii) design a simple and inexpensive device for applications.

Results

Shear-induced intracellular uptake

Our hypothesis is that controlled flow through microchannels can cause shear-induced loading of cells with macromolecules. As a first step toward testing this hypothesis, we exposed DU145 prostate cancer cells to controlled shear forces in a cone-and-plate cell-shearing injury device (CSID) that applied a uniform shear force to a monolayer of adherent cells in the presence of calcein (a cell-impermeant, green-fluorescent molecule), in the CSID. As shown in Figure 6.1, flow cytometry histograms of green fluorescence and display a control sample (i.e., no shear exposure) exhibiting innate autofluorescence and background noise, and a sample exposed to shear (i.e., 140 dynes/cm^2 for 300ms) displaying an increase in the number of cells with green fluorescence, indicating intracellular uptake of calcein. This result demonstrates that large transient shear forces can induce permeablization and cause intracellular uptake of molecules.

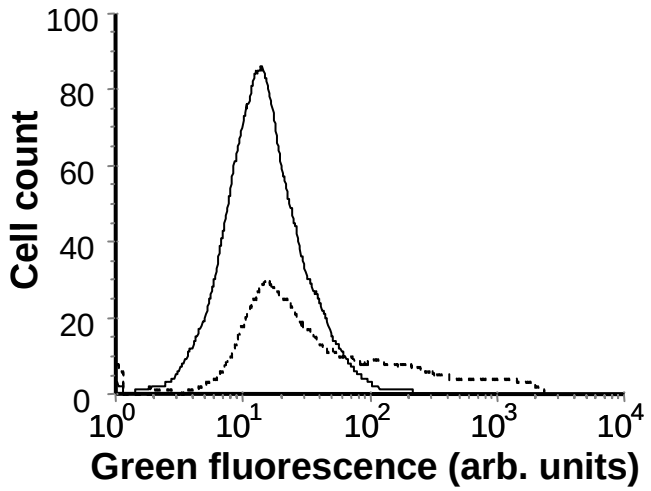

Figure 6.1: Flow cytometry histogram of green fluorescence displaying a control sample (solid line) and a sample exposed to shear in the CSID (dotted line), which exhibits an increase in green fluorescent indicting intracellular uptake of calcein.

Building from these results, we exposed cells in suspension to shear by flow through our fabricated microchannel device (Figure 3.2C). In Figure 6.2, representative flow cytometry and fluorescent microscopy results display intracellular uptake into viable cells after cells were exposed to fluidic shear in microchannels. The dashed curve in Figure 6.2A displays heterogeneous uptake that was typical at low shear conditions. The dotted curve in Figure 6.2A shows that higher shear caused intracellular uptake of calcein into a larger fraction of cells in a more homogenous manner. In Figure 6.2B, fluorescent microscopy displays cells with intracellular calcein and some dead cells, as stained with propidium iodide, verifying intracellular delivery of calcein into viable cells.

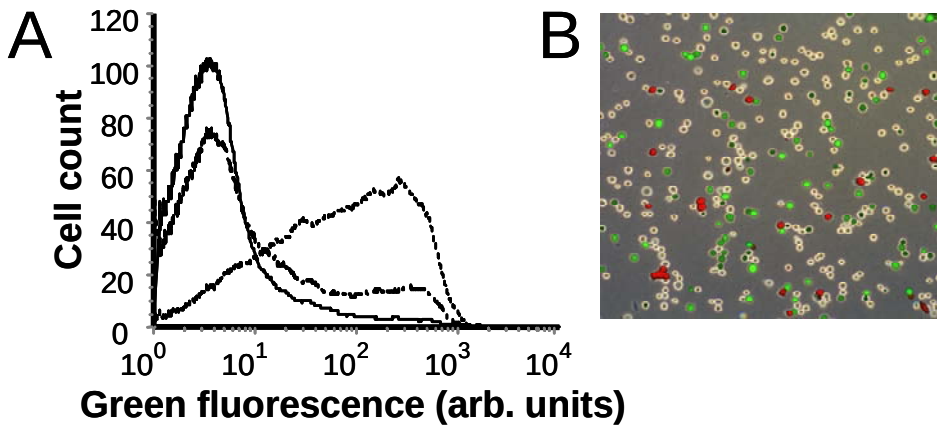

Figure 6.2: (A) Flow cytometry histogram of green fluorescence displaying a control sample and a sample subjected to low and high shear environments, which display an increase in green fluorescence indicting intracellular uptake of calcein. (B) Fluorescent miscrocopy image of cells after exposure to shear in microchannel flow, which depicts viable cells with intracellular uptake green-fluorescent calcein and non-viable cells stained with red-fluorescent propidium iodide.

Quantification of shear-induced bioeffects

Having demonstrated that controlled flow through microchannels can cause loading of cells with molecules, we further sought to systematically evaluate the effects of shear environment on uptake and loss of viability by flowing DU145 cells in suspension through microchannels of various dimensions. In Figure 6.3, the effects of fluid flow rate and microchannel diameter and length were examined. Fluid flow rate was varied up to 100ml/h, which was the maximum our apparatus could accommodate. Increased flow rate should increase the intensity of the shear force experience by a cell, while decreasing its duration. Microchannel diameter was varied down to 50 μm, which is approximately three times the cell diameter of 15-18 μm. Smaller diameters were found to clog and were therefore no used. Decreasing microchannel diameter should increase the shear intensity without changing its duration. Finally, microchannel length

was varied up to 250 μm, which was the maximum our apparatus could accommodate, due to the increased pressure drop associated with longer channels.

Figure 6.3 shows that significant effects on intracellular uptake and cell viability occurred under the different shearing conditions. In each graph, the total height of each bar represents the percent of cells remaining intact after shear exposure, which is subdivided into a black bar, representing the percent of viable cells with uptake (the typically desirable population), a grey bar, representing the percent viable cells without uptake (the apparently unaffected population), and a white bar, representing the percent of intact dead cells (the population stained with propidium iodide). All samples were normalized to the control sample (i.e., no shear exposure) taken to represent 100% viability and 0% uptake.

Figure 6.3 indicates that decreasing channel diameter and channel length each increased the number of cells with intracellular uptake (ANOVA, $P < 0.05$). A general trend in the viability could not be inferred, since at low shear the 250 μm channels display a higher viability and at high shear the 100 μm channels exhibit a higher viability. Increasing the flow rate over the range tested did not significantly change the intracellular uptake observed (ANOVA, $P > 0.05$). Overall, uptake by approximately 10% of cells was achieved with minimal viability loss and uptake in excess of 20% of cells was achieved with 20-50% viability loss. These results generally suggest that high shear conditions created by small diameter channels and short exposure times are favorable for affecting a large portion of the cell population and causing intracellular uptake.

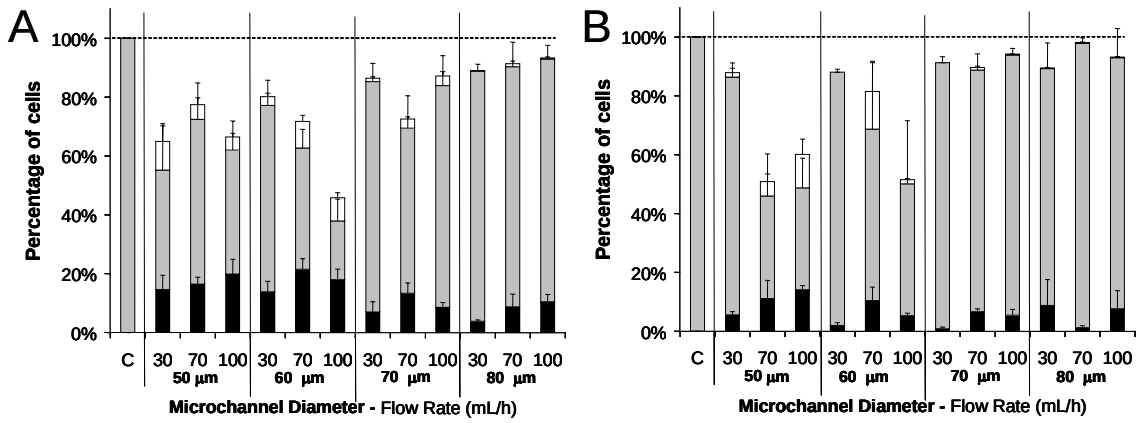

Figure 6.3: Cell viability and intracellular uptake populations following shear exposure within cylindrical microchannels of various dimensions. The total height of each bar represents the fraction of cells remaining intact, the size of the black stripe represents the fraction of cells with significant levels of intracellular uptake, the size of the grey stripe represents the fraction of cells that were apparently unaffected, and the size of the white bar represents the fraction of cells that were intact and dead. DU145 cells were subjected to shear by passage through microchannels of (A) 100 μm and (B) 250 μm channel length. Data in represent the averages of n ≥ 3 replicates with SEM shown.

To test the hypothesis that shear stress is responsible for the bioeffects, the average shear stress was estimated all of the flow conditions and graphed in Figure 6.4. The actual shear stress experienced by the cells is expected to be vary, becuase the velocity profile was not fully developed over the short channel lengths and regions of higher shear rates will exist near the channel wall and lower shear stress in the center of the channel. In Figure 6.4, uptake was shown to increase and viability was show to decrease with increasing average shear force (ANOVA, $P < 0.0001$). This result suggests that shear stress mediated the bioeffects, and that high shear forces are desirable for delivery to a larger number of cells. Differences between 100 μm (Figure 6.4A) and 250 μm (Figure 6.4B) channel length suggest that high shear for short durations are favorable to maintain high viability and delivery to a larger number of cells.

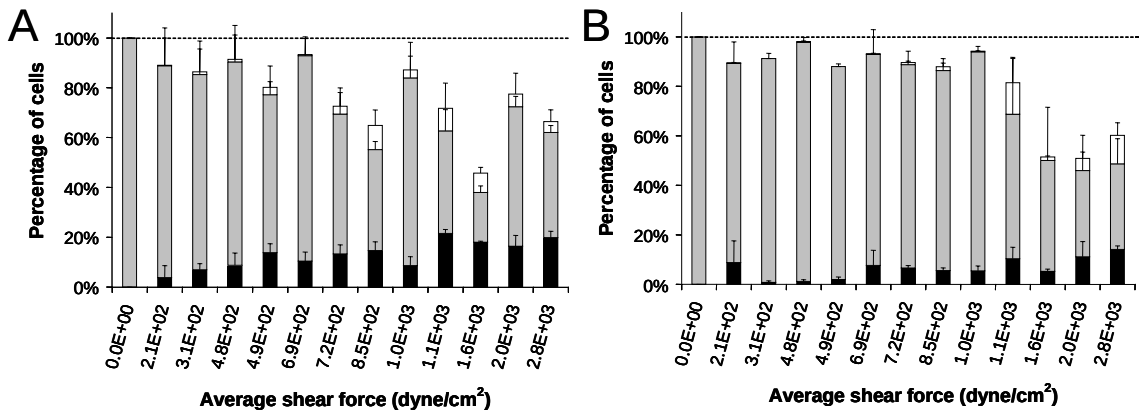

Figure 6.4: Correlation of cell viability and uptake measurements with average shear stress calculated for exposures within (A) 100 μm and (B) 250 μm channel lengths. The total height of each bar represents the fraction of cells remaining intact, the size of the black stripe represents the fraction of cells with significant levels of intracellular uptake, the size of the grey stripe represents the fraction of cells that were apparently unaffected, and the size of the white bar represents the fraction of cells that were intact and dead. Data in represent the averages of n ≥ 3 replicates with SEM shown.

Intracellular delivery of molecules by shear

We next wanted assess the breadth of molecules that could be loaded into cells by testing the uptake of different sized macromolecules. Molecules ranging in size from 0.6 to 2,000 kDa were incubated with cells and exposed to shear by flow through channels of 50 μm diameter and 100 μm lengths at a flow rate of 100 ml/h. As shown in Figure 6.5, all five of the molecules tested, including large dextrans and bovine serum albumin (BSA) were able to be loaded intracellularly by shear exposure. These findings show that large macromolecules can be delivered transiently shearing cells, which indicates that shear-induced disruptions to the plasma membrane barrier ar big enough to permit entry of large macromolecules (e.g. 2,000 kDA dextran). Moreover, this observation suggests that shear-induced loading of cells could be developed into a useful tool for intracellular

delivery of molecules with biological significance, such as intracellular stains, proteins and genetic material.

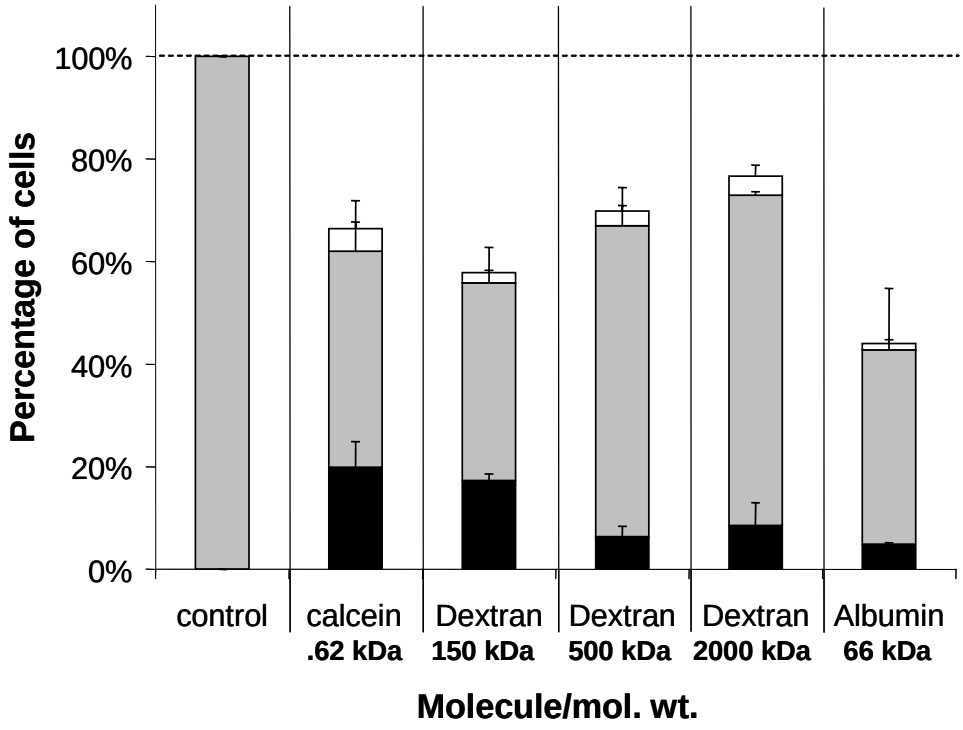

Figure 6.5: Intracellular delivery of various molecules by subjecting DU145 cells to shear in cylindrical microchannels with dimensions of 50 μm diameter and 100 μm channel length. The total height of each bar represents the fraction of cells remaining intact, the size of the black stripe represents the fraction of cells with significant levels of intracellular uptake, the size of the grey stripe represents the fraction of cells that were apparently unaffected, and the size of the white bar represents the fraction of cells that were intact and dead. Data in represent the averages of n ≥ 3 replicates with SEM shown.

Simplified device with conical microchannels

To facilitate practical use, we sought to design a simplified device that could be attached onto a syringe and allow one to manually expose cells to shear by passage through microchannels and thereby cause intracellular loading in the laboratory. Microchannels were fabricated in a 3 x 3 configuration, yielding nine channels, for higher

throughput and to reduce the incidence of channel clogging. Also, based on the observation that high stress for short durations is favorable, we created conical microchannels that maximized the shear stress just at the channel outlet (Figure 3.2B) (Martanto et al. 2005). Conical microchannels were drilled using the excimer laser in a trepanning mode to yield an inlet diameter of approximately 300 μm and exit diameter of 40 and 50 μm over a 250 μm channel length. To simulate simplified laboratory use, these channels were tested by manually dispensing the syringe containing approximately 3 ml of cell solution instead of using the syringe pump. As shown in Figure 6.6, this approach produced significantly improved results with higher viabilities and a larger percent of cells with intracellular uptake such that uptake. For example, uptake in 36% of cells was achieved while maintaining a cell viability of 80%. We believe this increased effectiveness was due to the use of conical channels that achieved a very short exposure to high shear stress. This work also illustrates that a simple, hand-operated device can be used to cause intracellular loading of molecules in a large number of cells.

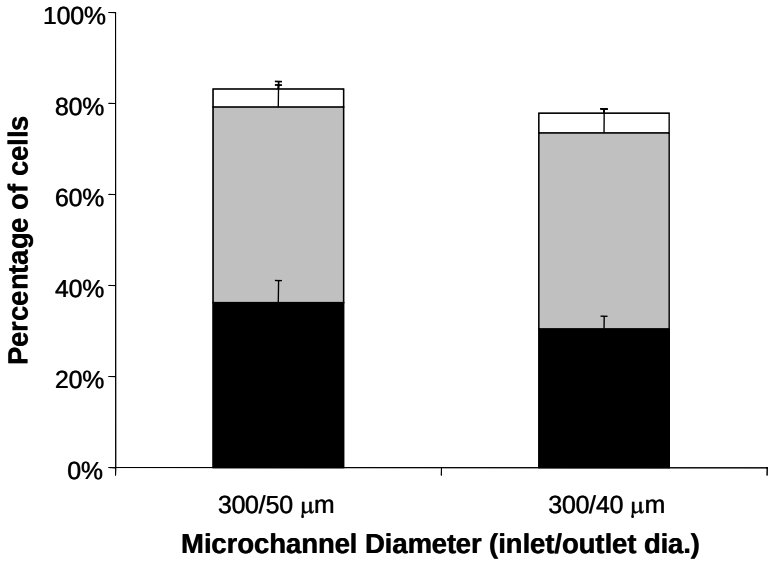

Figure 6.6: Intracellular uptake and viability populations after manually dispensing cells through conical microchannels. Microchannels were fabricated a 3 x 3 array (9 total channels) with inlet diameter of 300 μm and an outlet diameter of (A) 50 μm and (B) 40 μm. The total height of each bar represents the fraction of cells remaining intact, the size of the black stripe represents the fraction of cells with significant levels of intracellular uptake, the size of the grey stripe represents the fraction of cells that were apparently unaffected, and the size of the white bar represents the fraction of cells that were intact and dead. Data in represent the averages of n ≥ 3 replicates with SEM shown.

Discussion

In this study, intracellular delivery of molecules was evaluated by subjecting cells to shear stress by fluid flow in the controlled environment of a cone and plate shearing device and in a novel device that exploited the high shear environment of fluid flow through microchannels. Shear stress proved to be a functional mediator of intracellular uptake as we demonstrated the uptake of small and macromolecules into a large number of cells. Most importantly, this work led to the development of a simple and inexpensive device that can expose a large number of cells to shear, thereby delivering molecules into cells.

By evaluating the shearing environment in terms of the microchannel dimensions and geometry, we have concluded that the most favorable shearing environment for high uptake and viability is high magnitude shear for short durations, as illustrated by the conical microchannels. Conical microchannels were created with large inlet diameters and small outlet diameter, which were on the order of magnitude of the cell diameter. It is expected that the large inlet diameter (approximately 300 μm) produced insignificant shear forces on the cell as was observed in the large cylindrical channels, such as 70-80 μm diameters channels (more than three times smaller than the conical channel inlet). However, as the channels decreased diameter with the conical profile, higher velocities were achieved creating a shear environment similar to the small cylindrical channels, such as 50 μm diameter channels, yet with much shorter durations. We believe high magnitude shear and short exposure durations were the principle factors that led to higher viabilities and more cells with intracellular uptake.

A device for flowing fluid through the microchannels was created with the following design consideration: (i) allow coupling of a syringe and tubing for dispensing and collecting, respectively, (ii) provide a water tight seal around the microchannel disks to ensure fluid flow through the microchannels, and (iii) allow microchannel disks to be easily replaced within the device. The fabricated device, as shown in Figure 3.2 C, proved to be suitable for dispensing and collecting small volumes (3 – 10 ml) of cell solution, however, other designs could be imagined for flowing larger volumes of cell solution. A number of the samples tested with single channel disks (Figure 6.1 B) had the incidence of high resistance during fluid flow, which we attributed to cells or cellular debris accumulating in the channel and obstructing flow. Using micro-machining

techniques, we were able to create Mylar® disks with an array of microchannels (Figure 3.2 B) that nearly eliminated the incidence of clogging and allowed for higher throughput of the cell solution. The ease of use of this device with an array of conical microchannels was demonstrated by manually dispensing cell solution (Figure 6.6)

By demonstrating intracellular of small molecules to large macromolecules and proteins, this study showed the potential of our device to be useful for intracellular delivery of molecules in a number of biological applications. Intracellular delivery is pursued by a number of techniques such as electroporation, liposomes, viral vectors, and microinjection to deliver bioactive molecules to alter cellular processes and diagnostic molecules into cells to label cellular structures for live cell imaging and analysis. Possible areas that could benefit from this device include *in vitro* studies in biological laboratories, *ex vivo* cell based clinical therapies, biotechnology processes, and pharmaceutical laboratories for drug discovery and testing of intracellular targets.

In conclusion, we have demonstrated the potential of shear forces to cause intracellular uptake and have fabricated a novel device that uses shear to deliver molecules into a large number of cells. The advantages of this device are its low-cost, ease of use, ability to be used for high throughput systems, and effective intracellular delivery of small and large molecules. However, limitations of this device are its hetergeneous effect and loss of viability. Despite these limitations, we believe this device or one of similar design will be a beneficial tool to deliver molecules into cells for the biological, medical, or biotechnology community.

CHAPTER 7

CONCLUSIONS

The success of the next generation of medicinal treatments will not only require the discovery of new therapeutic drugs but will also greatly depend on new and more effective methods of drug delivery. Advancements to conventional drug delivery methods are aimed at reducing the inefficiencies of the delivery process, particularly by targeting specific cells or tissues and more effectively penetrating the cell membranes, which are impediments to drug transport. Inefficiencies in the delivery process lead to poor efficacy of the drug or gene and often require much higher doses, which causes higher costs and unwanted side effects. Ideally one would desire to administer a therapeutic agent that would effectively target and deliver to specific cells or tissues at high efficiency. Such a system would provide a great benefit in a broad range of drug delivery applications by increasing the efficacy of current drugs, lowering administrating costs, decreasing side effects, and promoting future gene therapy and drug design. Ultrasound-enhanced delivery is a novel and exciting technique that is being heavily researched because it offers the potential to address these issues by targeting intracellular delivery in a non- or minimally invasive manner.

In this study, we first sought to measure cavitation, which is the mechanism by which ultrasound induces intracellular delivery, as a means to monitor the kinetics of cavitation activity and predict bioeffects. During exposure of cell suspensions to ultrasound in an *in vitro* system, we used a passive cavitation detection system that allowed recording of sound emissions from cavitation activity. Recorded sound emissions were then processed by FFT analysis to derive the frequency spectrum. These

spectra showed characteristic features of bubble oscillation and collapse, including increased magnitudes at harmonics and increased levels of broadband noise. Generally, we found that the broadband noise increased sharply and peaked during the first 20 ms of ultrasound exposure and then decayed with a half-life of tens to hundreds of milliseconds until reaching a point of constancy. The sudden rise in broadband noise has been generally accepted to coincide with the initial collapse of stabilize microbubbles and the collapse of secondary bubbles. The decay in broadband noise is attributed to the destruction of secondary bubbles resulting in a lack of bubbles available for collapse. From measuring the peak broadband noise, the time to reach peak broadband noise, and the half-life at different frequencies, pressures, and microbubble concentrations, we found the kinetics greatly differed over these parameters. For instance, increasing pressure increased the peak broadband noise, whereas increasing frequency decreased the peak broadband noise, and increasing microbubble concentration did not consistently change the peak broadband noise In conclusion, we hypothesize that two factors principally control the kinetic activity of inertial cavitation in our system and hence the measured broadband noise: these are (1) the initial number of bubbles capable of undergoing inertial cavitation (i.e., bubbles within the size range for inertial cavitation, which depends primarily on acoustic pressure and frequency and Optison concentration) and (2) the rate of destruction of bubbles by inertial cavitation, which depends on the volume of the sample exposed to a pressure above the pressure threshold for inertial cavitation.

To obtain a measurement of the overall inertial cavitation activity, we used the time integral of broadband noise, termed cavitation dose, over the exposure duration.

We found that cavitation dose correlated broadly with bioeffects over a range of experimental and acoustic parameters, including acoustic pressure, exposure time, frequency, and microbubble concentration. We further showed that measuring the output parameter of broadband noise from cavitation emissions offers a means to predict bioeffects that is superior to the measurement of input parameters such as acoustic energy, which can not always predict the cavitation activity. Overall, these results demonstrate that passive cavitation detection and measurement of broadband noise is a unifying parameter that could be used as a feed-back measurement in the lab and potentially in the clinic to non-invasively measure cavitation and predict bioeffects.

In this study, we also investigated the use of ultrasound to cause targeted intracellular delivery into tissue, advancing this technique beyond previous experiments with *in vitro* cell suspensions. For these studies, we chose to focus on arterial tissue because it presents a favorable location for cavitation production (i.e., the blood stream) and a number of cardiovascular diseases could benefit from targeted drug delivery. We found that by exposing viable *ex vivo* porcine carotid arteries to ultrasound in the presence of microbubbles and a model drug, we could cause targeted intracellular delivery to endothelial and smooth muscle cells. Using confocal microscopy to image and then quantify the bioeffects, we found that at low to intermediate ultrasound energy, ultrasound can achieve targeted intracellular delivery into viable cells in 9 – 24% of exposed endothelial cells. These conditions also typically caused 7 - 25% endothelial cell death. Approximate ultrasound energy for *in vivo* applications can be deduced from these quantitative results. At high energy, intracellular delivery was targeted to smooth muscle cells, which was associated with denuding or death of proximal endothelial cells.

Furthermore, it was determined that the internal elastic lamina poses the main barrier to cavitation effects on medial cells and that high ultrasound energies are necessary for delivery to smooth muscle cells. From images of the artery after ultrasound exposure, the distribution of cells with uptake and death appeared as heterogeneously scattered patches, which are hypothesized to correspond to ultrasonic cavitation events. Lastly, we used intact arteries in a custom-designed chamber that allowed us to approximate physiologic conditions of pressure, tension, and fluid properties (i.e., by using whole blood). In these experiments, we found that bioeffects appeared similar to those measured in quantified experiments. In conclusion, this work supported the hypothesis that ultrasound-mediated cavitation can target intracellular uptake into endothelial cells. Furthermore, we have for the first time imaged the localized patterns of intracellular uptake and shown them to be heterogeneously scattered patches that may correspond to ultrasonic cavitation events. Using intact arteries as an *ex vivo* drug delivery model, this study showed that the same bioeffects occur at near physiologic conditions. These results exhibit ultrasound's advantages for causing targeted intracellular uptake into endothelial cells and smooth muscle cells and also the limitations due to heterogeneous uptake and loss of viability in the form of denuding and cell death. The understanding gained from these results can further guide research on this technique for drug or gene delivery applications to treat cardiovascular diseases and dysfunctions.

Lastly, in this study, we evaluated high shear stress exposure to cells in order to induce intracellular uptake. Shear stress from cavitation oscillations and collapse is commonly believed to be the primary mediator of intracellular uptake by ultrasound as well as in a number of other techniques such as shockwave exposure. Building from

these findings, we explored the use fluid flow through microfluidic channels to impart high shear forces for short durations on cells. Using this technique, we found that we could achieve intracellular uptake of small and large macromolecules into cells. We believe this phenomenon closely mimics the shearing mechanism by which ultrasound-mediated cavitation causes bioeffects. However, at optimal shearing conditions, intracellular uptake could be achieved in a large portion of the exposed cells in a more homogenous manner than with ultrasound exposure. We believe these optimal conditions exposed cells to a more homogeneous shear stress than the shear stress generated from localized cavitation bubbles during ultrasound exposure. In conclusion, we believe this method offers a simple, quick, inexpensive, and high-throughput method for delivering molecules into cells. We believe this method could be further developed for applications to intracellularly deliver bioactive molecules (e.g., genetic material or drugs) or diagnostic labeling probes in an *in vitro* laboratory setting or possibly for *ex vivo* clinical purposes.

Overall, this thesis presents data that advances ultrasound-enhanced drug delivery on two major fronts: (i) the challenge in controlling cavitation-mediated bioeffects *in vitro* were addressed based on cavitation detection and correlation of bioeffects with the unifying broadband noise measurement and (ii) the advancement of this method toward an *in vivo* application was furthered by the evaluation of this method to deliver molecules into cells in viable *ex vivo* tissue. From these findings, it is expected that the cavitation-mediated bioeffects could be controlled in an *in vivo* application by a feedback-measurement based on cavitation detection. Furthermore, the proper acoustic energies and treatment strategies (e.g., repeated exposures) for *in vivo* can be inferred from our

results with *ex vivo* arteries. Lastly, this thesis has presented a novel method for intracellular delivery by exposing cells to shear forces in fluid flow through microchannels. Delivery of small to large molecules was demonstrated and the near optimal shear environment was determined. It is expected that this method could be further developed to aid biological research or cell based therapies by delivery of bioactive or diagnostic molecules to *in vitro* cells in the lab or clinic.

CHAPTER 8

RECOMMENDATIONS

For future studies of ultrasound-enhanced drug delivery, I would recommend continuing to focus on drug and gene delivery to vascular tissue for treatment of cardiovascular diseases and dysfunctions. I believe the most probable scenario for ultrasound as a successful drug or gene delivery modality is employing ultrasound for targeted treatment to the cardiovascular system. Foremost, there is a need for a targeted drug delivery in the cardiovascular system for treatment of specific diseased sites such as atherosclerotic lesions (e.g. vulnerable plaques), restenosis post percutaneous interventions, and regions of ischemic tissues. Furthermore, I believe the cardiovascular system is an area in the body that is most conducive for ultrasonic delivery because cavitation can be readily produced in the blood, and drugs and microbubbles can easily access most of the cardiovascular system via intravenous injections and transport by blood flow. To advance ultrasound-enhanced drug delivery toward a clinical treatment, I would recommend concentrating on (1) delivery in *ex vivo* systems for optimization of delivery of various molecules and genetic material, (2) delivery in *in vivo* systems to determine the performance of this technique *in vivo*, (3) the inflammation and injury caused by this technique, and (4) employing this techniques for treating disease models in *in vivo* systems.

Building from the intact artery experiments in this thesis, I believe further *ex vivo* experiments in a system comprised of viable excised arteries maintained in an organ culture system offers an excellent way to study the ability of ultrasound for drug and gene delivery. Using this system, intracellular delivery of various molecules from small

molecules (as shown in this thesis) to macromolecules (e.g., proteins) into endothelial and smooth muscle cells can be studied. In addition, there has been an increase research on ultrasound for gene therapy, however, most have used *in vivo* systems and have not fully quantified the percent of cells with gene expression. An *ex vivo* system as described would offer an approach to quantify and image gene expression of reporter plasmids to fully determine the capabilities of this technique. Furthermore, many of these studies have not fully investigated the cavitation activity occurring during treatment and many have not characterized the ultrasound exposure (e.g. in terms of peak pressure, area of exposure, and exposure time). Many of these experiments have also employed DNA-loaded microbubbles, and it is not fully understood if this increases gene expression. I believe there is an area of need to understand the cavitation activity in terms of the type of cavitation (i.e., stable or inertial) and the level of cavitation that is inducing gene expression. Experiments could employ a cavitation detection system as used in this thesis to determine the type and level of cavitation. These studies could shed insight on the mechanism of cavitation-induced gene expression.

Future studies should also evaluate this technique in an *in vivo* setting for drug and gene delivery. Even though the *ex vivo* system provides an excellent system for study, it can not mimic the injury and healing response that would be experienced *in vivo*. Therefore, I would recommend experiments in animal models to evaluate the bioeffects of intracellular uptake or gene expression and the viability post ultrasound treatment. A possible limitation of this technique may be the injury and inflammation response from the physical effects of cavitation. Vascular injury by mechanical means such as angioplasty or stenting typically causes an inflammatory response in the form of platelet

adhesion, leukocyte recruitment, cellular responses such as endothelial apoptosis and smooth muscle cell proliferation, and release of proinflammatory and prothrombogenic cytokines. Such a response would be greatly undesired during treatment of the cardiovascular system, especially in the case of treating atherosclerotic plaques where inflammation could worsen the condition or cause thrombosis. The use of cavitation in the cardiovascular system, by combining microbubbles contrast agent and diagnostic ultrasound, has been deemed safe and used for many years. However, diagnostic ultrasound typically uses low energy - low pressure ultrasound that only mediates stable cavitation, whereas, intracellular delivery is commonly believed to require the more intense inertial cavitation. Inertial cavitation at high ultrasound energies has been found to cause some vascular injury by causing capillary rupture (Hwang et al. 2005), endothelial cell death, and denudation in *ex vivo* tissue, as shown in this thesis. It is critical to understand the injury and inflammatory reaction by ultrasound mediated cavitation to determine the safety and limitations of this technique before application in a clinical situation.

Based on the results of the recommend experiments and identifying intracellular targets or therapeutic genes, I believe treatment of diseases will be feasible and should be attempted in animal models. Understanding the capabilities for intracellular delivery, finding the optimal ultrasound conditions for proper cavitation activity, and knowing the limitations in terms injury and inflammation should allow for treatment strategies to induce targeted drug or gene delivery to a large portion of the exposed cells and have a therapeutic effect.

APPENDIX A: EQUIPMENT SCHEMATIC

INTRODUCTION

As described in Chapter 3 Methods, ultrasound was applied to a sample in a custom-built water bath. Figure A.1 displays a schematic of the equipment used to expose samples to ultrasound and record cavitation emissions. Samples were accurately placed within the bath by using a micropositioning system (Velmex). Ultrasound was produced at 1.1 and 3.1 MHz by a submersible piezoceramic transducer. An acoustic absorber was place at the opposing end of the tank to minimize acoustic reflections and standing wave formation. The response of the transducer was controlled by driving electronics that included: two function generators (Standford research instruments and Agilent), a RF amplifier (Electronic Navigation Industries), and a matching network. To record cavitation emissions, a focused hydrophone (Sonic Concepts) was placed perpendicular to ultrasound beam. The signal from the focused transducer was sent through a preamplifier before being recorded by a high-speed digitizer (National Instruments) in a local computer. The first function generator acted as the "switch" to turn the ultrasound "on" and "off" by creating a square wave where the ultrasound was turned "on" at a high voltage and "off" at a low voltage of the square wave. The square wave produced by the first function generator could be customized for the desired ultrasound "on" and "off" time (or duty cycle) as well as the number of bursts. The signal from the first function generator was sent to the computer to initialize recording of the ultrasound burst and to the second function generator as an external trigger to control the burst of ultrasound. The parameters of ultrasound (i.e., frequency and pressure) were

controlled by the second function generator by inputting the desired frequency and voltage amplitude of a sine wave.

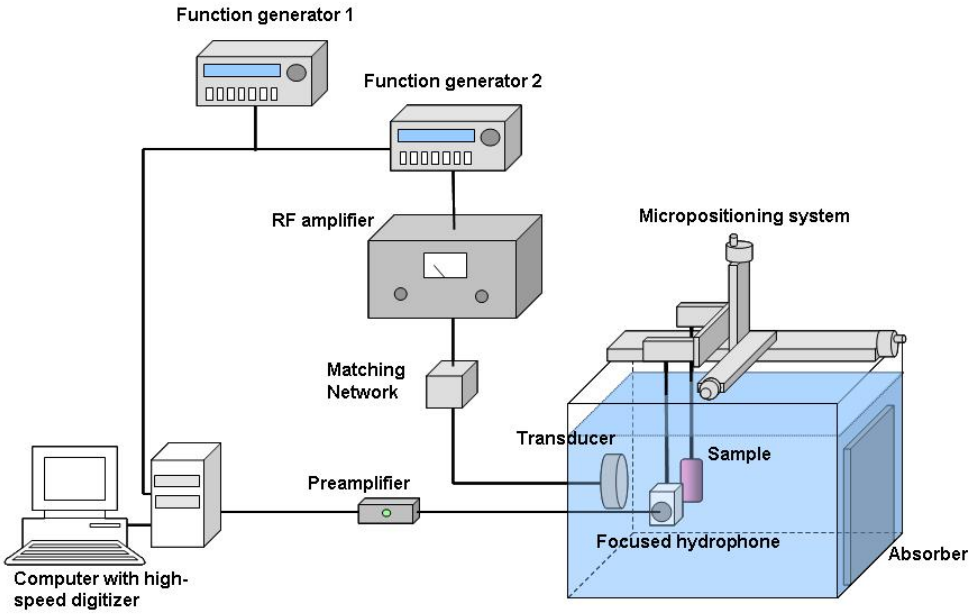

Figure A.1: Equipment schematic of the ultrasound bath and electronics.

APPENDIX B: CALIBRATION OF ULTRASOUND FIELD

INTRODUCTION

Mapping and calibration of the acoustic field produced by the ultrasound transducer was performed to determine the optimal location for sample placement and to calibrate the function generator voltage input to the ultrasound pressure output at the desired sample location.

METHODS

Mapping and calibration of the piezoceramic transducer was carried out as described in Chapter 3 Methods.

RESULTS

Mapping of the acoustic field

To determine the optimal sample location axially along the acoustic beam, the membrane hydrophone was used to find the focus and then moved axially to measure the pressure, as shown in Figure B.1A and B for 1.1 and 3.1 MHz, respectively. As shown in Figure B.1, the focus of each frequency was the location with the highest pressure measured, approximately at 5.1 - 5.4 cm from the transducer face for both frequencies. For both frequencies, there were also local maxima were the pressure peaked just before and after the focus. These local maxima are due to the constructive and destructive interference of the ultrasound as it is focused.

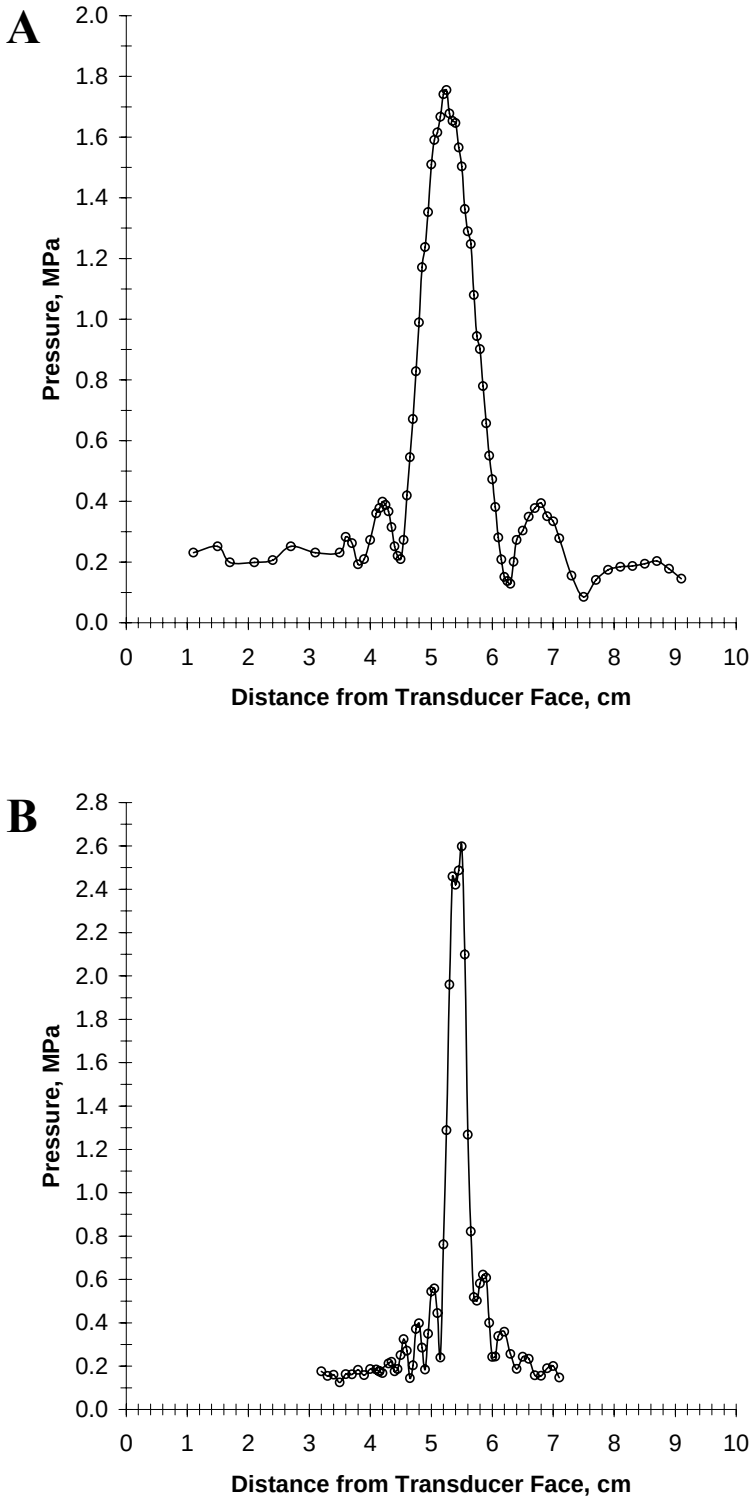

Figure B.1: Mapping of temporal-peak-negative presssure along the axis of the focused ultrasound beam emitted at (A) 1.1 and (B) 3.1 MHz

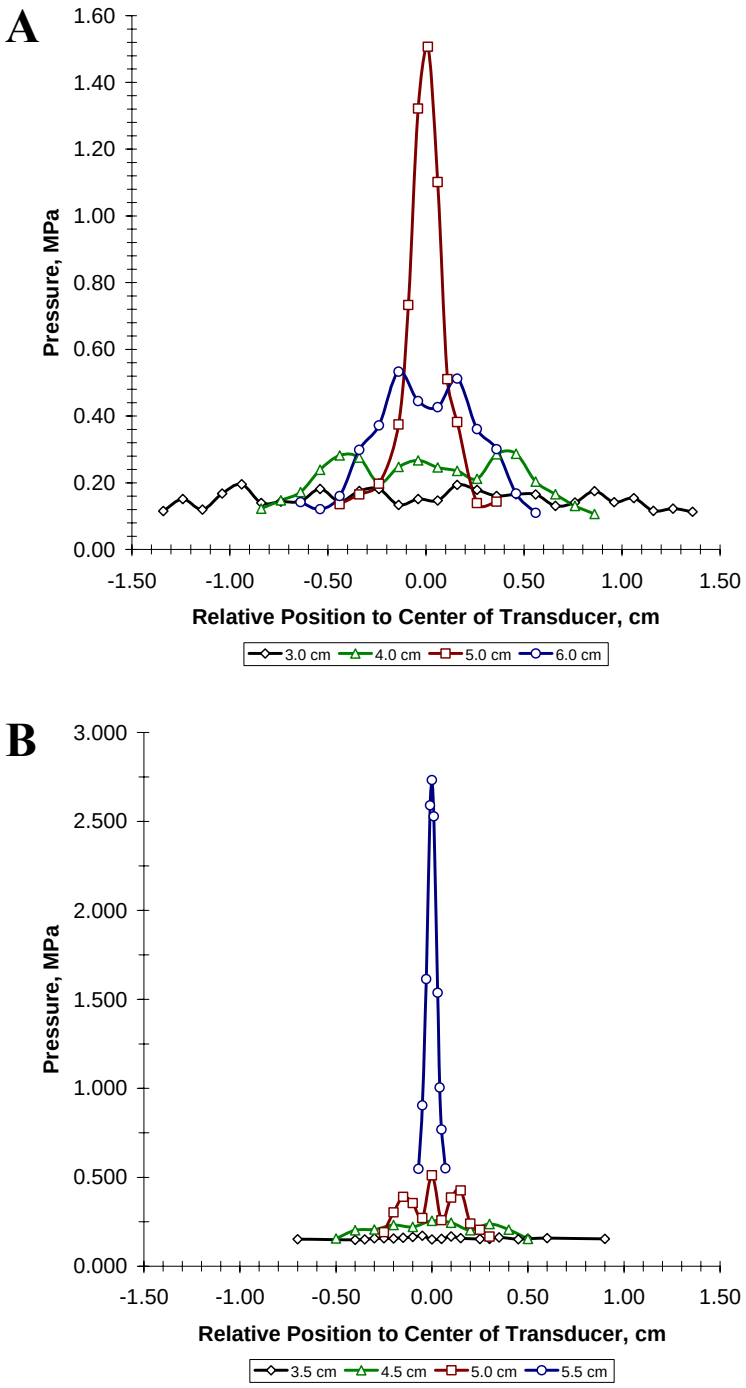

Figure B.2: Mapping of the temporal-peak-negative pressure transversely along the cross-section of the focused ultrasound beam emitted at (A) 1.1 and (B) 3.1 MHz

To measure the transverse width along the ultrasound beam, the hydrophone was moved perpendicular to the beam. In Figure B.2A and B, the transverse mapping of the acoustic beam is shown for 1.1 and 3.1 MHz, respectively. As shown in Figure B.2, the beam width decreases as hydrophone approaches the focus and increases passed the focus. To display the acoustic profile graphically, Figure B.3A and B displays the data of the transverse data along the axial distance from the transducer for 1.1 and 3.1 MHz, respectively. In Figure B.3, the width at half the amplitude is shown to display beam width.

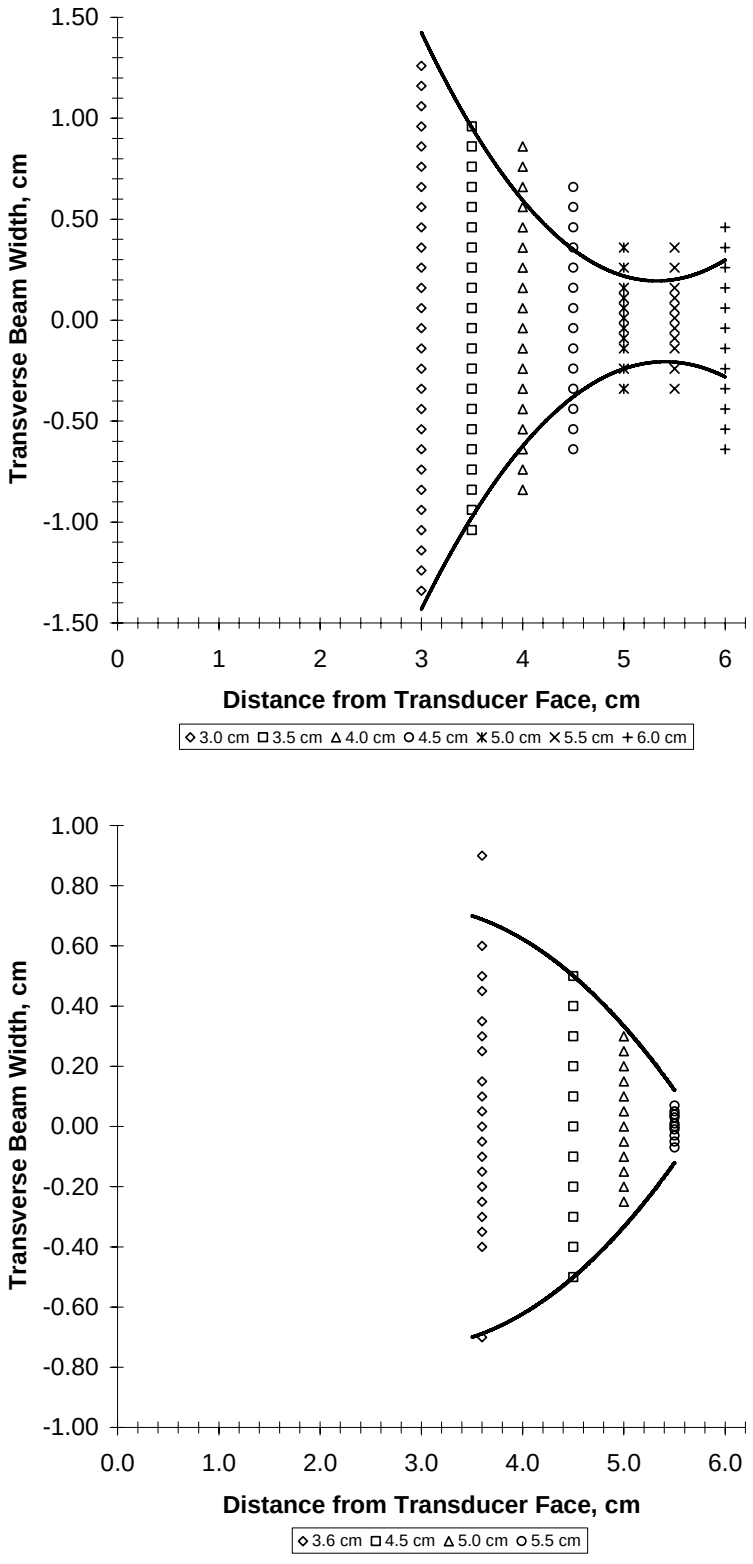

Figure B.3: Focused ultrasound beam profile of ultrasound emitted at (A) 1.1 and 3.1 MHz.

Based on these results, the sample location was chosen to be placed at the local maximum immediately prior to the focus. This location was chosen because of the wider beam width, approximately 10.4 mm and 2.4 mm wide at half-amplitude (-6 dB) for 1.1 and 3.1 MHz, respectively. A wider beam width allowed more of the sample to be exposed to ultrasound and the local maximum still allowed high pressures to be produced at this location.

To calibrate the input voltage to the output ultrasound pressure, the hydrophone was used find the focus and then moved towards the transducer to find the local maximum, the desired sample location. At this location, the voltage was varied from approximately 0.1 mVpp to 4.0 mVpp while measuring the pressure with the hydrophone. In Figure B.4, the calibration curve is shown for 1.1 and 3.1 MHz.

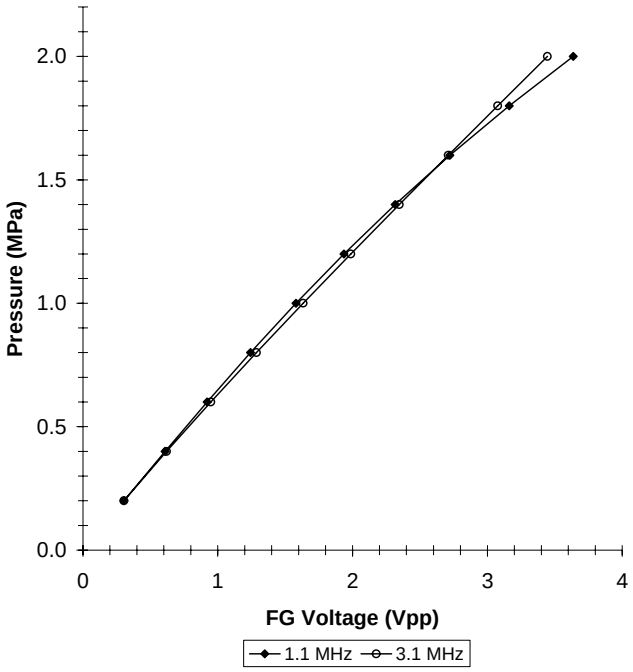

Figure B.4: Calibration of temporal-spatial-peak negative pressure with the function generator voltage at the local maximum prior to the focus.

APPENDIX C: MATLAB AND LABVIEW PROGRAMS

INTRODUCTION

LabVIEW and MATLAB programs were written to aid in recording and analyzing cavitation emissions, respectively. The LabVIEW program was written specifically to control the high-speed digitizer, which was installed in a personal computer and recorded the emissions in a digital format. A MATLAB program was then written to take the digital files of recorded cavitation emissions and apply Fast-Fourier Transforms (FFT) to the data to derive the frequency spectrum of cavitation emissions.

METHODS

LabVIEW programming

As described, in the Chapter 3 Methods the cavitation emissions were detected by a focused hydrophone that then sent the signal through a pre-amplifier before being recorded by a high-speed digitizer, which was controlled by a LabVIEW program. To prepare for a given experiment, a folder on the personal computer was created and named the proper date of the experiment. In the experiment folder, three other folders were created and named "Bursts", "Pictures", and "Spectrum Data". These folders were created to keep data organized as it was recorded and processed. An excel file was then created in the Spectrum Data folder and named "Conditions.xls". This file contained all the information needed by the high-speed digitizer to record the cavitation emission, including number of samples to be recorded for each burst, the number of bursts, the sampling rate, and the voltage range of the emissions. The voltage range was determined before an experiment in a pilot study by measuring output voltage from the

pre-amplifier during an ultrasound exposure to a sample containing Optison at the desired pressure, location and concentration, respectively. The Conditions file was saved as a text file in order to be read by the LabVIEW program. The LabVIEW program named "Long Acquistion-smb.vi" was opened. Figure C.1 displays the program's panel interface. Prior to recording, the electronics were connected in the correct configuration, the sample was placed in the desired location of the ultrasound apparatus, and the driving electronics settings were adjusted for the sample. To begin the exposure, the sample number was inputted into the LabVIEW program and the "Run" button was clicked with the mouse to start the program. At this point the LabVIEW program was running and waiting for a signal input that would trigger the recording. Immediately after starting the LabVIEW program, the ultrasound was applied by pressing the TRIG button the function generator. The output of the LabVIEW program for each sample were files named "sample #.dsc", "sample #.txt", and "sample #.I16". The ".dsc" file was a description file that could be opened in Notepad and listed parameters used by the LabVIEW program during the recording of each burst, including numbers of samples, sampling period, offset, gain, and timer. The ".txt" file contained information regarding the experimental parameters and the data and time of each sample recording. Lastly, the ".I16" file was a binary data file that contains recorded emission for each burst during ultrasound exposoure to a sample. Using the gain and offset in the ".dsc" file, the binary data could be converted into actual voltage data.

MATLAB programming

The MATLAB program "SpectraBNCorrelation" was used to analyze each experiments recording by reading the binary data, converting it to real voltage data,

applying FFT, analyzing regions of the frequency spectrum, writing the spectrum data to excel files, and graphing spectrum data. The inputs to the program were the date of the experiment the samples to be analyzed and the locations of the data files.

LABVIEW CODE

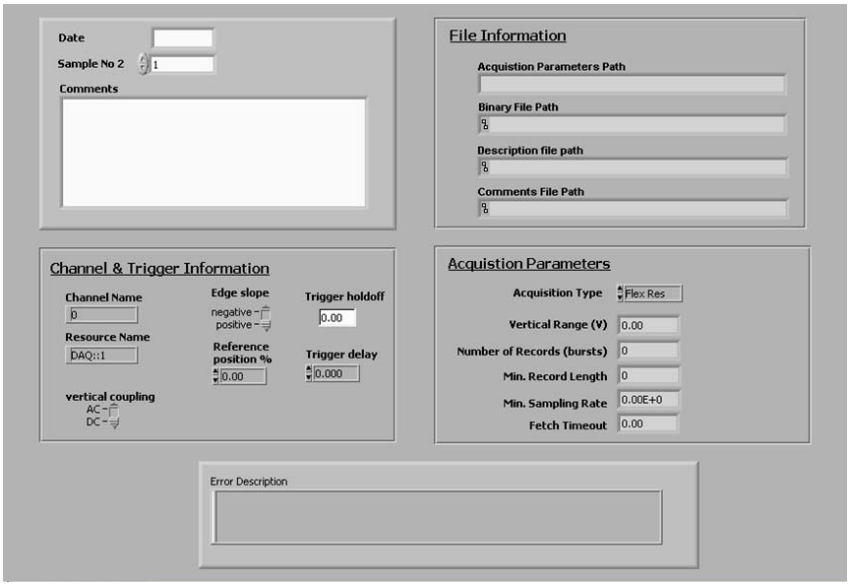

Figure C.1: Front panel of Labview program to control the high-speed digitizer for recording cavitation emissions. Program name: Long Acquistion-smb.vi.

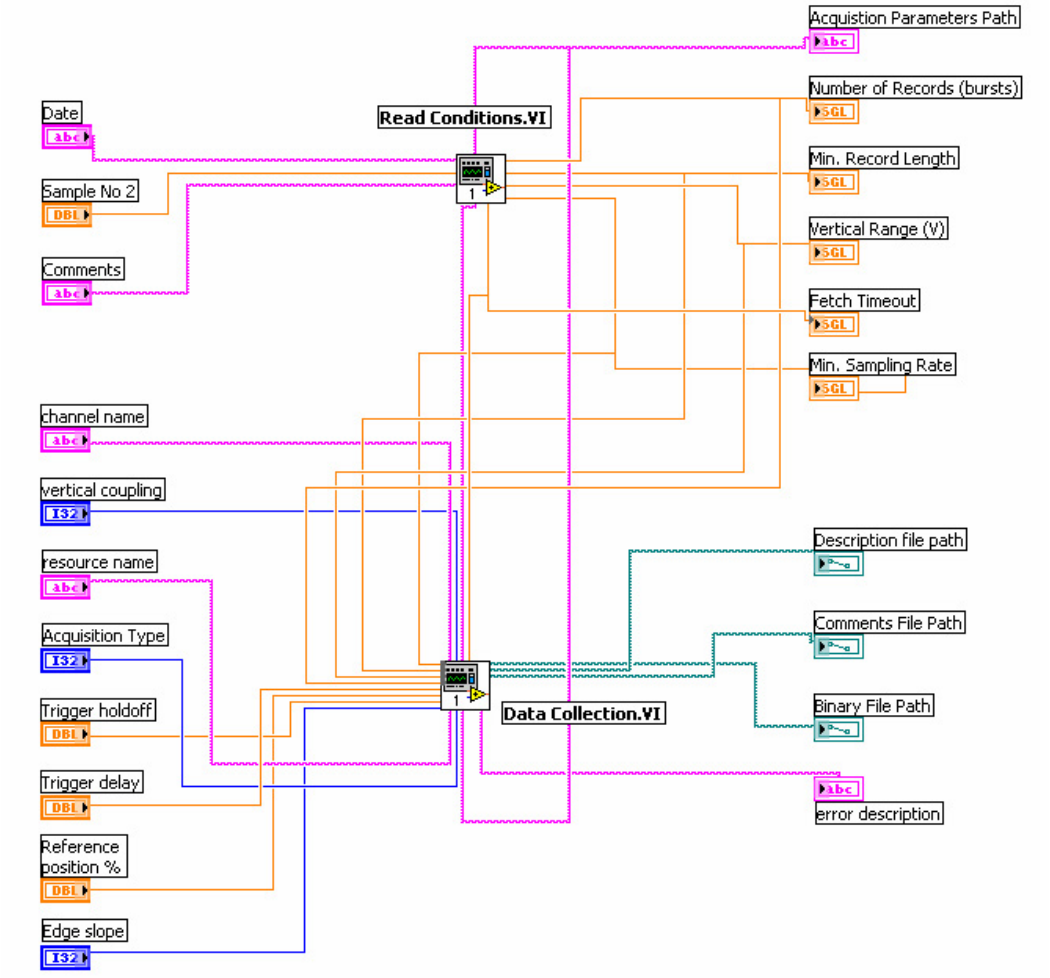

Figure C.2: Diagram view of Labview program: Long Acquistion-smb.vi.

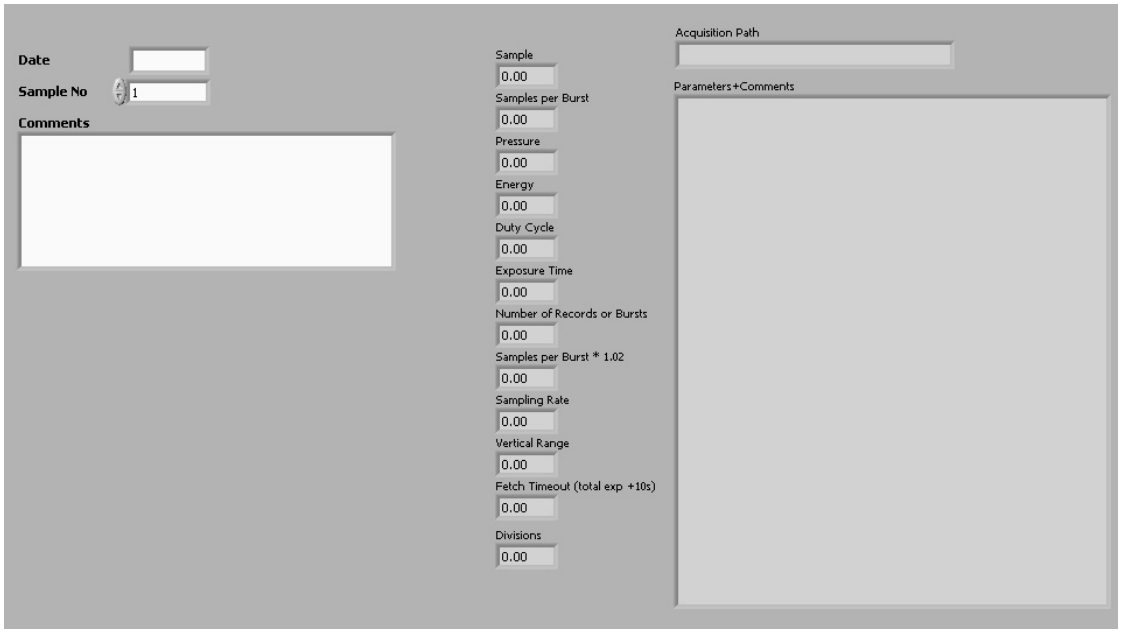

Figure C.3: Front panel of Labview program: Read Conditions-smb.vi. Sub-VI for Long Acquisition-smb.vi.

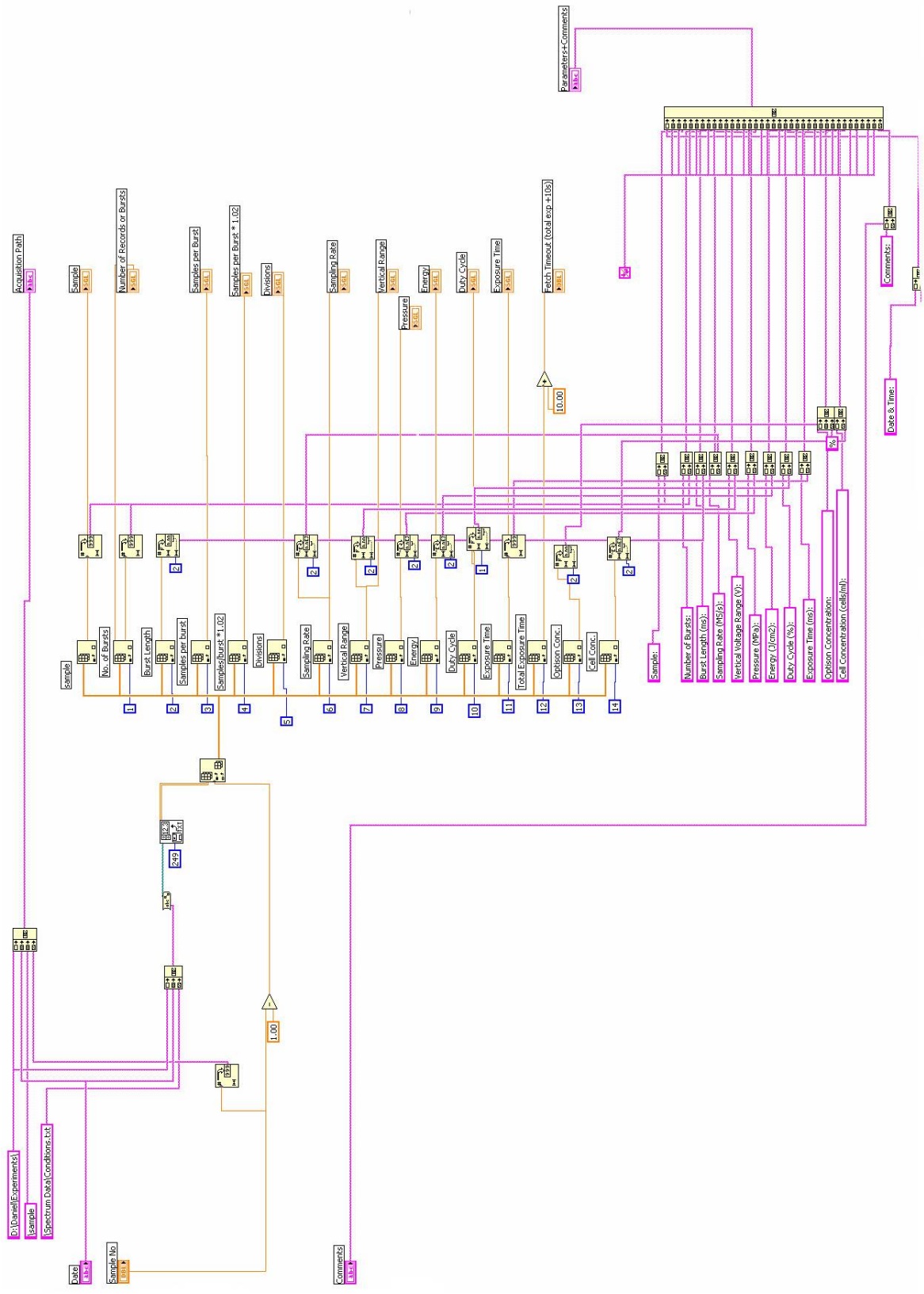

Figure C.4: Diagram view of Labview program: Read Conditions-smb.vi

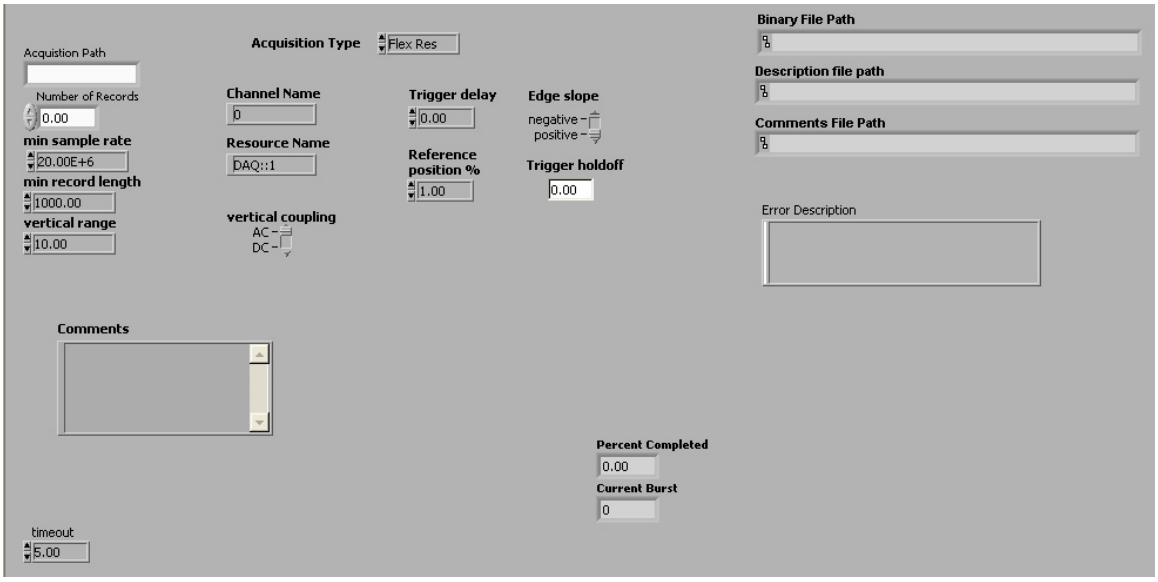

Figure C.5: Front panel of Labview program: Data Collection-smb.vi. Sub-VI for Long Acquisition-smb.vi.

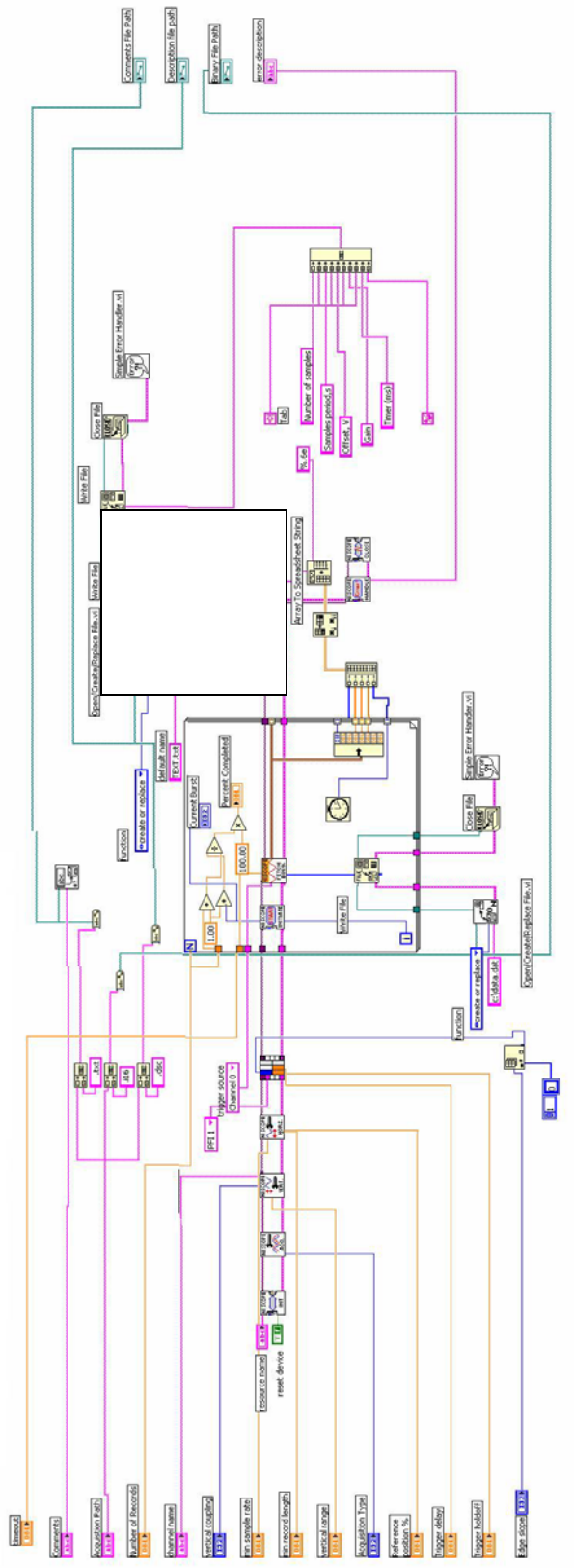

Figure C.6: Diagram view of Labview program: Data Collection-smb.vi

MATLAB CODE

```
%Spectrum Analysis Program - version 17.1
clear

Date='10-8-03';
sample_start=8;
sample_end=8;
DF=3.1e6;  %driving frequency

First_Burst_Only='Yes'
Make_Plots='Yes'
Print_Plots='No'
Write_Files='No'
Hanning_Window='No'

clc
Date
%Establish working directories
Data_dir=['E:\10-8-03\'];
% Data_dir=['E:\'];
Graph_dir=['B:\Experiments\',Date,'\Pictures\'];
Spec_dir=['B:\Experiments\',Date,'\Spectrum Data\'];
Desc_dir=['E:\10-8-03\'];
% Desc_dir=['E:\'];

%read conditions for experimental parameters
conditions=xlsread(['B:\Experiments\',Date,'\Spectrum Data\Conditions.xls']);  %read conditions file
% conditions=xlsread(['D:\Daniel\Experiments\',Date,'\Spectrum Data\Conditions.xls']);  %read conditions
file

c_samples=conditions(:,1);
c_bursts=conditions(:,2);
c_burst_length=conditions(:,3);
c_samplesperburst=conditions(:,4);
c_actualspb=conditions(:,5);
c_pressures=conditions(:,9);
c_energies=conditions(:,10);

max_bursts=(max(conditions(:,2)));
max_samples=(max(conditions(:,1)));

Max(1:max_bursts,1:max_samples,1:4)=0;
Ave(1:max_bursts,1:max_samples)=0;

if strcmp(sample_end,'Max')==1
   sample_end=max(c_samples);
end
['Samples to be analyzed: ',num2str(sample_start), ' through ', num2str(sample_end)]

for k=[sample_start:sample_end]    %index for samples analyzed
   File=['sample ',num2str(k)]

   if strcmp(First_Burst_Only,'Yes')==1
```

```
    Bursts =1
  else
    Bursts = c_bursts(k);       %Number of bursts to be analyzed
  end

  if Bursts >0;    %establishes if sample is a control and skips-controls should have 0 bursts in the conditions file

    ['Reading sample ',num2str(k),' i16 Binary File.....']
    fid1=fopen([Data_dir,File,'.i16'],'r','b'); %Open specific i16 binary file which contains the signal
    if fid1 ~= -1                    %establishes if file exists then proceeds-skips controls or samples not recorded, which have no files

      fid2=fopen([Desc_dir,File,'.dsc']);    %Open specific description file which contains the sampling frequency, signal gain and offset
      ds=fscanf(fid2,'%g',[5,inf])';          %creates a matrix 'ds' that contains the information from the description file
      fclose(fid2);

      ['Analyzing sample ',num2str(k),' - ',num2str(Bursts),' bursts.....']
      for j=1:Bursts    %index for burst of specified file


        fseek(fid1, 2*(j-1)*c_actualspb(k), 'bof'); %seeks within the binary file to start the fread at the correct burst
        y = fread(fid1,c_actualspb(k),'int16');  %reads the binary file

        %Read from the desciption matrix 'ds' for specific parameters for each burst
        Period=ds(j,2);  %Sampling Period
        fs=1/Period;     %Sampling Frequency
        fn=fs/2;         %Nyquist Frequency
        Gain=ds(j,4);    %Gain for binary data
        Offset=ds(j,3);  %Offset for binary data

        %Apply offset and gain to convert 'y' from binary data to real voltage data
        %Create relative time matrix for plotting
        y=y*Gain+Offset;
        t=0:Period:(length(y)-1)*Period;
        %
        if strcmp(Hanning_Window,'Yes')==1
          w=hann(length(y));
          y=y.*w;
        end



        %Cut acquisiton appropriately for 1 ms signal
        i=1;
        while y(i)<0.005
          i=i+1;
          if i>length(y), break, end
        end

        a1=i;
        a2=a1+12499;
        if a2 > 13500
```

```
    a2=13500;
    a1=a2-12499;
end
y3=y(a1:a2);
t3=0:Period:(length(y3)-1)*Period;


%Apply FFT, computing magnitude and phase

NFFT=2.^(ceil(log(length(y3))/log(2)));    %Next highest power of 2 greater than or equal to length of y2
FFTY=fft(y3,NFFT);                  %Take fft, padding with zeros, length(FFTY)==NFFT
NumUniquePts = ceil((NFFT+1)/2);        %Non-redundant points before Nyquist frequency
FFTY=FFTY(1:NumUniquePts);              %Keeping only non-redudant values
MY=abs(FFTY);                       %Magnitude
MY=MY*2;                            %Multiply by 2 to take into account the fact that we
%threw out second half of FFTX above
MY(1)=MY(1)/2;                      %Account for endpoint uniqueness
MY(length(MY))=MY(length(MY))/2;
MY=MY/length(y3);                   %We know NFFT is even. Scale the FFT so that it is not a function of the length of y2.
MYD=10*log10(MY);                   %Magnitude in decibels

F=(0:NumUniquePts-1)*2*fn/NFFT;         %Frequency for fft
F2=F/DF;                            %Frequency/Driving Frequency
R=2*fn/NFFT ;                       %Frequency Resolution


%Analyzing markers of cavitation
%Half Frequency
I=round(.5*DF/R);
a=I-5;
b=I+5;
MYDs=MYD(a:b);
MYs=MY(a:b);
Fs=F(a:b);
[C,I]=max(MYs);
max_h=MYs(I);
frequency_h=Fs(I)/1e6;

%Main Frequency
I=round(DF/R);
a=I-5;
b=I+5;
MYDs=MYD(a:b);
MYs=MY(a:b);
Fs=F(a:b);
[C,I]=max(MYs);
max_m=MYs(I);
frequency_m=Fs(I)/1e6;

%One and one half Frequency
I=round(1.5*DF/R);
a=I-5;
b=I+5;
MYDs=MYD(a:b);
```

```
MYs=MY(a:b);
Fs=F(a:b);
[C,I]=max(MYs);
max_oh=MYs(I);
frequency_oh=Fs(I)/1e6;

%Twice the Frequency
I=round(2*DF/R);
a=I-5;
b=I+5;
MYDs=MYD(a:b);
MYs=MY(a:b);
Fs=F(a:b);
[C,I]=max(MYs);
max_t=MYs(I);
frequency_t=Fs(I)/1e6;

% Broad band 1
%               a=round(1.9e6/R);
%               b=round(2.1e6/R);
% Broad band 2
c=round(2.3e6/R);
d=round(2.5e6/R);

%               MYs1=MY(a:b);
MYs2=MY(c:d);
%               ave=(sum(MYs1)+sum(MYs2))/(length(MYs1)+length(MYs2));
ave=(sum(MYs2)/length(MYs2));
ave2=10*log10(ave);

%Maximum of Magnitude with in these specified ranges (a and b above)
Max(j,k,1)=max_h;  %f/2
Max(j,k,2)=max_m;  %f
Max(j,k,3)=max_oh; %3/2f
Max(j,k,4)=max_t; %2f
Ave(j,k)=ave;     %broadband noise

if strcmp(Make_Plots,'Yes')==1
   %Plots

   figure(1);
   clf;
   plot(t3,y3);
   xlabel('Time (s)');
   ylabel('Voltage (V)'), grid on;
   ylim([-1 1]);
   xlim([0 .0015]);

   if strcmp(Print_Plots,'Yes')==1
      print('-djpeg','-f1','-r200',[Graph_dir,'Waveform-',File,' Burst ',num2str(j),'.jpg']);
   end

   %Magnitude in decibels Plot
   figure (2);
   clf;
   plot(F,MYD);
```

```
            xlim([0 fn]);
            ylim([-70 0]);
            ylabel('Magnitude [Decibels]'), grid on;
            xlabel('Frequency [Hertz]');
            title(['Burst ',num2str(j)]);

            if strcmp(Print_Plots,'Yes')==1
               print('-djpeg','-f1','-r300',[Graph_dir,'FFT-',File,' Burst ',num2str(j),'.jpg']);
            end

            figure (3);
            clf;
            plot(F2,MYD);
            xlim([0 fn/DF]); grid on;
            ylim([-70 0]);
            ylabel('Magnitude [Decibels]'), grid on;
            xlabel('Frequency/Driving Frequency [-]');

            if strcmp(Print_Plots,'Yes')==1
               print('-dbmp','-f1','-r300',[Graph_dir,'FFT-',File,' Burst ',num2str(j),'.jpg']);
            end

            figure (4);
            clf;
            plot(F,MY);
            xlim([0 fn]);
            ylim([0 1.25*max(MY)]);
            ylabel('Magnitude'), grid on;
            xlabel('Frequency [Hertz]');

            if strcmp(Print_Plots,'Yes')==1
               print('-djpeg','-f1','-r200',[Graph_dir,'FFT-',File,' Burst ',num2str(j),'.jpg']);
            end

            %              figure (5);
            %              clf;
            %              specgram(y3,NFFT,fs)
            %              title('Spectrogram')

         elseif strcmp(Make_Plots,'No')==1
         else
            'Make Plots Error'
            break
         end

      end
   end
   fclose(fid1);
 end
end

for i=1:max_samples
   M(i,1)=c_pressures(i);
   M(i,2)=Max(1,i,1); %Max value: (Burst, Sample File, four local maximum regions) %f/2
   M(i,3)=Max(1,i,2); %f
   M(i,4)=Max(1,i,3); %3/2f
```

```
   M(i,5)=Max(1,i,4); %2f
   M(i,6)=Ave(1,i);   %Broad Band measurement(Burst, Sample File)

end
fid = fopen([Spec_dir,'Maximums Burst 1.xls'],'w');
fprintf(fid,'%12.8f\t %12.8f\t %12.8f\t %12.8f\t %12.8f\t %12.8f\n',M');
fclose(fid);


for k=1:max_samples

   if c_bursts(k)~=0

      for j=1:c_bursts(k)

         B_h(j,k)=Max(j,k,1); %(k=Sample, j=Burst, Region)
         B_m(j,k)=Max(j,k,2);
         B_oh(j,k)=Max(j,k,3);
         B_t(j,k)=Max(j,k,4);
         BN(j,k)=Ave(j,k);
      end
   end

   if c_bursts(k)==0
      for j=1:1

         B_h(j,k)=Max(j,k,1); %(k=Sample, j=Burst, Region)
         B_m(j,k)=Max(j,k,2);
         B_oh(j,k)=Max(j,k,3);
         B_t(j,k)=Max(j,k,4);
         BN(j,k)=Ave(j,k);
      end
   end


   SumBN(1,k)=c_samples(k);
   SumBN(2,k)=c_pressures(k);
   SumBN(3,k)=c_bursts(k);
   SumBN(4,k)=c_energies(k);

   R=[0  0          6.00892E-06       0.000037581       0          4.59264E-06       9.88026E-06
         3.0802E-06       0          0          3.77178E-06       0          7.33868E-06       0.000006496
         0          1.04148E-05       0          1.65894E-05       0          0
   ];


   if c_pressures(k)==0
      R1=3.15e-6;
   elseif c_pressures(k)==0.5
      R1=3.51e-6 ;
   elseif c_pressures(k)==1.2
      R1=3.71e-6;
   elseif c_pressures(k)==1.7
      R1=3.62e-6;
   elseif c_pressures(k)==2.0
      R1=3.89e-6;
```

```
    end

    R2=R(k);

    SumBN(5,k)=0;
    if c_pressures(k)==0
       SumBN(5,k)=0;
       u(k)=c_bursts(k);

    elseif c_bursts(k) <=30
       i=1;
       u(k)=i;
       while BN(i,k)>R1
          SumBN(5,k)=SumBN(5,k)+BN(i,k);
          u(k)=i;
          i=i+1;
          if i>c_bursts(k)
             break
          end
       end
       SumBN(5,k)=SumBN(5,k)-(u(k)*R1);

    else
       i=31;
       SumBN(5,k)=sum(BN(1:30,k));
       u(k)=30;
       while BN(i,k)>R2
          SumBN(5,k)=SumBN(5,k)+BN(i,k);
          u(k)=i;
          i=i+1;
          if i>c_bursts(k)
             break
          end
       end
       SumBN(5,k)=SumBN(5,k)-(u(k)*R2);
    end
    SumBN(6,k)=u(k);

end

if strcmp(Write_Files,'Yes')==1

    q='%12.8f\n';
    for i=1:(max_samples-1)
       q=['%12.8f\t ',q];
    end

    ['Writing files to ',Spec_dir,'....']
    fid = fopen([Spec_dir,'Burst_h.xls'],'w');
    fprintf(fid,q,B_h');
    fclose(fid);

    fid = fopen([Spec_dir,'Burst_m.xls'],'w');
    fprintf(fid,q,B_m');
    fclose(fid);
```

```
    fid = fopen([Spec_dir,'Burst_oh.xls'],'w');
    fprintf(fid,q,B_oh');
    fclose(fid);

    fid = fopen([Spec_dir,'Burst_t.xls'],'w');
    fprintf(fid,q,B_t');
    fclose(fid);

    fid = fopen([Spec_dir,'Burst_BN.xls'],'w');
    fprintf(fid,q,BN');
    fclose(fid);

    fid = fopen([Spec_dir,'Sum_BN.xls'],'w');
    fprintf(fid,q,SumBN');
    fclose(fid);

elseif strcmp(Write_Files,'No')==1
else
    'Write Files Error'
    break
end
'Finished'
beep
```

APPENDIX D: INTACT ARTERY SAMPLE CHAMBER DESIGN

INTRODUCTION

A sample chamber was constructed to hold an intact artery in place during ultrasound exposure. The design considerations for this chamber were (i) to allow ultrasound to pass through the chamber and artery with minimal attenuation from the chamber, (ii) to hold the intact artery in place in a horizontal orientation, (iii) to allow media to be filled inside the artery to approximately physiologic pressure, (iv) to allow media to be filled inside the chamber, and (v) to allow the chamber to be attached to the micropositioning system for placement in the ultrasound bath. In Figure D.1A and B, a dimensional drawing and actual image of the intact artery sample chamber is shown, respectively. The chamber was constructed from acrylic plastic for the frame and walls of the chamber, Mylar plastic for the ultrasound windows, stainless steel cannulas, and polycarbonate compression fittings. The chamber was constructed such that the acrylic walls provided a strong frame and Mylar plastic windows could be attached with screws, providing an acoustically transparent window. A gasket would between the Mylar and acrylic was used to provide a water tight seal. An intact artery could be attached to metal cannulas by suturing thread, and cannulas were held in place by compression fittings on each of the acrylic frame, which also provide a water tight seal. Arteries could be filled with media through the metal cannulas media. A simple stopper was used to plug one end of the cannulas and some rubber tubing and three-way stop cock was used to allow fitting of pressure guage and provide seal. The chamber, itself, was filled via syringe and needle through a small hole in the top of the chamber, which was seal with a rubber

stopper. Lastly, the top of the chamber had a hole bored for a positioning rod and a set screw was used to hold it in place.

A

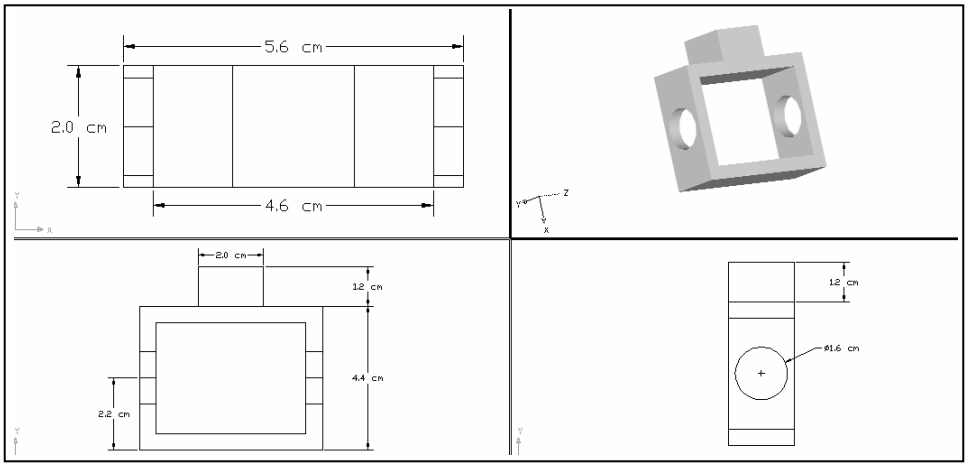

B

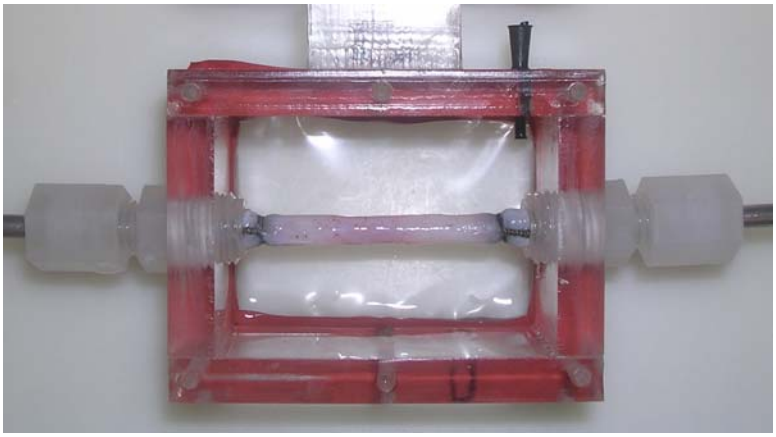

Figure D.1: (A) Mechanical drawing of intact artery chamber. (B) Real image of intact artery chamber with an ex vivo porcine carotid artery cannulated in the chamber

APPENDIX E: CONICAL TRANSDUCER HOUSING

INTRODUCTION

A conical transducer housing was designed and constructed in order to have a portable means to produce ultrasound outside of the water bath (e.g., exposure to animal models or *ex vivo* tissue samples). The design considerations were (i) to have a housing that would hold the transducer, (ii) provide a water tight seal, (iii) allow the housing to be filled with water, and (iv) allow mounting a micropositioning system. In Figure E.1, a dimensional drawing of the conical housing is shown. The housing was constructed such that the transducer would fit inside the back of the cylindrical portion of the housing with a water tight seal. At the other end, a plastic window could be mounted, also with a water tight seal. This window was typically thin mylar plastic to provide an acoustically transparent window. Near the top of the cylindrical section of the housing a small hole was bored for filling the housing with water and could be plugged with a simple rubber stopper. The angle of the conical portion was approximately equal to the ultrasound beam and was important to allow the ultrasound to be more easily targeted. The housing could allow be mounted to a microposition system via tapped holes on the transducer cover. To further couple the cone to a sample an ultrasonic gel could be used to provide a medium for the ultrasound.

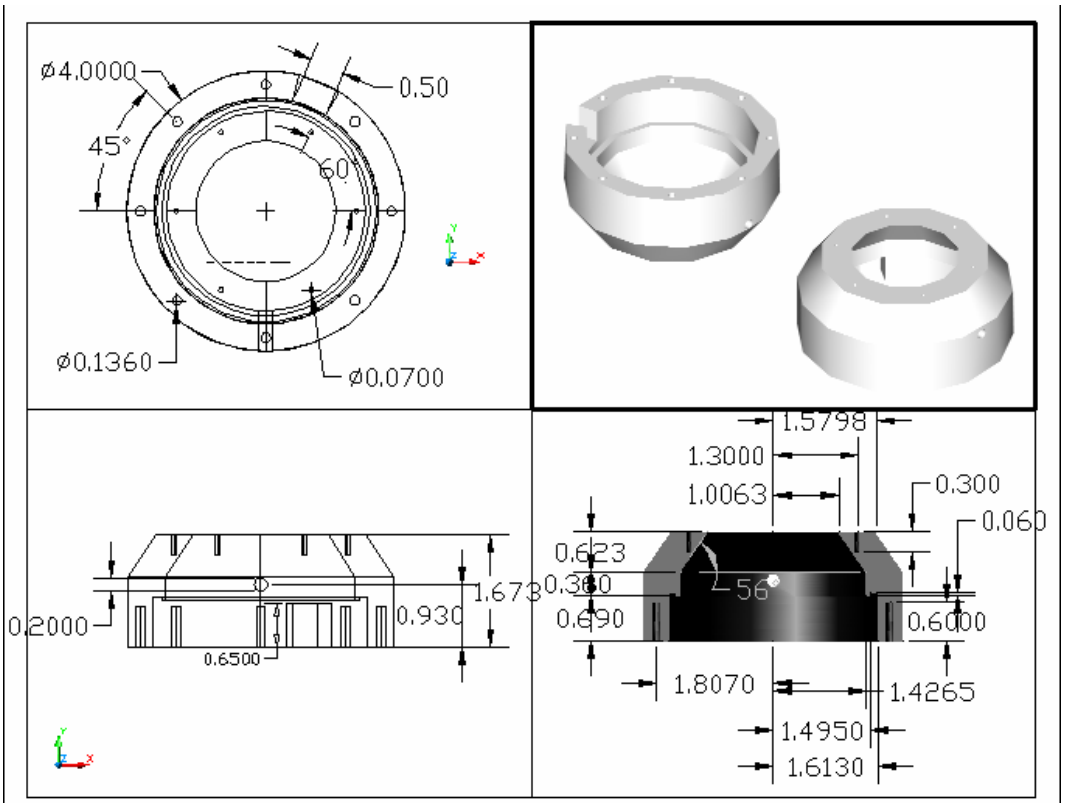

Figure E.1: Mechanical drawing for conical transducer housing.

APPENDIX F: CAVITATION IN HIGH VISCOSITY SOLUTIONS

INTRODUCTION

The use of cavitation in the body is being explored for many uses including diagnostic imaging, drug delivery, heating tissues and destroying cells and tissue. Inertial cavitation is of particular interest for drug delivery applications and is currently studied for uses in drug delivery to organs and tissues, including kidneys, myocardium, vascular tissue, brain, skeletal muscle, spinal cord, and many cancerous tumors. In each of these scenarios, cavitation production is desired to be produced in interstitial spaces or in the blood presenting locations were cavitation may be limited due to effects such as viscosity. To study the extent to which viscosity limits inertial cavitation activity, we used our established cavitation detection system to measure cavitation is solutions of varying viscosities.

METHODS

High viscosity solutions

Solutions of glycerin (Sigma, St. Louis, MO) and deionized-distilled water were mixed in concentrations ranging from 0 to 85 wt% of glycerin to create twelve solutions with viscosities ranging from 0.9 cP (pure water) to 85.5 cP (85 wt% glycerin). Viscosities were determined by measuring each solution using a u-tube viscometer (Cannon Instrument Company, State College, PA). In Figure F.1 viscosity measurements are graphed for measured and literature values, which show close agreement.

Ultrasound apparatus and cavitation Detection

The ultrasound apparatus and cavitation detection system was used as described in the Chapter 3 Methods.

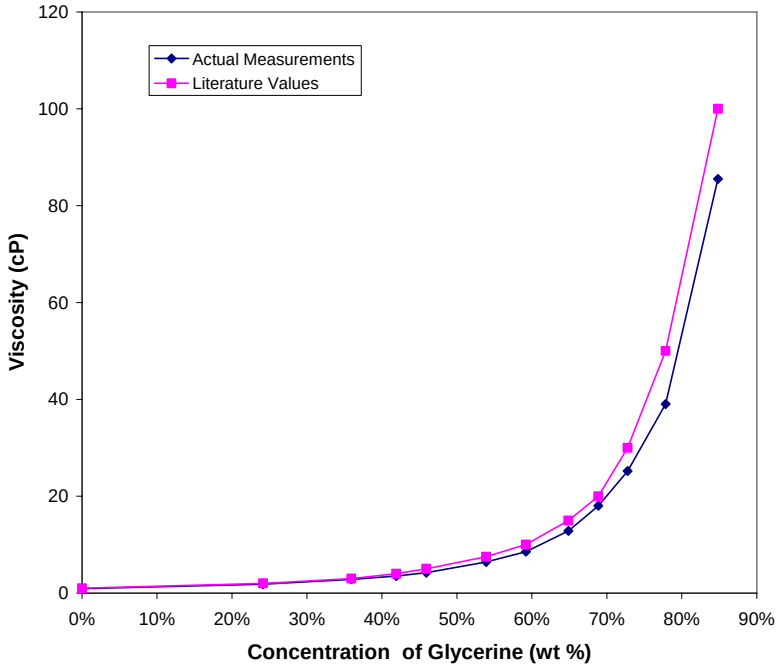

Figure F.1: Literature and measured values of the calibration of viscosity with concentration of glycerine in a water-glycerine mixture.

Experimental Protocol

Similar to the protocol in the methods described in Chapter 3, samples were prepared by adding Optison® at a concentration of 1.7% v/v (~ 1.1 x 10^7 bubble/ml) to 0.5 ml of each glycerin-water solution immediately before ultrasound exposure. Ultrasound was exposed at 1.1 MHz to each glycerin-water solution with Optison® at 0.5, 1.0, 1.5, and 2.0 MPa for 3000 ms of exposure time at a 1% duty cycle while simultaneously recording cavitation emissions.

RESULTS

Using our established cavitation detection system and method of analyzing inertial cavitation based on broadband noise, we recorded cavitation emissions and analyzed the broadband noise signal over the exposure time for each ultrasound exposure. In Figure F.2, broadband noise measurements are shown for each solution over a 3000 ms exposure of ultrasound at 0.5, 1.0, 1.5, 2.0 MPa. The higher viscosity solutions display a reduction in cavitation activity as indicated by the lower levels of broadband noise, which is most distinctive at ultrasound exposure of 2.0 MPa (Figure F.2D). Lower viscosities display a higher in the peak broadband noise and sustained higher levels of broadband noise over the exposure time first hundred of milliseconds.

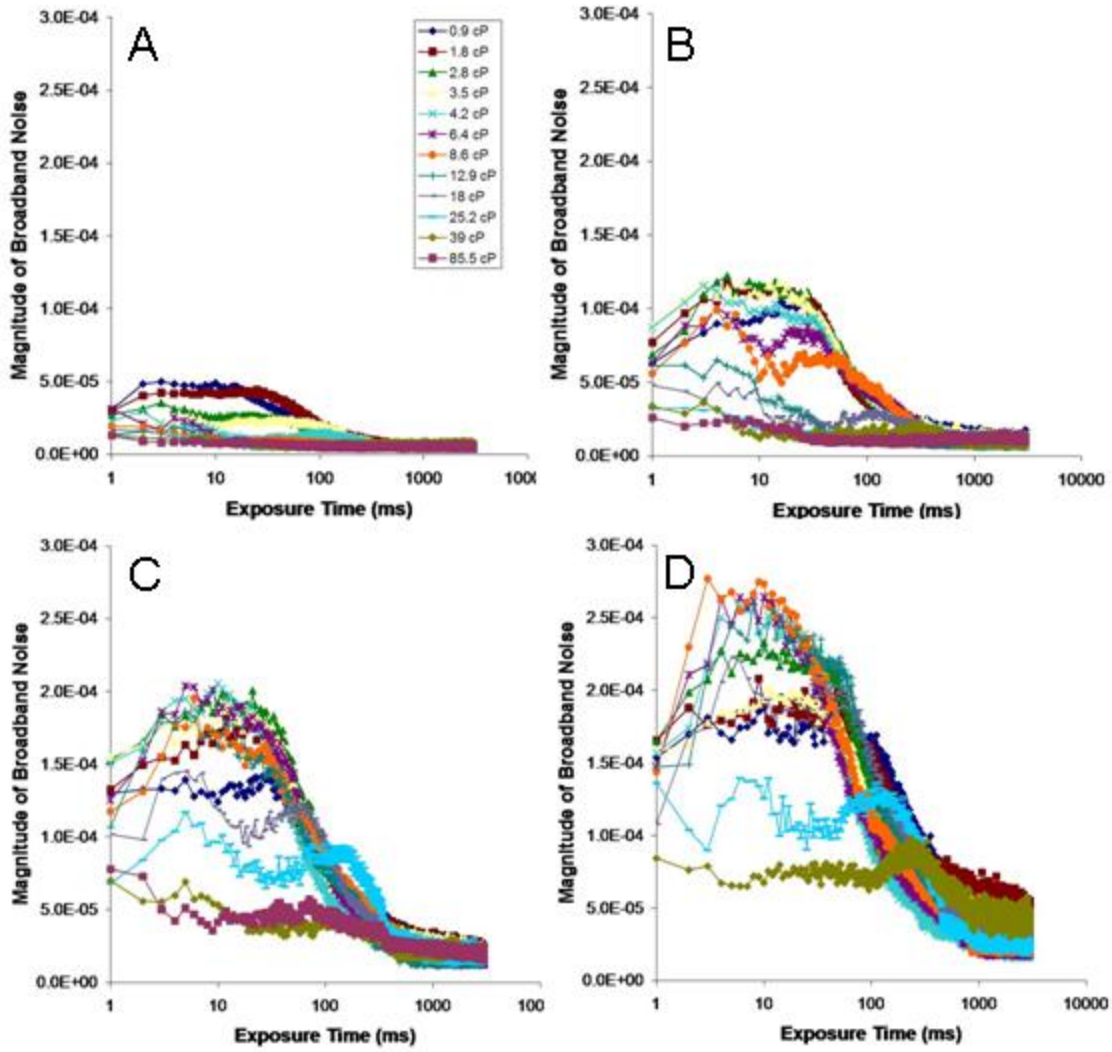

Figure F.2: Broadband noise measurements of recorded cavitation emissions produced in glycerine-water solutions of various viscosities mediated by ultrasound at (A) 0.5, (B) 1.0, (C) 1.5 and (D) 2.0 MPa for a 3000 ms exposure time.

To further analyze the results presented in Figure F.2, the broadband noise was integrated over the exposure time to calculate the inertial cavitation dose, a measure of inertial cavitation activity over the exposure time. As shown in Figure F.3, the inertial cavitation dose increases with increasing pressure as expected from previous results. With respect to viscosity, the inertial cavitation dose decreased significantly with

increasing viscosity. This data suggests that biological fluids such as blood, which has a viscosity of 3-4 cP, will reduce the cavitation activity compared to water (1 cP). This effect of viscosity appears to be more significant at the lower pressures, since the high pressures sustained a high inertial cavitation dose whereas the lower pressures diminished the inertial cavitation dose at 5-6 cP at 0.5 MPa.

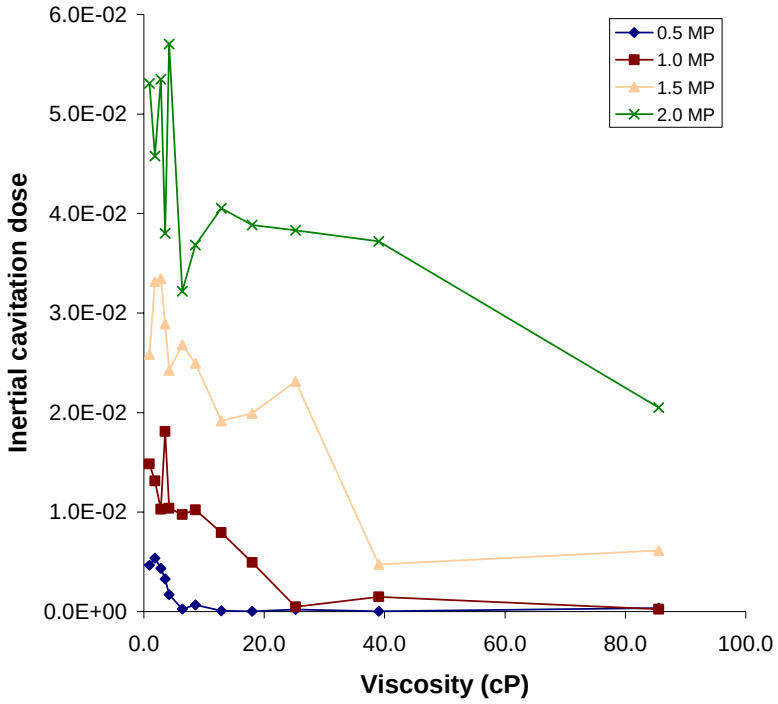

Figure F.3: Measured inertial cavitation dose at various viscosities and peak-negative ultrasound pressure.

REFERENCES

Aliabadi HM, Lavasanifar A. Polymeric micelles for drug delivery. Expert Opin Drug Deliv 2006; 3: 139-62.

Allen JS, Roy RA, Church CC. On the role of shear viscosity in mediating inertial cavitation from short-pulse megahertz-frequency ultrasound. iEEE Trans Ultrason Ferroelectr Freq Control 1997; 44: 743-751.

Amabile PG, Waugh JM, Lewis TN et al. High-efficiency endovascular gene delivery via therapeutic ultrasound. J Am Coll Cardiol 2001; 37: 1975-80.

America ASo ANSI Technical Report: Bubble Detection and Cavitation Monitoring 2002

Apfel RE. Sonic effervescence: A tutorial on acoustic cavitation. J Acoust Soc Am 1997; 101: 1227-1237.

Azzam T, Domb AJ. Current developments in gene transfection agents. Curr Drug Deliv 2004; 1: 165-93.

Baker AH, Kritz A, Work LM, Nicklin SA. Cell-selective viral gene delivery vectors for the vasculature. Exp. Physiol. 2005; 90: 27-31.

Barber K, Mala RR, Lambert MP et al. Delivery of membrane-impermeant fluorescent probes into living neural cell populations by lipotransfer. Neurosci Lett 1996; 207: 17-20.

Barry BW. Novel mechanisms and devices to enable successful transdermal drug delivery. Eur J Pharm Sci 2001; 14: 101-14.

Batheja P, Thakur R, Michniak B. Transdermal iontophoresis. Expert Opin Drug Deliv 2006; 3: 127-38.

Beach KW. 1975-2000: a quarter century of ultrasound technology. Ultrasound Med Biol 1992; 18: 377-88.

Beeri R, Guerrero JL, Supple G et al. New efficient catheter-based system for myocardial gene delivery. Circulation 2002; 106: 1756-9.

Bekeredjian R, Grayburn PA, Shohet RV. Use of ultrasound contrast agents for gene or drug delivery in cardiovascular medicine. J Am Coll Cardiol 2005; 45: 329-35.

Belanger AC. Vascular anatomy and physiology: an introductory text. Pasadena, Calif.: Appleton Davies, 1990.

Brayman AA, Coppage ML, Vaidya S, Miller MW. Transient poration and cell surface receptor removal from human lymphocytes in vitro by 1 MHz ultrasound. Ultrasound Med Biol 1999; 25: 999-1008.

Brayman AA, Lizotte LM, Miller MW. Erosion of artificial endothelia in vitro by pulsed ultrasound: acoustic pressure, frequency, membrane orientation and microbubble contrast agent dependence. Ultrasound Med. Biol. 1999; 25: 1305-20.

Burkoth TL, Bellhouse BJ, Hewson G et al. Transdermal and transmucosal powdered drug delivery. Crit Rev Ther Drug Carrier Syst 1999; 16: 331-84.

Chen WS, Brayman AA, Matula TJ, Crum LA. Inertial cavitation dose and hemolysis produced in vitro with or without Optison(R). Ultrasound Med Biol 2003; 29: 725-37.

Chen WS, Matula TJ, Crum LA. The disappearance of ultrasound contrast bubbles: observations of bubble dissolution and cavitation nucleation. Ultrasound Med Biol 2002; 28: 793-803.

Chesler NC, Conklin BS, Hand H-C, Ku DN. Simplified ex vivo artery culture techniques for porcine arteries. J. Vasc. Invest. 1998; 4: 123-127.

Chien YW. Novel drug delivery systems. New York: M. Dekker, 1992.

Cines DB, Pollak ES, Buck CA et al. Endothelial cells in physiology and in the pathophysiology of vascular disorders. Blood 1998; 91: 3527-61.

Clarke MS, McNeil PL. Syringe loading introduces macromolecules into living mammalian cell cytosol. J Cell Sci 1992; 102 (Pt 3): 533-41.

Cochran SA, Prausnitz MR. Sonoluminescence as an indicator of cell membrane disruption by acoustic cavitation. Ultrasound Med Biol 2001; 27: 841-50.

Coleman AJ, Saunders JE. A review of the physical properties and biological effects of the high amplitude acoustic field used in extracorporeal lithotripsy. Ultrasonics 1993; 31: 75-89.

Conti S, Polonelli L, Frazzi R et al. Controlled delivery of biotechnological products. Curr Pharm Biotechnol 2000; 1: 313-23.

Cooke JP. The endothelium: a new target for therapy. Vasc Med 2000; 5: 49-53.

Correas JM, Bridal L, Lesavre A et al. Ultrasound contrast agents: properties, principles of action, tolerance, and artifacts. Eur Radiol 2001; 11: 1316-28.

Crum LA. Sonoluminescence. Physics Today 1994; 47: 22-29.

Daniels S, Kodama T, Price DJ. Damage to red blood cells induced by acoustic cavitation. Ultrasound Med Biol 1995; 21: 105-11.

Davis C, Fischer J, Ley K, Sarembock IJ. The role of inflammation in vascular injury and repair. J Thromb Haemost 2003; 1: 1699-709.

Davis SP, Martanto W, Allen MG, Prausnitz MR. Hollow metal microneedles for insulin delivery to diabetic rats. IEEE Trans Biomed Eng 2005; 52: 909-15.

Dice JF. Microinjected ribonuclease A as a probe for lysosomal pathways of intracellular protein degradation. J Protein Chem 1988; 7: 115-27.

Doukas AG, Flotte TJ. Physical characteristics and biological effects of laser-induced stress waves. Ultrasound Med Biol 1996; 22: 151-164.

Doukas AG, Kollias N. Transdermal drug delivery with a pressure wave. Adv Drug Deliver Rev 2004; 56: 559-579.

Duncan R, Spreafico F. Polymer conjugates. Pharmacokinetic considerations for design and development. Clin Pharmacokinet 1994; 27: 290-306.

Edelman ER, Kost J, Bobeck H, Langer R. Regulation of drug release from polymer matrices by oscillating magnetic fields. J Biomed Mater Res 1985; 19: 67-83.

Evans EA, Waugh R, Melnik L. Elastic Area Compressibility Modulus of Red-Cell Membrane. Biophysical Journal 1976; 16: 585-595.

Everbach EC, Makin IR, Azadniv M, Meltzer RS. Correlation of ultrasound-induced hemolysis with cavitation detector output in vitro. Ultrasound Med Biol 1997; 23: 619-24.

Feldman LJ, Steg G. Optimal techniques for arterial gene transfer. Cardiovasc Res 1997; 35: 391-404.

Feril LB, Kondo T, Zhao QL et al. Enhancement of ultrasound-induced apoptosis and cell lysis by echo-contrast agents. Ultrasound Med Biol 2003; 29: 339-345.

Flint EB, Suslick KS. The Temperature of Cavitation. Science 1991; 253: 1397-1399.

Forsberg F, Shi WT, Goldberg BB. Subharmonic imaging of contrast agents. Ultrasonics 2000; 38: 93-8.

Gardlik R, Palffy R, Hodosy J et al. Vectors and delivery systems in gene therapy. Med Sci Monit 2005; 11: RA110-RA121.

Gehl J. Electroporation: theory and methods, perspectives for drug delivery, gene therapy and research. Acta Physiol Scand 2003; 177: 437-47.

Gershlick AH. Drug eluting stents in 2005. Heart 2005; 91 Suppl 3: iii24-31.

Goldberg BB, Liu JB, Forsberg F. Ultrasound contrast agents: a review. Ultrasound Med Biol 1994; 20: 319-33.

Goyal P, Goyal K, Vijaya Kumar SG et al. Liposomal drug delivery systems--clinical applications. Acta Pharm 2005; 55: 1-25.

Greenleaf WJ, Bolander ME, Sarkar G et al. Artificial cavitation nuclei significantly enhance acoustically induced cell transfection. Ultrasound Med Biol 1998; 24: 587-95.

Gupta B, Levchenko TS, Torchilin VP. Intracellular delivery of large molecules and small particles by cell-penetrating proteins and peptides. Adv Drug Deliv Rev 2005; 57: 637-51.

Guzman HR, McNamara AJ, Nguyen DX, Prausnitz MR. Bioeffects caused by changes in acoustic cavitation bubble density and cell concentration: A unified explanation based on cell-to-bubble ratio and blast radius. Ultrasound in Medicine and Biology 2003; 29: 1211-1222.

Guzman HR, Nguyen DX, Khan S, Prausnitz MR. Ultrasound-mediated disruption of cell membranes. I. Quantification of molecular uptake and cell viability. J Acoust Soc Am 2001; 110: 588-96.

Guzman HR, Nguyen DX, Khan S, Prausnitz MR. Ultrasound-mediated disruption of cell membranes. II. Heterogeneous effects on cells. J Acoust Soc Am 2001; 110: 597-606.

Guzman HR, Nguyen DX, McNamara AJ, Prausnitz MR. Equilibrium loading of cells with macromolecules by ultrasound: effects of molecular size and acoustic energy. J Pharm Sci 2002; 91: 1693-701.

Hanahan D, Weinberg RA. The hallmarks of cancer. Cell 2000; 100: 57-70.

Hashiya N, Aoki M, Tachibana K et al. Local delivery of E2F decoy oligodeoxynucleotides using ultrasound with microbubble agent (Optison) inhibits intimal hyperplasia after balloon injury in rat carotid artery model. Biochem Biophys Res Commun 2004; 317: 508-14.

Heller LC, Ugen K, Heller R. Electroporation for targeted gene transfer. Expert Opin Drug Deliv 2005; 2: 255-68.

Hofheinz RD, Gnad-Vogt SU, Beyer U, Hochhaus A. Liposomal encapsulated anti-cancer drugs. Anticancer Drugs 2005; 16: 691-707.

Hollis B, Thilaganathan B. Role of ultrasound in obstetrics. Current Obstetrics and Gynaecology 2001; 11: 78-85.

Holmes SA, Whitfield HN. The current status of lithotripsy. Br J Urol 1991; 68: 337-44.

Huber PE, Mann MJ, Melo LG et al. Focused ultrasound (HIFU) induces localized enhancement of reporter gene expression in rabbit carotid artery. Gene Ther. 2003; 10: 1600-7.

Huber PE, Mann MJ, Melo LG et al. Focused ultrasound (HIFU) induces localized enhancement of reporter gene expression in rabbit carotid artery. Gene Ther 2003; 10: 1600-7.

Hwang JH, Brayman AA, Reidy MA et al. Vascular effects induced by combined 1-MHz ultrasound and microbubble contrast agent treatments in vivo. Ultrasound Med Biol 2005; 31: 553-64.

Jensen KD, Nori A, Tijerina M et al. Cytoplasmic delivery and nuclear targeting of synthetic macromolecules. J Control Release 2003; 87: 89-105.

Johnson-Saliba M, Jans DA. Gene therapy: optimising DNA delivery to the nucleus. Curr Drug Targets 2001; 2: 371-99.

Kamaev PP, Hutcheson JD, Wilson ML, Prausnitz MR. Quantification of optison bubble size and lifetime during sonication dominant role of secondary cavitation bubbles causing acoustic bioeffects. J Acoust Soc Am 2004; 115: 1818-25.

Kennedy JE. High-intensity focused ultrasound in the treatment of solid tumours. Nat Rev Cancer 2005; 5: 321-7.

Kerkis A, Hayashi MA, Yamane T, Kerkis I. Properties of cell penetrating peptides (CPPs). IUBMB Life 2006; 58: 7-13.

Kipshidze NN, Porter TR, Dangas G et al. Novel site-specific systemic delivery of Rapamycin with perfluorobutane gas microbubble carrier reduced neointimal formation in a porcine coronary restenosis model. Catheter Cardiovasc Interv 2005; 64: 389-94.

Klibanov AL. Microbubble contrast agents: targeted ultrasound imaging and ultrasound-assisted drug-delivery applications. Invest Radiol 2006; 41: 354-62.

Koch S, Pohl P, Cobet U, Rainov NG. Ultrasound enhancement of liposome-mediated cell transfection is caused by cavitation effects. Ultrasound Med Biol 2000; 26: 897-903.

Kodama T, Doukas AG, Hamblin MR. Shock wave-mediated molecular delivery into cells. Bba-Mol Cell Res 2002; 1542: 186-194.

Koike H, Tomita N, Azuma H et al. An efficient gene transfer method mediated by ultrasound and microbubbles into the kidney. J Gene Med 2005; 7: 108-16.

Kompella UB, Lee VH. Delivery systems for penetration enhancement of peptide and protein drugs: design considerations. Adv Drug Deliv Rev 2001; 46: 211-45.

Kondo I, Ohmori K, Oshita A et al. Treatment of acute myocardial infarction by hepatocyte growth factor gene transfer: the first demonstration of myocardial transfer of a "functional" gene using ultrasonic microbubble destruction. J Am Coll Cardiol 2004; 44: 644-53.

Kondo T, Kodaira T, Kano E. Free radical formation induced by ultrasound and its effects on strand breaks in DNA of cultured FM3A cells. Free Radic Res Commun 1993; 19 Suppl 1: S193-S200.

Lagneaux L, de Meulenaer EC, Delforge A et al. Ultrasonic low-energy treatment: a novel approach to induce apoptosis in human leukemic cells. Exp Hematol 2002; 30: 1293-301.

Langer R. New methods of drug delivery. Science 1990; 249: 1527-33.

Langer R. Drug delivery and targeting. Nature 1998; 392: 5-10.

Langer R. Drug delivery. Drugs on target. Science 2001; 293: 58-9.

Lauterborn W, Ohl CD. Cavitation bubble dynamics. Ultrasonics Sonochemistry 1997; 4: 65-75.

Leighton TG. The Acoustic Bubble. London: Academic Press, 1994.

Li S. Electroporation gene therapy: new developments in vivo and in vitro. Curr Gene Ther 2004; 4: 309-16.

Liu J, Lewis TN, Prausnitz MR. Non-invasive assessment and control of ultrasound-mediated membrane permeabilization. Pharm Res 1998; 15: 918-924.

Liu Y, Yang H, Sakanishi A. Ultrasound: Mechanical gene transfer into plant cells by sonoporation. Biotechnol Adv 2005;

Lokhandwalla M, Sturtevant B. Mechanical haemolysis in shock wave lithotripsy (SWL): I. Analysis of cell deformation due to SWL flow-fields. Phys Med Biol 2001; 46: 413-437.

Lu QL, Liang HD, Partridge T, Blomley MJ. Microbubble ultrasound improves the efficiency of gene transduction in skeletal muscle in vivo with reduced tissue damage. Gene Ther 2003; 10: 396-405.

Madeddu P. Therapeutic angiogenesis and vasculogenesis for tissue regeneration. Exp Physiol 2005; 90: 315-26.

Madersbacher S, Marberger M. High-energy shockwaves and extracorporeal high-intensity focused ultrasound. J Endourol 2003; 17: 667-72.

Madersbacher S, Pedevilla M, Vingers L et al. Effect of high-intensity focused ultrasound on human prostate cancer in vivo. Cancer Res 1995; 55: 3346-51.

Malecki M, Kolsut P, Proczka R. Angiogenic and antiangiogenic gene therapy. Gene Ther. 2005; 12 Suppl 1: S159-69.

Marin A, Sun H, Husseini GA et al. Drug delivery in pluronic micelles: effect of high-frequency ultrasound on drug release from micelles and intracellular uptake. J Control Release 2002; 84: 39-47.

Martanto W, Baisch SM, Costner EA et al. Fluid dynamics in conically tapered microneedles. Aiche Journal 2005; 51: 1599-1607.

McCarron PA, Olwill SA, Marouf WM et al. Antibody conjugates and therapeutic strategies. Mol Interv 2005; 5: 368-80.

McNeil PL, Murphy RF, Lanni F, Taylor DL. A method for incorporating macromolecules into adherent cells. J Cell Biol 1984; 98: 1556-64.

McNeil PL, Steinhardt RA. Plasma membrane disruption: Repair, prevention, adaptation. Annu Rev Cell Dev Bi 2003; 19: 697-731.

Mehier-Humbert S, Bettinger T, Yan F, Guy RH. Plasma membrane poration induced by ultrasound exposure: Implication for drug delivery. J Control Release 2005; 104: 213-222.

Melan MA. Overview of cell fixation and permeabilization. Methods Mol Biol 1994; 34: 55-66.

Melo LG, Gnecchi M, Pachori AS et al. Endothelium-targeted gene and cell-based therapies for cardiovascular disease. Arterioscler Thromb Vasc Biol 2004; 24: 1761-74.

Miller AP, Nanda NC. Contrast echocardiography: new agents. Ultrasound Med Biol 2004; 30: 425-34.

Miller DL, Dou CY. Membrane damage thresholds for pulsed or continuous ultrasound in phagocytic cells loaded with contrast agent gas bodies. Ultrasound Med Biol 2004; 30: 405-411.

Miller DL, Pislaru SV, Greenleaf JE. Sonoporation: mechanical DNA delivery by ultrasonic cavitation. Somat Cell Mol Genet 2002; 27: 115-134.

Miller DL, Quddus J. Lysis and sonoporation of epidermoid and phagocytic monolayer cells by diagnostic ultrasound activation of contrast agent gas bodies. Ultrasound Med Biol 2001; 27: 1107-13.

Miller MW, Miller DL, Brayman AA. A review of in vitro bioeffects of inertial ultrasonic cavitation from a mechanistic perspective. Ultrasound Med Biol 1996; 22: 1131-54.

Mitragotri S. Healing sound: the use of ultrasound in drug delivery and other therapeutic applications. Nat Rev Drug Discov 2005; 4: 255-60.

Mitragotri S, Blankschtein D, Langer R. Ultrasound-mediated transdermal protein delivery. Science 1995; 269: 850-3.

Mittle S, Makaryus AN, Mangion J. Role of contrast echocardiography in the assessment of myocardial rupture. Echocardiography 2003; 20: 77-81.

Miura S, Tachibana K, Okamoto T, Saku K. In vitro transfer of antisense oligodeoxynucleotides into coronary endothelial cells by ultrasound. Biochem Biophys Res Commun 2002; 298: 587-90.

Mukherjee D, Wong J, Griffin B et al. Ten-fold augmentation of endothelial uptake of vascular endothelial growth factor with ultrasound after systemic administration. J Am Coll Cardiol 2000; 35: 1678-86.

Mulholland SE, Lee S, McAuliffe DJ, Doukas AG. Cell loading with laser-generated stress waves: The role of the stress gradient. Pharmaceut Res 1999; 16: 514-518.

Neppiras EA. Subharmonic and other Low-Frequency Emission from Bubbles in Sound-Irradiated Liquids. The Journal of the Acoustical Society of America 1968; 46: 587-601.

Neppiras EA. Acoustic Cavitation. Physics Reports 1980; 61: 160-251.

Netz RR, Schick M. Pore formation and rupture in fluid bilayers. Phys Rev E 1996; 53: 3875-3885.

Ng KY, Liu Y. Therapeutic ultrasound: its application in drug delivery. Med Res Rev 2002; 22: 204-23.

Niidome T, Huang L. Gene therapy progress and prospects: nonviral vectors. Gene Ther. 2002; 9: 1647-52.

Ohl CD, Wolfrum B. Detachment and sonoporation of adherent HeLa-cells by shock wave-induced cavitation. Bba-Gen Subjects 2003; 1624: 131-138.

Panyam J, Labhasetwar V. Targeting intracellular targets. Curr Drug Deliv 2004; 1: 235-47.

Pierce AD. Acoustics: an introduction to its physical principles and applications. New York: McGraw-Hill Book Co., 1981.

Pine JL, Smith LJ, Haws MJ, Gingrass MK. Ultrasound-assisted lipoplasty. Plast Surg Nurs 2003; 23: 101-8; quiz 109.

Prado GR, Ross JD, DeWeerth SP, LaPlaca MC. Mechanical trauma induces immediate changes in neuronal network activity. J Neural Eng 2005; 2: 148-58.

Prausnitz MR. Microneedles for transdermal drug delivery. Adv Drug Deliv Rev 2004; 56: 581-7.

Quarck R, Holvoet P. Gene therapy approaches for cardiovascular diseases. Curr Gene Ther 2004; 4: 207-23.

Rapoport N. Combined cancer therapy by micellar-encapsulated drug and ultrasound. Int J Pharm 2004; 277: 155-62.

Rau KR, Guerra A, Vogel A, Venugopalan V. Investigation of laser-induced cell lysis using time-resolved imaging. Appl Phys Lett 2004; 84: 2940-2942.

Ray R, Shah AM. NADPH oxidase and endothelial cell function. Clin. Sci. (Lond.) 2005; 109: 217-26.

Rosen H, Abribat T. The rise and rise of drug delivery. Nat Rev Drug Discov 2005; 4: 381-5.

Rosenzweig BP, Nayar AC, Varkey MP, Kronzon I. Echo contrast-enhanced diagnosis of atrial septal defect. J Am Soc Echocardiogr 2001; 14: 155-7.

Saia F, Marzocchi A, Serruys PW. Drug-eluting stents. The third revolution in percutaneous coronary intervention. Ital. Heart. J. 2005; 6: 289-303.

Saltzman WM. Drug delivery: engineering principles for drug therapy. Oxford; New York: Oxford University Press, 2001.

Sapra P, Tyagi P, Allen TM. Ligand-targeted liposomes for cancer treatment. Curr Drug Deliv 2005; 2: 369-81.

Sato Y. Molecular diagnosis of tumor angiogenesis and anti-angiogenic cancer therapy. Int J Clin Oncol 2003; 8: 200-6.

Schlicher RK, Radhakrishna H, Tolentino TP et al. Mechanism of intracellular delivery by acoustic cavitation. Ultrasound Med Biol 2006; 32: 915-24.

Sharif F, Daly K, Crowley J, O'Brien T. Current status of catheter- and stent-based gene therapy. Cardiovasc Res 2004; 64: 208-16.

Sharif F, Daly K, Crowley J, O'Brien T. Current status of catheter- and stent-based gene therapy. Cardiovasc. Res. 2004; 64: 208-16.

Simoes S, Filipe A, Faneca H et al. Cationic liposomes for gene delivery. Expert Opin Drug Deliv 2005; 2: 237-54.

Smith SC, Jr., Jackson R, Pearson TA et al. Principles for national and regional guidelines on cardiovascular disease prevention: a scientific statement from the World Heart and Stroke Forum. Circulation 2004; 109: 3112-21.

Song W, Sun Q, Dong Z et al. Antiangiogenic gene therapy: disruption of neovascular networks mediated by inducible caspase-9 delivered with a transcriptionally targeted adenoviral vector. Gene Ther 2005; 12: 320-9.

Stein WD, Lieb WR. Transport and diffusion across cell membranes. Orlando: Academic Press, 1986.

Stubbe BG, De Smedt SC, Demeester J. "Programmed polymeric devices" for pulsed drug delivery. Pharm Res 2004; 21: 1732-40.

Sundaram J, Mellein BR, Mitragotri S. An experimental and theoretical analysis of ultrasound-induced permeabilization of cell membranes. Biophys J 2003; 84: 3087-101.

Suslick KS. Sonochemistry. Science 1990; 247: 1439-1445.

Tachibana K. Emerging technologies in therapeutic ultrasound: thermal ablation to gene delivery. Hum Cell 2004; 17: 7-15.

Taniyama Y, Tachibana K, Hiraoka K et al. Local delivery of plasmid DNA into rat carotid artery using ultrasound. Circulation 2002; 105: 1233-9.

Teupe C, Richter S, Fisslthaler B et al. Vascular gene transfer of phosphomimetic endothelial nitric oxide synthase (S1177D) using ultrasound-enhanced destruction of plasmid-loaded microbubbles improves vasoreactivity. Circulation 2002; 105: 1104-9.

Thom T, Haase N, Rosamond W et al. Heart disease and stroke statistics--2006 update: a report from the American Heart Association Statistics Committee and Stroke Statistics Subcommittee. Circulation 2006; 113: e85-151.

Thorpe PE. Vascular targeting agents as cancer therapeutics. Clin. Cancer Res. 2004; 10: 415-27.

Tozer GM, Kanthou C, Baguley BC. Disrupting tumour blood vessels. Nat Rev Cancer 2005; 5: 423-35.

Tsutsui JM, Xie F, Porter RT. The use of microbubbles to target drug delivery. Cardiovasc Ultrasound 2004; 2: 23.

Tyle P, Agrawala P. Drug delivery by phonophoresis. Pharm Res 1989; 6: 355-61.

Unger EC, Hersh E, Vannan M et al. Local drug and gene delivery through microbubbles. Prog Cardiovasc Dis 2001; 44: 45-54.

Unger EC, Porter T, Culp W et al. Therapeutic applications of lipid-coated microbubbles. Adv Drug Deliv Rev 2004; 56: 1291-314.

Veronese FM, Pasut G. PEGylation, successful approach to drug delivery. Drug Discov Today 2005; 10: 1451-8.

Vyas SP, Singh A, Sihorkar V. Ligand-receptor-mediated drug delivery: an emerging paradigm in cellular drug targeting. Crit Rev Ther Drug Carrier Syst 2001; 18: 1-76.

Wu J, Ross JP, Chiu JF. Reparable sonoporation generated by microstreaming. J Acoust Soc Am 2002; 111: 1460-4.

Young LS, Searle PF, Onion D, Mautner V. Viral gene therapy strategies: from basic science to clinical application. J Pathol 2006; 208: 299-318.

VITA

Daniel Martin Hallow was born in Madison, Indiana on January 3, 1979. He graduated from Madison Consolidated High School in June 1997. He then attended Rose-Hulman Institute of Technology in Terre Haute, Indiana, and in 2001, he graduated Magna Cum Laude from Rose-Hulman with a Bachelor of Science in Chemical Engineering. In August 2001, he attended the Georgia Institute of Technology in Atlanta, Georgia where he was accepted as a Ph.D. candidate in the School of Chemical and Biomolecular Engineering. His dissertation title was "Measurement and Correlation of Acoustic Cavitation with Cellular and Tissue Bioeffects." He defended his doctoral thesis on August 18, 2006 and obtained his Ph.D. in Chemical Engineering with a minor in Biomedical Engineering in December 2006.